**High-resolution shear-wave reflection profiling to image offset in unconsolidated near-surface sediments**

**By**



**Bevin L. Bailey**

Submitted to the Department of Geology and the Graduate Faculty of the University of Kansas in partial fulfillment of the requirements for the degree of Master of Science 2014.

_____

Chairperson: Richard D. Miller

_____

Don Steeples

_____

Jennifer A. Roberts

Date Defended: April 4th, 2014

The Thesis Committee for Bevin L. Bailey

certifies that this is the approved version of the following thesis:

**High-resolution shear-wave reflection profiling to image offset in unconsolidated near-surface sediments**

_____

Chairperson Richard D. Miller

Date approved: April 4th, 2014

## Abstract

S-wave reflection profiling has many theoretical advantages, when compared to P-wave profiling, such as high-resolution potential, greater sensitivities to lithologic changes and insensitivity to the water table and pore fluids, and could be particularly useful in near-surface settings. However, S-wave surveys can be plagued by processing pitfalls unique to near-surface studies such as interference of Love waves with reflections, and the stacking of Love waves as coherent noise, leading to possible misinterpretations of the subsurface. Two lines of S-wave data are processed and used to locate previously unknown faults in Quaternary sediments in a region where earthquake activity poses a threat to surface structures. This study provides clear examples of processing pitfalls such as Love waves with hyperbolic appearances on shot gathers, and a CMP section with coherent noise that is easily misinterpreted as reflections. This study demonstrates pros and cons of using SH reflection data in the near surface.

## Acknowledgments

First and foremost I would like to thank my advisor, Dr. Richard Miller, for all his guidance, help and support throughout my time at the University of Kansas and the Kansas Geological Survey. His work ethic and command of knowledge are something I aspire to. I would like to thank Don Steeples for giving me a chance at KU and for his excellent guidance and support throughout my time here. I would also like to thank my other committee member Jennifer Roberts for her guidance.

I would like to thank Rich Markiewicz and the U.S. Bureau of Reclamation for allowing me to use this data. I would also like to acknowledge the Exploration Services staff at the KGS for all of their assistance and efforts. In particular, Shelby Peterie, Julian Ivanov and Brett Bennett provided me with exceptional support and assistance. Also, thanks to Brett Wedel and Joe Anderson for their support in field data collection.

## Table of Contents

**Abstract** ..... **iii**
**Acknowledgments** ..... **iv**
**Table of Contents** ..... **v**
**List of Figures** ..... **vii**
**Chapter 1: Introduction** ..... **1**
1.1 Shear-wave Theory ..... 3
1.2 Near-surface applications of S-waves ..... 7
1.3 Shear-wave pitfalls ..... 11
1.4 Extended Correlation ..... 14
1.5 Love-wave inversion for surface elevation static corrections ..... 17
1.6 Problem Statement ..... 19
**Chapter 2: Data Acquisition and Analysis** ..... **21**
2.1 Site ..... 21
2.2 Geologic and Structural Setting ..... 24
2.3 Acquisition ..... 28
2.4 Standard Correlation Processing ..... 30
2.5 Shear-wave processing pitfalls ..... 62
**Chapter 3: Extended Correlation** ..... **68**
3.1 Line 1 Extended Correlation ..... 72
3.2 Line 2 Extended Correlation ..... 79
**Chapter 4: Inversion of Love waves for surface statics** ..... **86**
4.1 Line 1 surface elevation corrections ..... 87
4.2 Line 2 surface elevation corrections ..... 95
**Chapter 5: Geologic Interpretation** ..... **104**
5.1 Line 1 Interpretation ..... 106
5.2 Line 2 Interpretation ..... 113
**Chapter 6: Discussion** ..... **119**
6.1 Standard Correlation ..... 119
6.2 S-wave processing pitfalls ..... 120
6.3 Extended Correlation ..... 123
6.4 Love wave inversion and surface elevation corrections ..... 123
6.5 Geologic interpretation ..... 124
6.6 Other applications ..... 124

6.7 Future research .....126
**Conclusion .....126**
**References.....127**

## List of Figures

Figure 1. Stress vs. strain graph ..... 4
Figure 2: Incident shear-wave on ground surface. ..... 7
Figure 3: Extended Correlation ..... 16
Figure 4. Synthetic seismogram corresponding dispersion curves for Rayleigh waves and Love waves ..... 19
Figure 5. Location of Ogden and Willard Bay Reservoir ..... 23
Figure 6. Proximity map of site to the Wasatch Fault ..... 23
Figure 7. Map of the Great Basin. ..... 26
Figure 8. Shoreline of Lake Bonneville with location of the present-day Great Salt Lake shoreline.. ..... 26
Figure 9. An Ogden area rock column ..... 27
Figure 10. Location of Line 1 and Line 2 along A. V. Watkins dam. ..... 29
Figure 11. View of the waffle plate used for S-wave acquisition. ..... 29
Figure 12. Basic processing flow used for Lines 1 and 2 S-wave data for both conventional and extended correlation. ..... 32
Figure 13. Percentages of time spent on different parts of processing. ..... 33
Figure 14. Shot gather from Line 1 ..... 35
Figure 15. Shot gather from Line 2 ..... 37
Figure 16. Amplitude spectra for Line 1 ..... 38
Figure 17. Alternate amplitude spectrums of Line 1and Line 2 ..... 39
Figure 18. Line 2 shot record from Line 2 with Love waves ..... 40
Figure 19. Zoomed in shot gather from Line 2 ..... 41
Figure 20. Shot record from Line 2 showing muted data ..... 42
Figure 21. An NMO corrected CMP gather from Line 2 ..... 43
Figure 22. Line 2 CMP stack before and after statics ..... 44
Figure 23. Portion of Line 2 stacked time section before migration ..... 45
Figure 24. Portion of Line 2 stacked time section after migration ..... 46
Figure 25. Portion of Line 2 depth section. ..... 47
Figure 26. Diagram of how Lines 1 and 2 are split up for display purposes into SW and NE sections. ..... 48
Figure 27. NE portion of Line 1 stacked migrated time section. ..... 49
Figure 28. SW portion of Line 1 migrated time section ..... 50
Figure 29. NE portion of Line 2 migrated time section ..... 51
Figure 30. SW portion of Line 2 migrated time section. ..... 52
Figure 31. NE portion of Line 1 depth section. ..... 53
Figure 32. SW portion of Line 1 depth section ..... 54
Figure 33. NE portion of Line 2 depth section ..... 55
Figure 34. SW portion of Line 2 depth section ..... 56

Figure 35. NE portion of Line 1 depth section interpreted. ..... 58
Figure 36. SW portion of Line 1 depth section interpreted ..... 59
Figure 37. NE portion of Line 2 depth section interpreted ..... 60
Figure 38. SW portion of Line 2 depth section interpreted ..... 61
Figure 39. A synthetic seismograph showing only dispersive Love waves. ..... 63
Figure 40. Shot record from Line 2 zoomed in to show Love-waves and reflections ..... 64
Figure 41. A section of Line 2 with the Love-waves unmuted ..... 65
Figure 42. Frequency bandwidth for final stacked section of Line 2 ..... 66
Figure 43. Amplitude spectra of Line 2 final stacked section ..... 66
Figure 44. Shot gather from Line 2 showing harmonic distortion ..... 67
Figure 45. The self-truncating extended correlation method ..... 69
Figure 46. Shot record from Line 2 correlated using standard Vibroseis correlation ..... 70
Figure 47. Shot gather from Line 2 extended using self-truncating extended correction. ..... 71
Figure 48. Section of Line 1 extended correlation data showing low coherency. ..... 73
Figure 49. Section of the Line 1 extended correlation section ..... 74
Figure 50. Section 1 of Line 1 extended correlation stacked section ..... 75
Figure 51. Section 2 of Line 1 extended correlation stacked section. ..... 76
Figure 52. Section 3 of Line 1 extended correlation stacked section. ..... 77
Figure 53. Section 4 of Line 1 extended correlation stacked section. ..... 78
Figure 54. Shot gather from Line 2 using the self-truncating extended correlation method ..... 80
Figure 55. Shot gather from Figure 37 with high-frequency noise removed ..... 81
Figure 56. Section 1 of Line 2 extended correlation stack. ..... 82
Figure 57. Section 2 of Line 2 extended correlation stack. ..... 83
Figure 58. Section 3 of Line 2 extended correlation stack. ..... 84
Figure 59. Section 4 of Line 2 extended correlation stack. ..... 85
Figure 60. Dispersion curves examples from Line 1 ..... 88
Figure 61. Line 1 $V_S$ profile from the inversion of Love waves. ..... 89
Figure 62. MALW and MASW comparison for Line 1. ..... 90
Figure 63. Three layer model for the Vs profile for Line 1 ..... 91
Figure 64. Surface elevations in ft from station numbers 1100 to 1585 for Line 1. ..... 91
Figure 65. Surface elevation correction model for Line 1. ..... 92
Figure 66. Line 1 with surface elevation corrections applied ..... 93
Figure 67. Line 1 with no surface elevation corrections applied ..... 94
Figure 68. Dispersion curve examples from Line 2. ..... 97
Figure 69. Vs profile from inverted Love waves for line 2. ..... 98
Figure 70. MALW and MASW comparison for Line 2. ..... 99
Figure 71. 3 layer model based on Vs profile from the inversion of Love waves for Line 2 ..... 100
Figure 72. Line 2 surface elevations ..... 100
Figure 73. Surface elevation correction model for Line 2 ..... 101

Figure 74. A portion of the Line 2 stacked section that has been corrected for surface elevation statics ..... 102
Figure 75. Original stacked section with no surface elevation corrections applied ..... 103
Figure 76. Ogden area representative rock column ..... 105
Figure 77. General geologic descriptions of sediments of both lines provided by the U. S. Bureau of Reclamation ..... 105
Figure 78. Approximate location of Line 1 along the A. V. Watkins dam ..... 107
Figure 79. Geologic interpretation of Line 1 based on wells drilled by the U.S. Bureau of Reclamation ..... 108
Figure 80. Map of the Weber Delta district in relation to the approximate location of the southern portion of the Willard Bay Reservoir ..... 109
Figure 81. NE portion of Line 1 with one possible interpretation shown ..... 111
Figure 82. SW portion of Line 1 with one possible interpretation shown ..... 112
Figure 83. Location of Line 2 along the A.V. Watkins dam where geologic information is available ..... 114
Figure 84. Geologic interpretation of Line 2 based on wells drilled by the U.S. Bureau of Reclamation ..... 115
Figure 85. NE portion of Line 2 with one possible interpretation shown ..... 117
Figure 86. SW portion of Line 2 with one possible interpretation shown ..... 118
Figure 87. Amplitude spectra from Line 1 and Line 2 ..... 122

# Chapter 1: Introduction

Researchers in the engineering, environmental and mining branches of geophysics are highly interested in the elastic properties of the near-surface and their effects on seismic wave propagation. Important material properties such as stiffness and lithology are desired information in near-surface studies for applications in the hydrogeological, geotechnical, mineral and petroleum resources, and geo-hazard fields within the engineering, environmental and mining branches of geophysics. For some applications, shear-wave (S-wave) reflection surveys have theoretical advantages over comparable compressional-wave (P-wave) surveys, both for hydrocarbon exploration and the engineering and environmental community (Helbig and Mesdag, 1982; Tatham and Stewart, 1993). However, P-wave reflection signal is routinely easier to generate, record and process compared to S-wave reflection data, making it the preferential choice for imaging the subsurface (Tatham and Stewart, 1993).

The hydrocarbon exploration industry benefits from the acquisition of converted P-SV waves, where SV is the vertically polarized S-wave (Bansal and Gaiser, 2013; Tatham and Stewart, 1993). These benefits include lithology discrimination and rock properties determination, verification of the presence of fluids, anisotropy determination, the ability to image structure through gas saturated media, the identification and characterization of fractures and time lapse monitoring, increased resolution, and determination of depth (Bansal and Gaiser, 2013; Kendall and Davis, 1996). The hydrocarbon exploration industry's goals are generally to produce images of deep petroleum-bearing structures, characterize reservoirs by determining lithology, porosity and fluid content, and to make specific determinations for well locations. These goals make the converted P-SV wave the ideal candidate for realizing the benefits of S-waves. The downgoing P-wave travels at faster velocities than a pure S-wave, and the reflected

energy reaches recording devices as an SV-wave. This is beneficial because both P- and S-wave data are then available for determining material properties such as $V_P\backslash V_S$ ratios, material stiffness, presence of fluids, etc. In addition, if P-waves are attenuated due to the presence of pore fluids, the unaffected S-wave data is also available.

The near-surface community has been struggling with, evaluating, and improving the use of SH-waves, the horizontally polarized S-wave, since the 1990's (Hasbrouck, 1991). Near-surface characterization is becoming more and more important as population increases (Haines and Ellefsen, 2010). Increased population growth is in turn increasing demand for clean water and industrial minerals creating a need for a better understanding of the near-surface, including hydrogeological, geotechnical, mineral and petroleum resources, and geo-hazard investigations (Haines and Ellefsen, 2010). Shallow S-wave reflection surveys are capable of providing higher resolution images of the near-surface, particularly in saturated or partially saturated environments and environments where P-waves can travel up to 10 times faster than equivalent S-waves such that wavelengths of S-waves are smaller, even if S-wave frequencies are lower (Goforth and Hayward, 1992; Haines and Ellefsen, 2010). However, processing of S-wave reflection data can have inherent and devastating pitfalls and difficulties associated with the presence of coherent noise on shot records that must be overcome to avoid misinterpretation of the subsurface (Miller et al., 2001).

## 1.1 Shear-wave Theory

In the seismic method, mechanical waves are recorded after they propagate through the earth from a source to a sensor. As seismic waves move through the ground, they exert an external force on the materials that deforms the matrix of the rocks they pass through (Telford et al., 1976). These external forces oppose the internal forces of the materials, but once the mechanical force is removed, the internal forces allow the materials to return to their original state. A fluid will resist volume changes, though not changes in shape. A fluid can take on any shape, but its overall volume will not be permanently changed when transient external forces act upon it. This property of materials returning to an original size and shape after deforming forces have been removed is known as elasticity. A theoretically perfectly elastic material is one that is completely restored to its original condition after linear deformation. If a material is stressed beyond its elastic limit, some form of permanent deformation will occur and the material will not return to its original size and shape. If the deformation is small, rocks can be considered perfectly elastic without significant error. The forces that are applied externally to a body and the changes that result can be related by the theory of elasticity.

Stress on a body is defined as the ratio of the force to the area over which the force is applied (Sheriff, 2006). Stress can be normal, where the force is perpendicular to the area, or stress can be shearing, where the force is parallel or tangential to the area. If the force is neither parallel nor perpendicular, it can be broken down into normal and shear stress components. Changes in shape, called strains, occur when an elastic body is subjected to stress. Strain can also be resolved into normal strains and shearing strains.

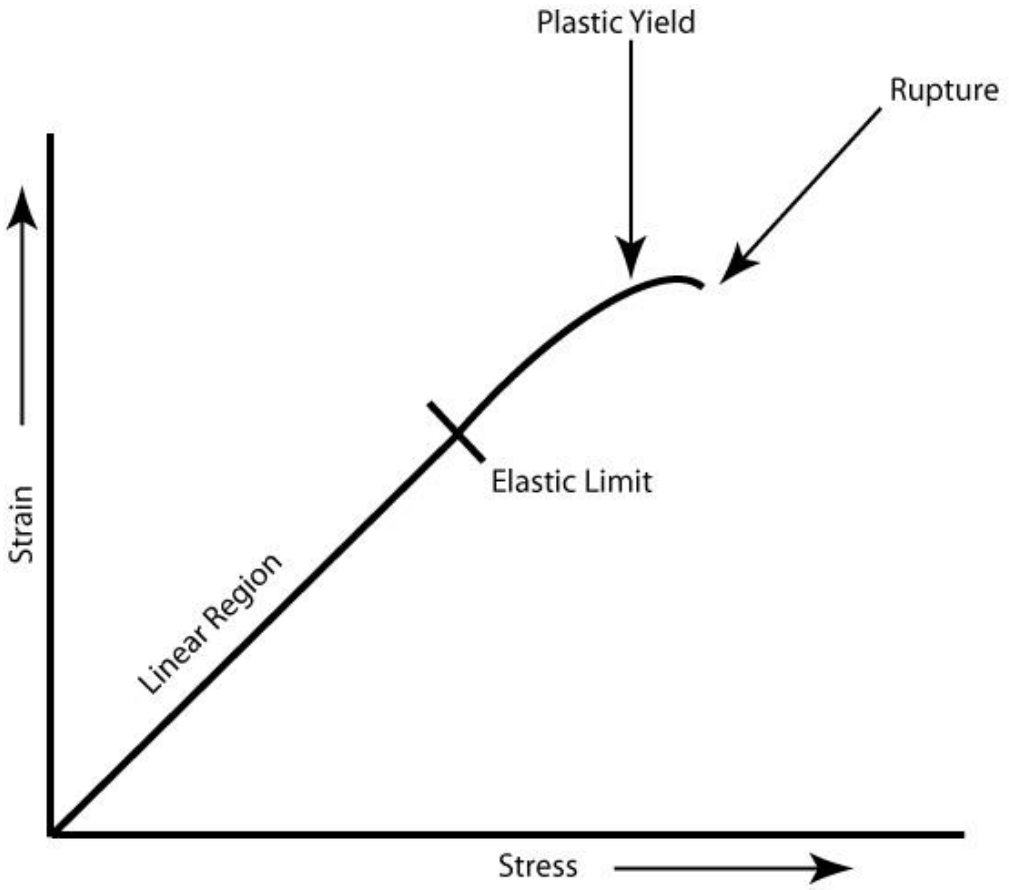


Figure 1. Stress vs. strain graph. An elastic modulus is defined by the ratio of stress to strain (Modified from Sheriff and Geldart, 1995).

An elastic modulus is defined as the ratio of stress to strain (Figure 1) (Mussett and Khan, 2000; Telford et al., 1976). The stronger the material, the higher the value of the modulus, making the strain produced by a given stress smaller. There are several types of moduli that are relevant to seismic waves. The bulk modulus ($k$), is a measure of the incompressibility of a material, or how much force is needed to change the volume of the material without changing its shape. The bulk modulus is mostly sensitive to pore material (fluids) and is defined as follows:

$$k = -\frac{P}{\Delta} \tag{1}$$

where P is the pressure and Δ is the dilatation, or the change in volume per unit volume (Telford et al., 1976). The shear modulus (μ) is a measure of the ability of a material to resist shearing, or the force needed to change the shape of a material, without changing its volume (Telford et al., 1976). The shear modulus is defined as follows:

$$\mu = \frac{\frac{\Delta F}{A}}{\frac{\Delta l}{l}} = \frac{Stress}{Strain} \tag{2}$$

where ΔF/A is the shearing stress and Δl/l is the shear displacement divide by the length of the area being acted upon by the tangential force ΔF.

For seismic waves, in general:

$$Velocity\ of\ waves = \sqrt{\frac{Restoring\ Stress}{Appropriate\ Mass}} \tag{3}$$

where the appropriate mass is the density (ρ) of a material such as rock. Longitudinal, or P-waves, cause both a change in size and shape so both the bulk modulus (*k*), and the shear modulus (μ) is involved. P-wave velocity is as follows:

$$V_p = \sqrt{\frac{k + \frac{4}{3}\mu}{\rho}} \tag{4}$$

Transverse, or S-waves, waves cause only a change in shape and no change in volume, so only the shear modulus (μ) is involved in the following equation for S-waves:

$$V_s = \sqrt{\frac{\mu}{\rho}} \tag{5}$$

The shear modulus (μ) is important to engineers for site response and material strength. This relates to basic safety characterization of buildings and structures exposed to dynamic forces such as seismic waves produced by earthquakes, wind or vibrations from manmade technology (Stumpel, 1984). High amplitudes and low frequencies from geohazards such as seismic waves from earthquakes decrease the shear modulus, which decreases a material's ability to resist the forces it is experiencing (Stumpel, 1984).

P-waves, or longitudinal waves, have particle motion in the direction of propagation. S-wave particle motion is perpendicular to the direction of propagation but can be in any direction in the perpendicular plane (Figure 2). S-wave motion can be resolved into two components of polarization. Horizontally polarized S-waves have motion parallel to the surface of the ground and are known as the SH, or horizontal component. Vertically polarized S-waves have motion perpendicular to the ground surface and are known as the SV, or vertical component. Plane polarized S-waves have either only SH, or only SV motion (Sheriff and Geldart, 1995). SH waves have particle motion parallel to a boundary and are considered autonomous in that all transmitted and reflected energy are also SH-waves, and there is no conversion at a boundary (Helbig and Mesdag, 1982; Waters, 1987). SV-waves however, can transmit and reflect SV waves, as well as generate P-waves at interfaces. SV waves can in turn be generated by P-waves at interfaces (Helbig and Mesdag, 1982).

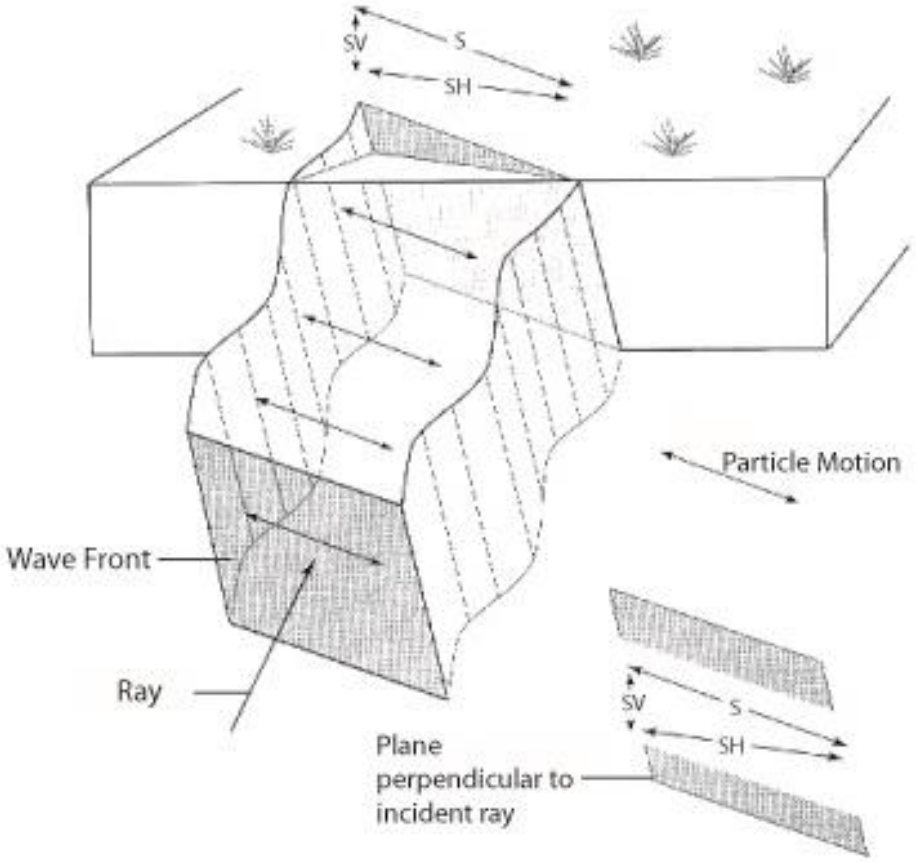


Figure 2: Incident shear-wave on ground surface. SH and SV particle motion is perpendicular to the direction of travel indicated by the ray (Modified from Burger et al., 2006).

## 1.2 Near-surface applications of S-waves

The exploration industry's goals are usually to locate hydrocarbons in sedimentary rock environments that are several hundred to several thousand meters deep (Johnson and Clark, 1992; Stewart et al., 2003). For the deeper hydrocarbon exploration targets, P-SV conversion, rather than S-S, is the most useful method for industry for a number of reasons (Stewart et al., 2003). P-SV conversion is characterized by a downgoing P-wave that is reflected and converted

at an interface and travels back to the surface as an upgoing SV-wave. Compared to S-S measurements, P-SV is relatively inexpensive, is an effective way of obtaining S-wave information, and it is broadly applicable (Stewart et al., 2003). S-wave properties relating rock type and lithology can be measured and subsurface images can be improved with P-SV analysis (Stewart et al., 2003). P-SV data has applications in the imaging of hydrocarbon associated structures and hydrocarbon saturated sediments, lithology estimation, anisotropy analysis, fluid description, and reservoir monitoring (Stewart et al., 2003).

Pure SH surveys are typically used by the near-surface community where noise suppression, polarized nature and improved resolution potential on shallow, relatively thin layers is the main goal (e.g. Bexfield et al., 2006; Guy et al., 2003; Haines and Ellefsen, 2010; Pugin et al., 2002; Pugin et al., 2007). Most conventional high-resolution seismic reflection data are P-wave (e.g. Hunter et al., 1984; Jongerius et al., 1985; Miller and Steeples, 1990). Though this method has been a useful and less complicated tool for imaging the subsurface, resolution can still be a difficulty encountered with the use of P-waves. In saturated sediments on land, sources can generally produce frequencies in the range of a few hundred Hertz (Dobecki, 1993). The equation for wavelength is:

$$\lambda = \frac{V}{F} \tag{6}$$

where $V$ is velocity and $F$ is frequency. For these subsurface conditions it is possible to achieve shorter wavelengths for the slower velocities of S-waves thereby achieving higher resolution. High-resolution does not necessarily depend on high frequency (Dobecki, 1993). Given a P-wave velocity and some dominant frequency, the wavelength will be longer than the wavelength given an S-wave velocity and the same dominant frequency (Dobecki, 1993). For example,

given a P-wave velocity of 1,500 m/s in saturated sediments and a dominant frequency of 100 Hz, a P wavelength would be around 15 m. Given the ¼ wavelength resolution criterion, resolution would be around 3.75 m. Given an S-wave velocity of around 180 m/s in saturated sediments, and a dominant frequency of 100 Hz a wavelength would be around 1.8 m. This gives a resolution of about half a meter.

S-wave energy traveling with horizontal particle motion (SH waves) has no conversion at boundaries and therefore travel the entire path from source to receiver as SH-waves (Helbig and Mesdag, 1982; Young and Hoyos, 2001). SV-waves on the other hand, can be converted to P-waves at interfaces (Helbig and Mesdag, 1982; Young and Hoyos, 2001).

Much of the P-wave seismic energy can be reflected at the water table (Haines and Ellefsen, 2010). Reflections below or adjacent to the water table can become obscured by the strong water table reflection. This does not occur when using SH polarized waves, as they are sensitive to the properties of the grain framework, and are not affected as much by the presence of pore fluids. Though S-waves are relatively insensitive to pore fluids, it is still possible to have an impedance contrast between dry materials and the water table when the materials are different, allowing S-waves to detect saturation changes and lithological boundaries within an aquifer, as well as the base of the aquifer (Stumpel, 1984).

When surface conditions consist of dry, coarse-grained or loose material, high frequency P-waves can be difficult to generate and an S-wave survey may succeed where a P-wave survey fails (Pullan et al., 1990). For partially saturated sediments and gas-containing sediments, S-waves have lower absorption than P-waves, allowing for more penetration by S-waves (Stumpel, 1984). Fractures and fault zones can be better located because S-waves can have a higher reflection coefficient than P-waves for air or water-filled cracks. Using S-waves allows the shear

modulus of fault zones to be assessed. S-wave velocities generally correlate well to properties of many lithologies. With the combination of P-wave and S-wave velocity measurements giving even more insight into lithology and material properties in the form of Vp/Vs ratio and Poisson's ratio (Haines and Ellefsen, 2010; Tatham and Stewart, 1993).

There are numerous examples of studies in the literature where S-wave reflection surveying has been successfully used for near-surface applications. The applications fall into five major categories:

- Investigations to map a bedrock surface under thick alluvium (Goforth and Hayward, 1992; Hunter et al., 1984; Pugin et al., 2013).
- Imaging of relatively shallow packages of unconsolidated saturated sediments to map and determine stratigraphy (Bexfield et al., 2006; Haines and Ellefsen, 2010; Hunter et al., 2002; Pugin et al., 2004; Pugin et al., 2007; Young and Hoyos, 2001; Carr et al., 1998; Deidda and Ranieri, 2001).
- Detecting and determining faults and fault structure, deformation due to active faults, and detection of fractures and joints (Benson and Mustoe, 1991; Wang et al., 2003; Woolery et al., 1993; Woolery and Street, 2002; Shtivelman et al., 1998; Kurahashi and Inazaki, 2007).
- Determination of geological and mechanical properties of near-surface materials for engineering purposes (Inazaki et al., 2001; Krawczyk et al., 2013; Pugin et al., 2002).
- Detecting near-surface geohazards and determining Vs structure for geohazard assessment and precautions (Benjumea et al., 2001; Guy et al., 2003; Harris, 2010; Inazaki, 2004; Krawczyk et al., 2012; von Steht et al., 2008; Inazaki, 2005).

The aforementioned studies use S-waves due to their increased resolution potential at equivalent and lesser frequencies, their sensitivity to lithology independent of pore fluid, avoiding problems associated with high reflectivity of P-wave energy at the water table, and to determine material and mechanical properties.

The literature on shallow shear-wave reflection surveys is lacking detailed information about the difficulties and pitfalls associated with shear-wave reflection processing. Miller et al., (2001), touches on some of the problems, however a more in-depth review of these issues is necessary. The resolution and detail of these reflection data provide first-time glimpses at structures and depositional features speculated on but never imaged. This study highlights detrimental processing pitfalls and difficulties that can arise when working with shallow, unreversed polarity SH data, and the need for a customized approach to provide accurate results.

### 1.3 Shear-wave pitfalls

More caution and attention to detail is required to avoid processing pitfalls with S-wave surveys, compared to P-wave surveys. The potential accuracy and fidelity of S-wave reflection profiling depends upon whether or not reflections can be clearly identified and separated from coherent noise (primarily Love waves) consistently record to record (Miller et al., 2001). In S-wave reflection profiling, reflections are not the only possible hyperbolic events with the source point apex (Kelly, 1983). Coherent noise in the form of dispersive Love waves can appear hyperbolic on shot gathers and easily stack on CMP sections resulting in incorrectly interpreted cross-sections (Miller et al., 2001). Love waves are surface waves that have a velocity of

$$V_L \approx 0.9V_S \tag{7}$$

(Burger et al., 2006), consist only of SH-motion and to propagate require the presence of a low-velocity layer overlying a high-velocity layer or sub-layer (Sheriff and Geldart, 1995). Love waves cause particle motion in a horizontal line that is perpendicular to the direction of propagation. This study reaffirms that Love waves can have a hyperbolic appearance on shot gathers (Kelly, 1983) with arrival times consistent with shallow targets and can stack coherently, leading to possible misinterpretation of the subsurface.

Other challenges in S-wave surveying include the difficulty of producing and propagating broad bandwidth S-waves, in particular, with a vibratory source (Garotta, 1999). Broad bandwidth S-waves are desired to maximize resolution in layers to resolve impedance changes. A compressional vibratory source loads (depresses) the ground with the weight of the system. Then the mass, relative to the baseplate, moves up and down vertically, allowing the Earth to rebound elastically from the depression due to preloading. This results in transmission through the earth at a peak force potential equal to its own weight (Garotta, 1999). For a compressional source, the ground force is equal to the weighted sum of the baseplate and reaction mass accelerations:

$$F_g = M_r A_r + M_b A_b \tag{8}$$

where $F$ is the ground force, $M_r$ and $A_r$ are the mass and acceleration of the reaction mass respectively, and $M_b$ and $A_b$ are the mass and acceleration of the baseplate respectively (Wei et al., 2010). Decoupling with a compressional vibrator occurs when the weight holding the base plate down is exceeded by the ground force (Schrodt, 1987). Decoupling can produce harmonic distortion, which arises from a nonlinear process, and is observed when frequency-modulated

mechanical vibrators are overdriven for given near-surface conditions on land (Seriff and Kim, 1970).

S-wave vibrators also load the ground using the mass of the system, but attempt to move the earth in a horizontal side-to-side motion consistent with desired particle motion. Some researchers (e.g. Ghose, 2002), assume that the ground-force equation for a compressional vibrator can also be used for a shear vibrator. However, it is only possible for an S-wave vibrator to transmit a force equal to the product of its own weight and the friction between the base plate and the ground (Garotta, 1999), which raises the question of whether using the ground force equation for a compressional vibrator with a shear vibrator is appropriate. Decoupling occurs with shear vibrators when the ground force exceeds the horizontal force with frictional forces factored in:

$$M_r A_r + M_b A_b > \mu_s mg \tag{9}$$

For a mass weighing 141 kg, a baseplate weighing 168 kg, and the gravitational acceleration of 9.8 m/s$^2$, the theoretical ground force for a shear vibrator (if calculated using the ground force equation for a compressional vibrator) would be about 3,028 N. However, if the friction coefficient $\mu_s$ is equal to anything less than 1, the horizontal force will be exceeded by the ground force and decoupling will occur. Therefore, using the ground-force equation for compressional vibrators with a shear vibrator is inappropriate as the horizontal motion, friction and decoupling are not taken into account.

For P- and S-wave signal of the same bandwidth and center frequency, the resolution improvement potential of S-waves is greater based on much slower S-wave velocities in comparison to those of P-waves in unconsolidated saturated materials (Miller et al., 2001).

However, taking advantage of these slower S-wave velocities can be difficult due to the challenge of recording high dominant reflection-frequency S-wave data that does not suffer from excessive attenuation. Narrow bandwidth and low signal-to-noise ratio is a recognized problem with S-waves. These issues can inhibit the greater resolution potential and contribute to processing challenges such as frequency filtering narrow bandwidth data, thus reducing the bandwidth further. Other problems that can arise are having signal and noise with the same dominant frequencies, and enhancement of near-offset Love waves arriving within the noise cone with velocity filtering. As evidenced in this study and in Miller et al., (2001), the accurate separation of reflections from Love waves within the first several hundred milliseconds is difficult because of the hyperbolic shape and because of geologic settings consisting of loose, unconsolidated material where the velocity changes very minimally with depth.

### 1.4 Extended Correlation

Based on the listen time used to record these uncorrelated Vibroseis S-wave data, the slower than expected velocities meant desired depths were not reached using conventional correlation approaches to form the seismic record. Extended Vibroseis correlation is typically used when exploration-scale seismic data is used to illuminate deep basement or mantle information at a regional or crustal scale (Allmendinger and Zapata, 2000; Best, 1991; Okaya and Jarchow, 1989). This extended correlation approach has never been documented in the literature with near-surface data. This study provides an example of the effectiveness of using this technique on near-surface data to obtain the returns from deeper reflections. It is clear this

can be a practical technique for near-surface applications from time-depths of interest being deeper than expected to a lack of previous seismic studies and velocity structure to guide survey design. This can result in acquired data that do not meet the depth objectives. Though general lithology information may be available, material velocities can vary considerably, especially in the near-surface (Zimmer et al., 2007).

There are two types of extended Vibroseis correlation: the fixed-bandwidth method and the self-truncating method **(**Figure 3**)**. Fixed-bandwidth extended Vibroseis correlation truncates the sweep to simulate a longer listening time (Okaya and Jarchow, 1989). Self-truncating extended correlation truncates the sweep to a length equal to the time remaining at each sample beyond the listen time (Okaya and Jarchow, 1989). Bandwidth is better preserved as it gradually diminishes with extra correlation time with the self-truncating method. Prior to the extended listen time, bandwidth is maintained as in standard correlation, so this method can be applied without sacrificing resolution within the original listening time (Okaya and Jarchow, 1989).

To use an extended correlation method, the original uncorrelated field data must be available. Typically it is suggested that upsweep data should be used for extended correlation because frequencies in the later portion of the sweep are attenuated and generally do not penetrate to the maximum target depth (Okaya and Jarchow, 1989). This attenuation with depth means reflections from deeper depths have lower frequencies, and therefore correlating a truncated downsweep would eliminate those critical lower frequencies (Okaya and Jarchow, 1989). No studies have been published on the use of a downsweep with extended correlation.

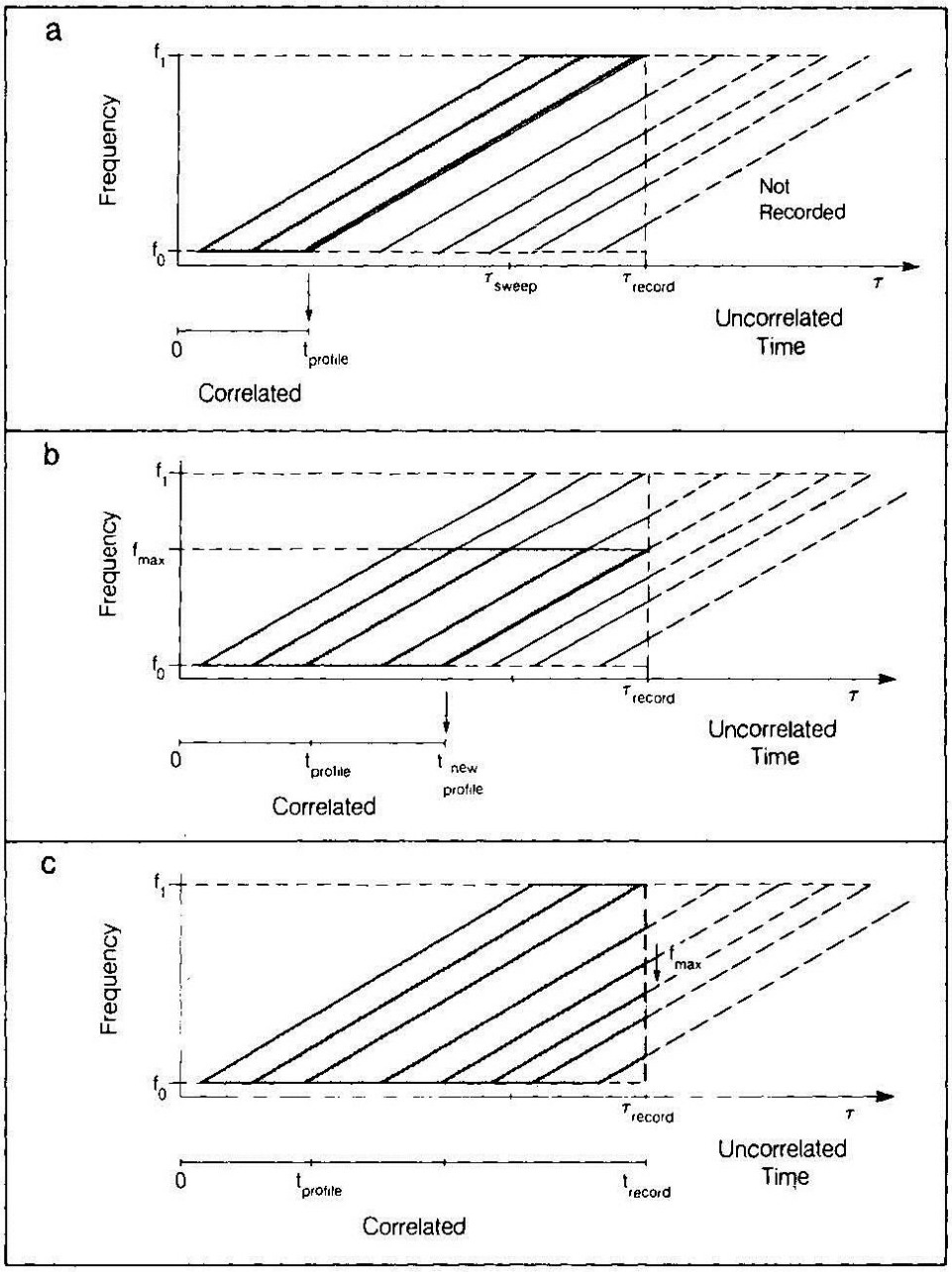


Figure 3: a. Conventional Vibroseis crosscorrelation. b. The fixed-bandwidth extended correlation method where the sweep frequencies are truncated and the record is extended. c. The self-truncating method whereby the correlation operator truncates on its own (From Okaya and Jarchow, 1989)

### 1.5 Love-wave inversion for surface elevation static corrections

Compared to P-wave statics, S-wave statics can be difficult, especially in saturated sediments, because S-wave velocity in near-surface inhomogeneous materials have greater variability than P-wave velocities, and shear velocity is less affected by the water table (Garotta, 1999). For these reasons shear statics can have much larger variations relative to compressional statics. Many studies (Park et al., 1999; Xia et al., 1999) use the MASW (multi-channel analysis of surface waves), which employs Rayleigh waves (the result of interfering P- and SV waves) to determine near-surface S-wave velocity structure. This very shallow velocity function might be used in correcting for surface elevation statics. Since the S-wave reflection data collected in this survey are in the SH orientation, MASW in determining near-surface velocity structure and surface statics would not be appropriate because of its SV orientation.

With the SH polarized data comes Love waves, making MALW (multi-channel analysis of Love waves) an ideal candidate for use with this SH reflection data. No examples could be found in the literature of the inversion of Love waves being used in the near-surface community for shallow S-wave velocities and static corrections, despite Love wave inversion being more stable in theory with less non-uniqueness than Rayleigh wave inversion (e.g. (Mari, 1984; Safani et al., 2005; Safani et al., 2006; Xia, 2009; Xia et al., 2010; Xia, 2009). This may be in large part because the acquisition of SH wave data is more difficult than acquiring vertical component surface wave data (Xia, 2009).

The MALW method (Xia et al., 2010) requires the same three general steps used in MASW; collection of surface wave data, dispersion curve image creation and inversion (Park et al., 1999; Xia et al., 1999). Since the use of raw uncorrelated field data is preferred for multi-channel analysis, swept sources such as Vibroseis are the ideal source choice (Park et al., 1999;

Xia et al., 1999). In MASW/MALW surveys, data are collected using the same basic field configurations and acquisition routines as CMP P- and S- reflection surveys (Park et al., 1999; Xia et al., 1999). Therefore, the Love waves acquired as part of this data set (with a Vibroseis source) should be ideal for the MALW process.

The next step, and one of the most critical in MALW processing, is the generation of a dispersion curve, which is later used to generate the $V_S$ profile (Park et al., 1999; Xia et al., 1999). Dispersion curves for Rayleigh waves and Love waves differ in appearance (Figure 4). Surface waves by their very nature are dispersive, meaning each frequency increment has a different phase velocity. This dependence results in different wavelengths at each frequency that is propagated (Park et al., 1999; Xia et al., 1999). Dispersion curves are displayed as phase velocity versus frequency, and analysis involves picking by the user before the data inversion portion.

An iterative inversion process is used to calculate the $V_S$ profile from the dispersion curves (Park et al., 1999; Xia et al., 1999). An initial earth model, consisting of velocity (in the MALW case only S-wave velocity), density, and thickness parameters is the starting point for the iterative inversion process (Park et al., 1999; Xia et al., 1999). When inversion is complete, a model for surface-elevation statics can be created based on the $V_S$ profile. Average velocities for each layer can be used for elevation corrections.

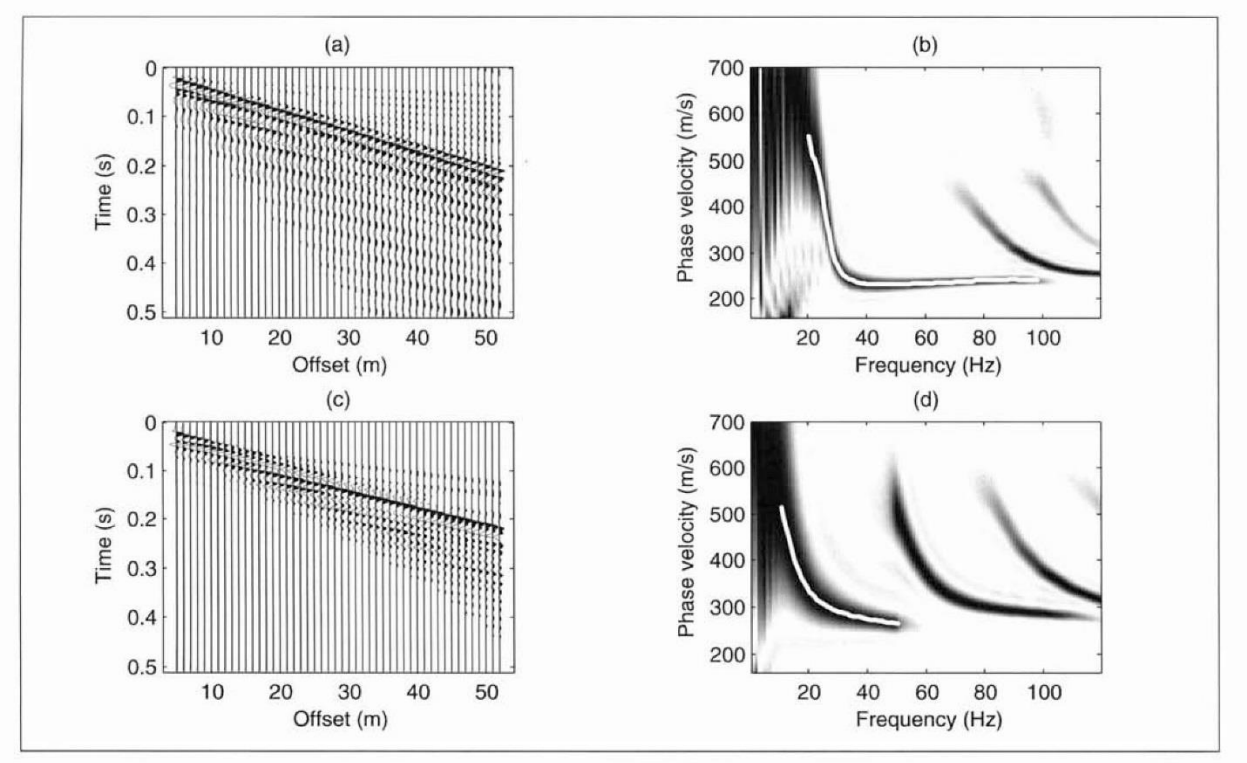


Figure 4. Synthetic seismogram (a) and corresponding dispersion curves (b) for Rayleigh waves and synthetic seismogram (c) and corresponding dispersion curves (d) for Love waves (From Safani et al., 2006).

## 1.6 Problem Statement

Two lines of S-wave reflection data were collected using a vibratory shear source and SH-oriented geophones at a dam site near Ogden, Utah. These data were collected as part of a site-characterization project focusing on a man-made dam in a high-risk seismic zone adjacent to a large active fault. As part of a large seismic program principally S-wave data were collected to obtain a high-resolution S-wave seismic sections and $V_s$ structure of Quaternary sediments adjacent to the dam. These data were used to aid in locating any unknown faults and to predict the mechanical material behavior in the presence of a range of ground motion. This study

provides information on the $V_s$ structure at the site and identifies previously unknown faults in the Quaternary sediments.

Shallow SH-wave studies have provided high-resolution images of the near-surface for a number of different applications, as previously referenced in the introduction. However, there is little information in the referenced literature about the many pitfalls and difficulties of processing the range of data recorded for these different applications, especially as it relates to coherent source noise. Additional pitfalls are associated with narrow bandwidth filtering and having signal and noise with the same dominant frequencies. Near-offset Love wave higher modes arriving within the noise cone with apparent velocity consistent with reflections represent understudied problems potentially under-addressed in previous studies.

The processing of the S-wave data at this site has been riddled with difficulties. As evidenced by these data, Love waves with a hyperbolic appearance on shot records can easily be CMP stacked and then misinterpreted as reflections, masking the true reflections and worse yet provide inaccurate appraisal of geohazards. In addition, power lines were present at the site along one line resulting in electric and mechanical noise in these data. Harmonic distortion caused by decoupling of the base plate from the Earth can also be seen in some of the shot records resulting from the nature of the vibratory source used to produce S-waves, the variability of ground coupling, and the drive producing the ground force (Reust, 1995). Data presented here demonstrates why extreme caution must be taken when separating true reflecting events from coherent noise and the detail necessary to produce accurate images and that despite narrow bandwidths and various noise sources, the collection and processing of this type of data provides valuable information for site characterization.

The S-wave velocities recorded at this site were slower than expected, resulting in the listen time being too short. Therefore desired depths were not obtained using conventional Vibroseis correlation. The extended Vibroseis correlation technique was used as a possible remedy to this problem. The literature available on extended Vibroseis correlation lacks examples where the technique has been used in near-surface situations. A bonus coming from this study is that the use of extended Vibroseis correlation on near-surface data was not only possible, but useful.

While the use of inversion of Love-waves for near-surface velocity structure and surface elevation static corrections is not an often used procedure in the near-surface community, this study shows the benefit and the potential of using this technique with SH reflection data.

# Chapter 2: Data Acquisition and Analysis

## 2.1 Site

A.V. Watkins Dam is located in Box Elder County, 12 miles northwest of Ogden, Utah (Figure 5). Information on the state of the dam foundation is needed to appraise if the dam structure is in need of repair. Prior seepage and leakage within the foundation and the embankment have increased the probability of dam failure if the dam is modified for increased capacity. Failure has the potential to result in uncontrolled release of reservoir waters and could lead to the loss of life.

The Willard Bay Reservoir is the water body retained by A.V. Watkins dam and was constructed in 1964. It has no natural drainage outlets and is used as an off-channel storage facility. The Willard Canal feeds the Willard Bay Reservoir from the Slaterville diversion dam

which is located 8 miles to the south. Water is also returned to the Weber River by way of the Willard Canal. The reservoir provides irrigation, municipal, recreational, and industrial water to heavily populated areas east of the Great Salt Lake.

A.V. Watkins Dam is an earthen structure that sits atop primarily lacustrine deposits of sand, silt and clay in the ancient Lake Bonneville basin. The dam contains over 17 million cubic yards of material and holds back the 10,000 acre Willard Bay reservoir. At its maximum height, the dam is 36 feet high and is more than 14.5 miles long. The dam has had previous near-failures due to piping and internal erosion of foundation soils, but there is also a seismic hazard from the nearby Wasatch Fault (Figure 6). There would certainly be loss of life and property damage if dam failure occurred with the reservoir at maximum capacity. A site-response model to ground movement originating from along the Wasatch Fault and associated faults is necessary to establish long-term safety requirements based on historically possible earthquakes and to determine what retrofitting is required to optimize the dam's resistance to ground motion. This study focuses on the seismic S-wave reflection data collected at this site.

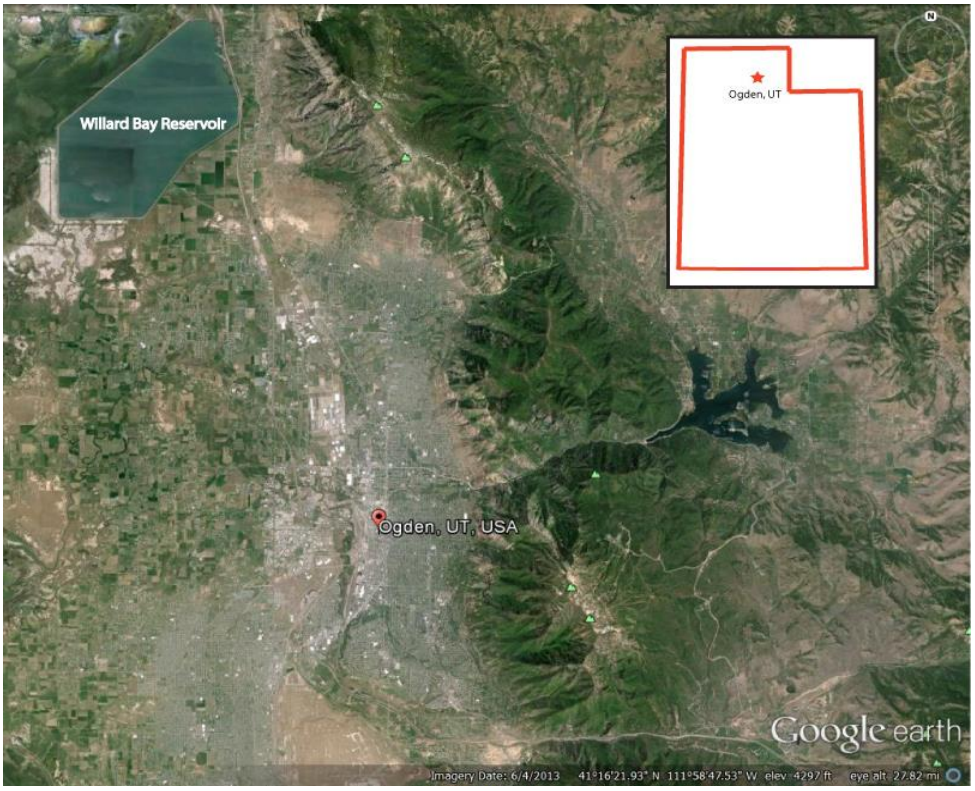


Figure 5. Location of Ogden and Willard Bay Reservoir (site) in north-central Utah.

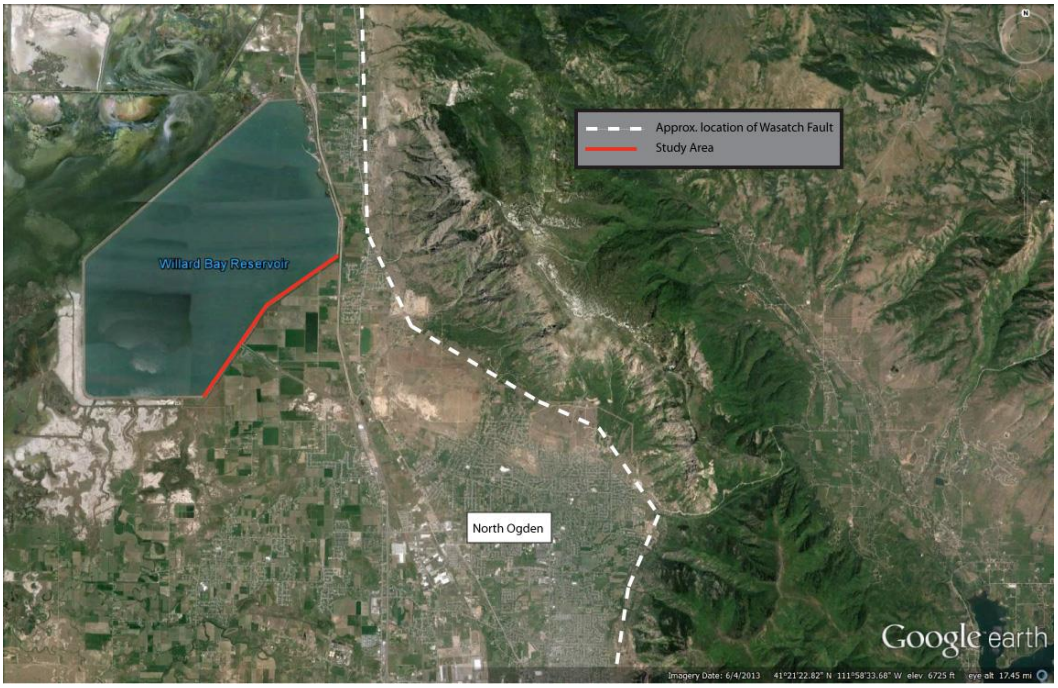


Figure 6. Proximity of site to the Wasatch Fault. Data was collected along the two lines shown.

The collection of seismic data at this site was complicated by a number of noise factors affecting data quality, including electrical and mechanical noise from nearby high-tension power lines, cultural noise from boats on the water and vehicles on an interstate highway adjacent to the site, train traffic approximately 1 mile east of the dam, as well as the source noise that is always present but whose character changes with each site.

## 2.2 Geologic and Structural Setting

The A. V. Watkins Dam and associated Willard Bay Reservoir is located in the Basin and Range physiographic province of Utah, and specifically in the Great Basin section (Banner, 1992) (Figure 7). The Great Basin of the Basin and Range physiographic province is characterized by wide, sediment-filled valleys separated by north-south trending mountain ranges (Banner, 2006). This dam site is on the eastern margin of the present day Great Salt Lake. The Great Salt Lake is a remnant of the Pleistocene fresh-water Lake Bonneville, which formed due to extensive normal faulting in the area (Eardley, 1938; Lemons and Chan, 1999). The Willard Bay Reservoir is located within the boundary of the ancient Lake Bonneville shoreline and on the eastern boundary of the Great Salt Lake (Figure 8).

Sediments that fill the basin adjacent to and underneath the site consist of hundreds of meters of Quaternary basin-fill deposits overlain by pre-Lake Bonneville Lake deposits, Lake Bonneville deposits (lacustrine sands, silts and clays), and post-Bonneville alluvium and colluvium from the nearby Wasatch Front (Pre-Cambrian crystalline rocks such as schist, gneiss, pegmatites and granites) (Eardley, 1938; Hintze, 2005). A stratigraphic column of an Ogden area rock column shows the near-surface geology to consist of a Late Eocene tuff overlain by a sequence of Pliocene-Miocene valley-fill deposits over 3000 ft thick, overlain by up to 100 ft of Quaternary alluvium and soil, and Lake Bonneville deposits (Hintze, 2005) (Figure 9).

Willard Bay Reservoir is located immediately adjacent to the active Wasatch Fault of the Wasatch Range**.** The active Wasatch fault represents a hazard with respect to the safety and stability of the A. V. Watkins Dam, particularly because this site is located on the edge of a deep sedimentary basin. This is particularly troublesome because conversion of body waves to surface waves can occur at the margins of basins and surface waves represent the source of most damage-causing ground motion (Joyner, 2000). To predict potential earthquake-induced ground motion and amplification, the near-surface velocity structure is of utmost importance, especially knowledge of $V_s$ structure (von Steht et al., 2008). Since sedimentary basins are known to amplify surface waves, contributing to strong ground motion (Joyner, 2000), and water-saturated clayey sediments are subject to intense shaking and potential liquefaction during an earthquake (von Steht et al., 2008), characterization of velocity structure and material properties at this site were needed to determine the safety of the dam and fitness for enhanced storage.


Figure 7. Map of the Great Basin, characterized by the Basin and Range physiographic province. Site location shown by red star. (Modified from Hintze, 2005).

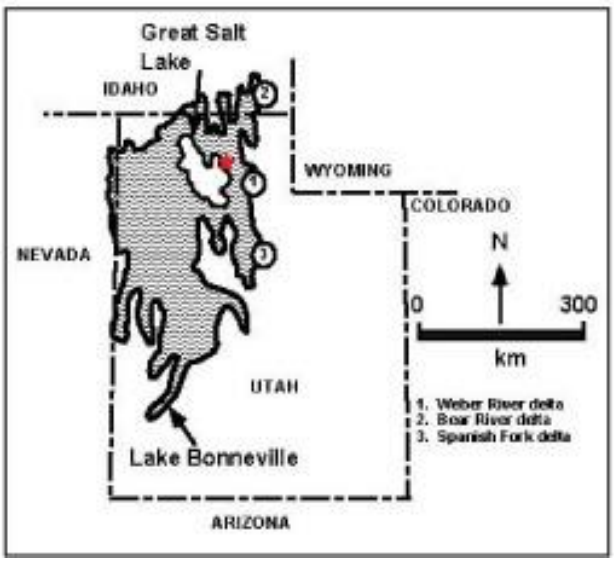


Figure 8. Highest shoreline of Pleistocene Lake Bonneville with location of the present-day Great Salt Lake shoreline. Red star indicates location of site. (Modified from Lemons and Chan, 1999).

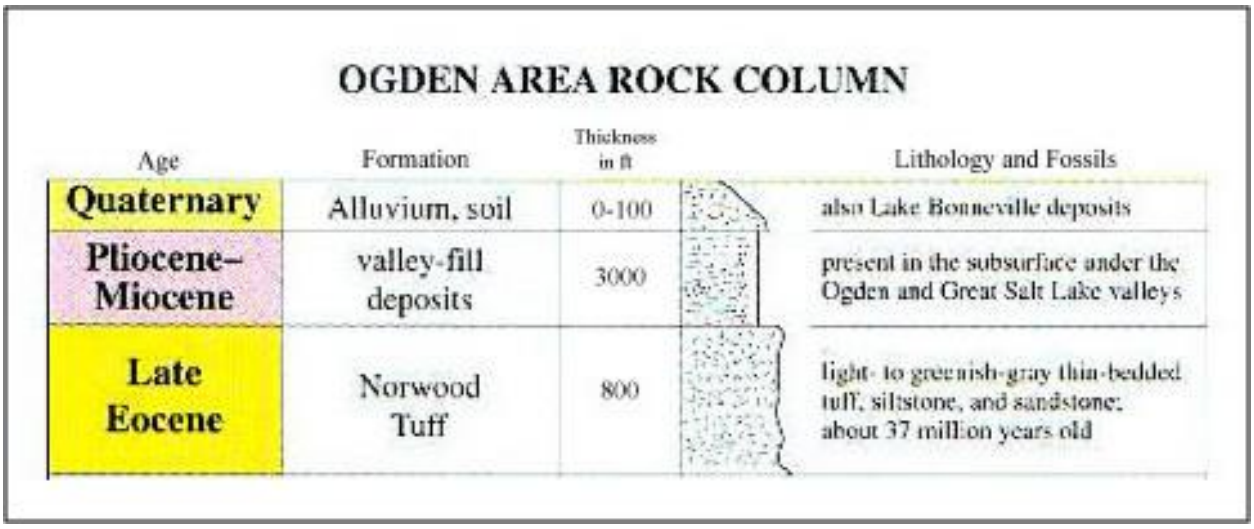


Figure 9. An Ogden area rock column. The red bracket indicated the part of the rock column that this study may image. (Modified from Hintze, 2005)

## 2.3 Acquisition

A series of seismic surveys was conducted at this site to help evaluate the risk of potential ground motion to surface structures. Acquisition was designed to image as shallowly as possible while still recording energy returning from depths of up to 3,500 ft. This required long spread lengths, long offsets, split-spread geometries, broad-bandwidth source energy, and closely spaced receiver stations. To effectively image both near surface and deeper data, four types of data were collected to optimize the accuracy and resolution, including MASW (multi-channel analysis of surface waves), tomography, and P- and S-wave reflection data. All four types of data were collected along two, ¾ mile long lines, oriented SW to NE parallel to the downstream toe of the dam structure, with a 480-channel Geometrics Geode distributed seismograph system enhanced with LTU Ethernet boosters (Figure 10).

The focus of this study is on the S-wave reflection data, which was collected with an IVI minivib 1 vibrator equipped with a waffle plate (Figure 11) that delivered a 10-second upsweep of 20-200 Hz, with a 12-second listen time. For each station, three uncorrelated and unstacked records were recorded using single 14 Hz geophones oriented to be sensitive to SH energy to optimize the resolution and signal-to-noise ratio on processed sections. Receiver and source spacing was 10 ft.


Figure 10. Location of Line 1 and Line 2 along A. V. Watkins dam.

Figure 11. View of the waffle plate with teeth used for S-wave acquisition.

## 2.4 Standard Correlation Processing

In general the common-midpoint (CMP) approach was used for the processing of both lines of S-wave data. S-wave data were processed using proprietary software of the Kansas Geological Survey, including SeisUtilities, WinSeis, SurfSeis and LWSeis. Since data was recorded uncorrelated in the field, pre-processing steps included conversion of raw data, Vibroseis whitening (Coruh and Costain, 1983), and conventional Vibroseis correlation. The basic processing flow for the S-wave data is shown in Figure 12, with percentage of time spent on the main parts of processing in Figure 13.

For standard processing, conventional Vibroseis correlation was performed using the full sweep length before any muting was done. The Vibroseis method employs a frequency-modulated source sweep to transmit seismic energy into the ground (Brittle et al., 2000; Ristow and Jurczyk, 1975). The earth sensor responses produce a wiggle trace that is recorded with the earth response and an embedded sweep that must be compressed to a zero-phase wavelet to see unique reflections from layers with different physical properties, which can be done by using cross-correlation of the synthetic sweep or pilot trace with the recorded trace (Brittle et al., 2000; Yilmaz, 1987). Cross-correlation by definition shows the degree to which two waveforms, or time series, resemble each other by determining the time lag at which they are most similar (Yilmaz, 1987).

For a swept source in the time domain, the basic convolutional model says that the recorded trace, $x(t)$, is equal to the reflectivity of the geology, or Earth's response, $r(t)$, convolved with the sweep, $s(t)$:

$$x(t) = r(t) * s(t) \tag{10}$$

where * is the convolutional operator (Brittle et al., 2000). In the frequency domain, sweep deconvolution is based on the same convolutional model and can be written:

$$X(f) = R(f)S(f) \tag{11}$$

where X(f) is the recorded trace in the frequency domain, R(f) is the reflectivity in the frequency domain, and S(f) is the sweep in the frequency domain. The sweep is removed through division (Brittle et al., 2000).

By cross-correlating the sweep with the recorded trace in the time domain, a deconvolved sweep is obtained from the following equation:

$$x_{cc}(t) = r(t) * s(t) \otimes sw(t) \tag{12}$$

where *sw(t)* is the sweep input into the ground, and $\otimes$ is the cross-correlation operator (Brittle et al., 2000). The length of the sweep subtracted from the length of the uncorrelated Vibroseis record gives the length of the resulting correlated record (Yilmaz, 1987). Standard correlation gave a record of 1800 ms in length (Figure 14).

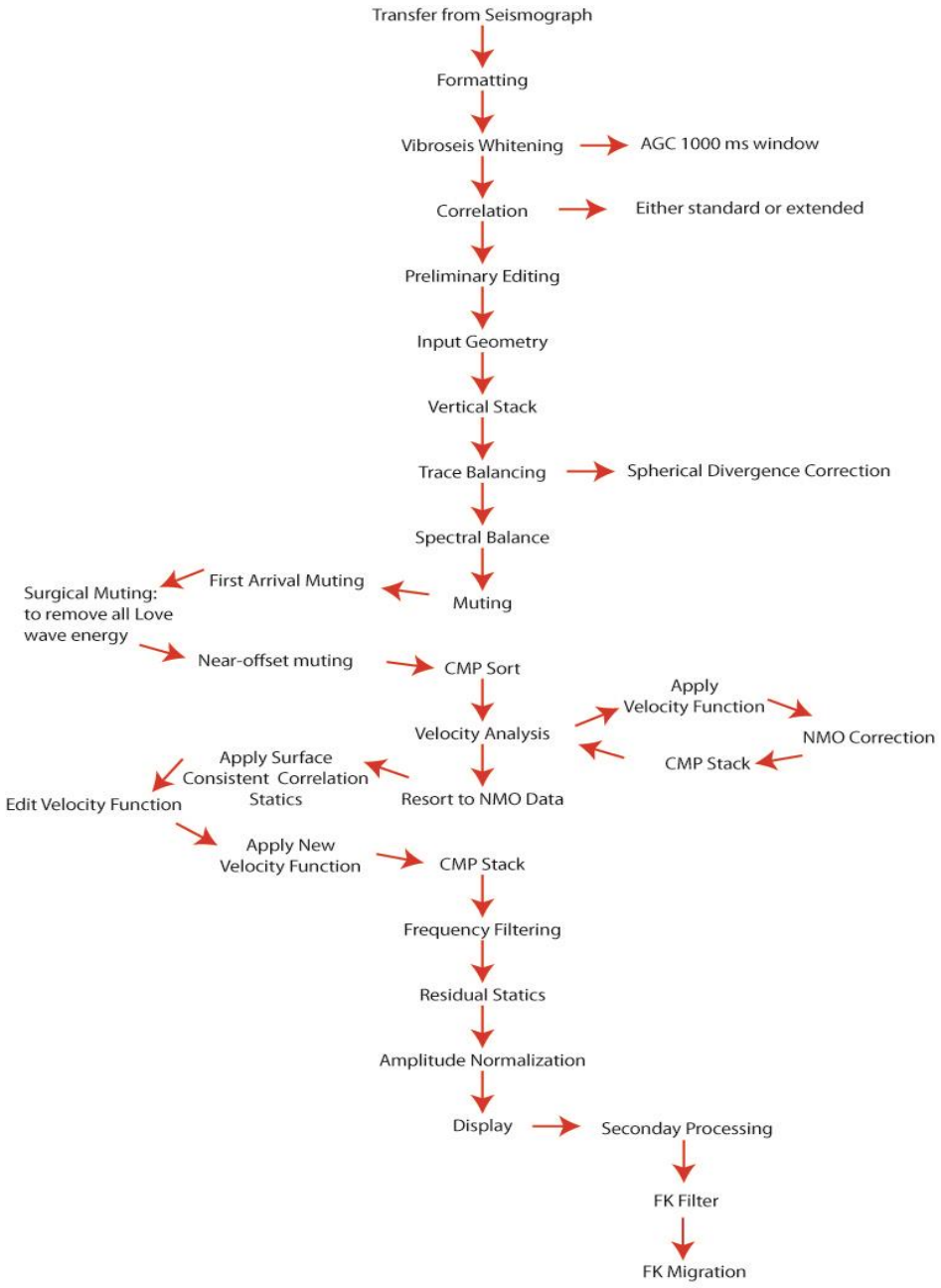


Figure 12. Basic processing flow used for Lines 1 and 2 S-wave data for both conventional and extended correlation.

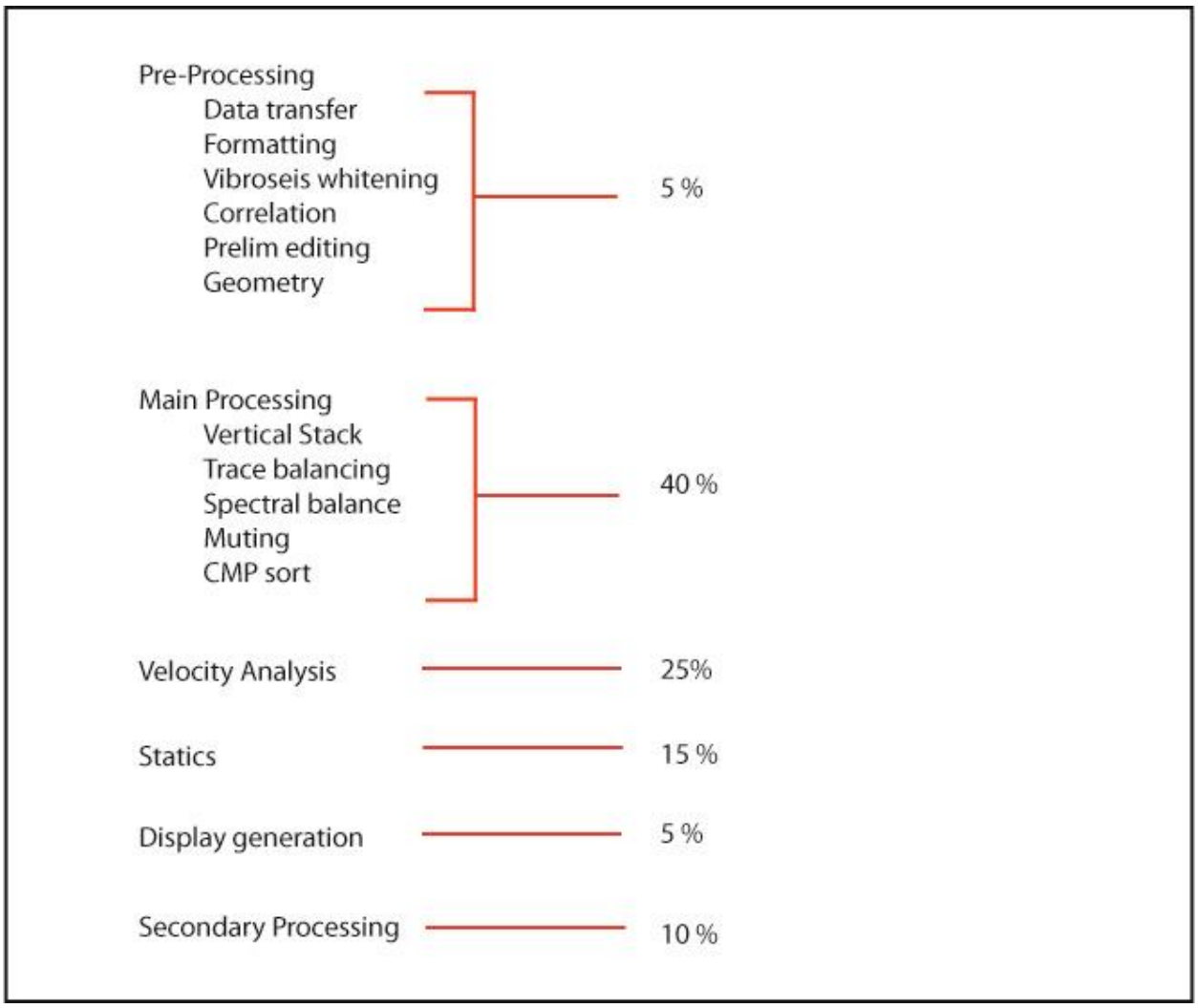


Figure 13. Percentages of time spent on different parts of processing.

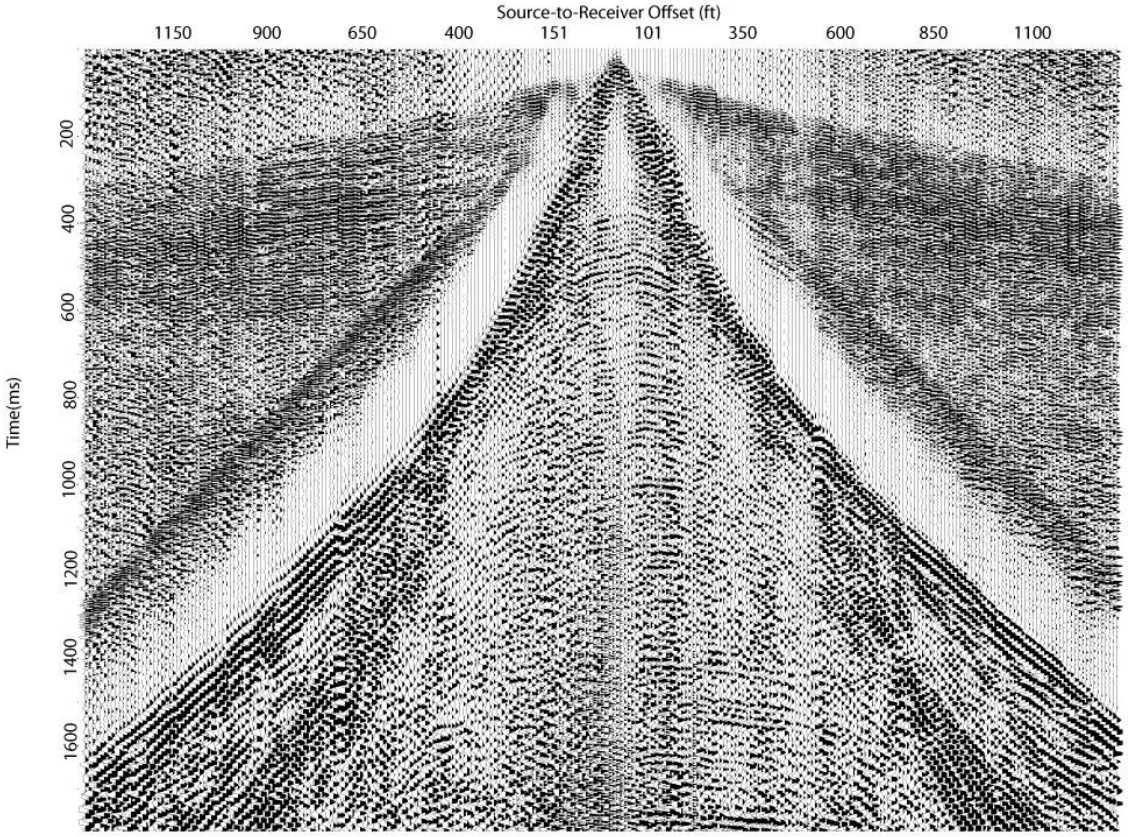


A.

Figure 14. (A) Shot gather from Line 1 with a 500 ms gain applied.

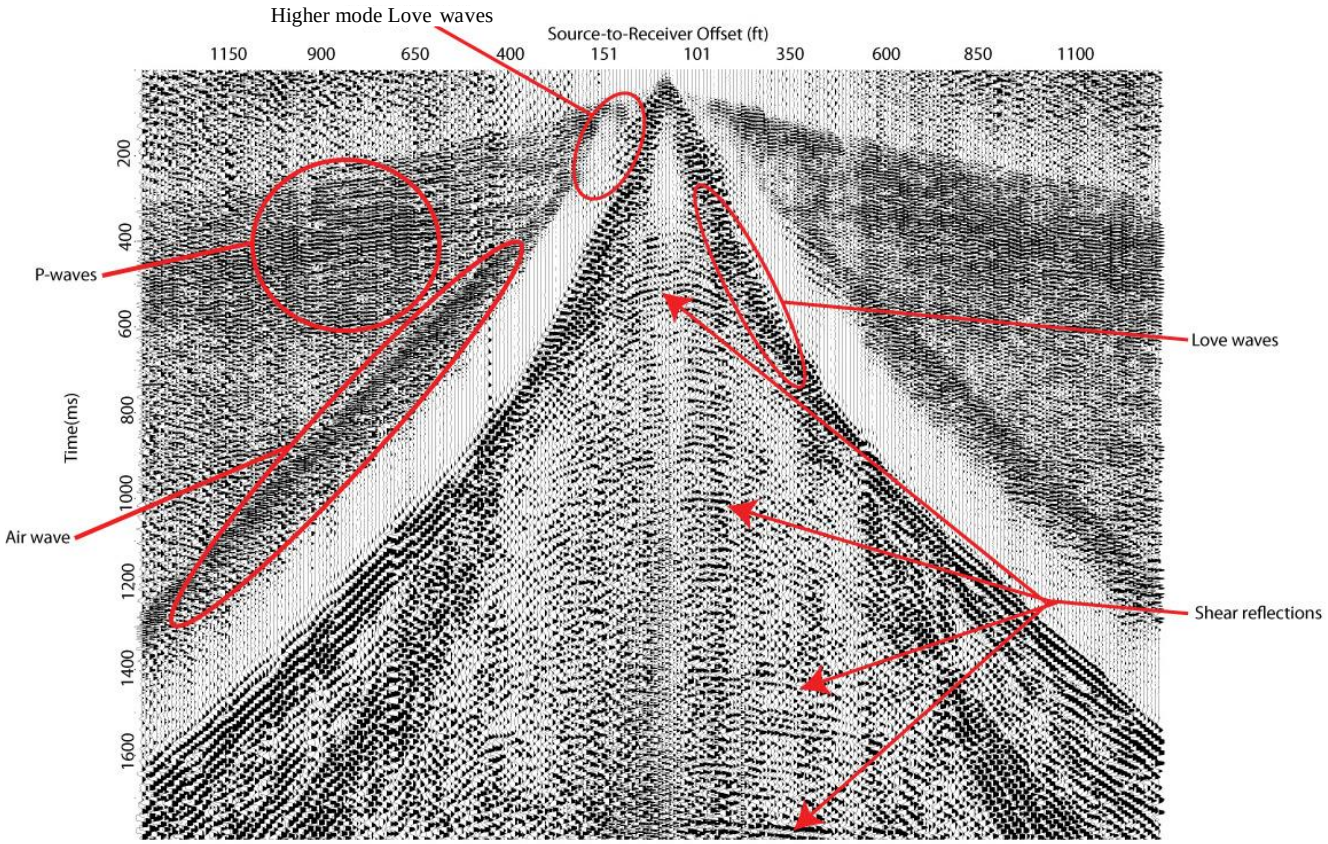


B.

Figure 15. (B) Interpreted shot gather from Line 1 with a 500 ms gain applied.

After preliminary editing to remove extra or noisy traces, the three shot gathers that were recorded at each station were vertically stacked in an attempt to cancel noise and enhance coherent reflections, thus improving signal-to-noise ratio. The quality of data is noticeably different on Lines 1 and 2. Line 1 data quality is poorer than that of Line 2 (Figure 15), in that reflections are more obscured and the data are noisier. The amplitude spectrums of both lines after correlation are shown in Figure 14. The amplitude spectrum for Line 1 shows a large quantity of random noise that has proven difficult to remove because the noise consists of many frequencies. Acquisition notes state Line 1 had a variable surface and that the vibrator pad was

rattling as data collection occurred. This is another source of noise which reduces the quality of Line 1 data below than that of Line 2.

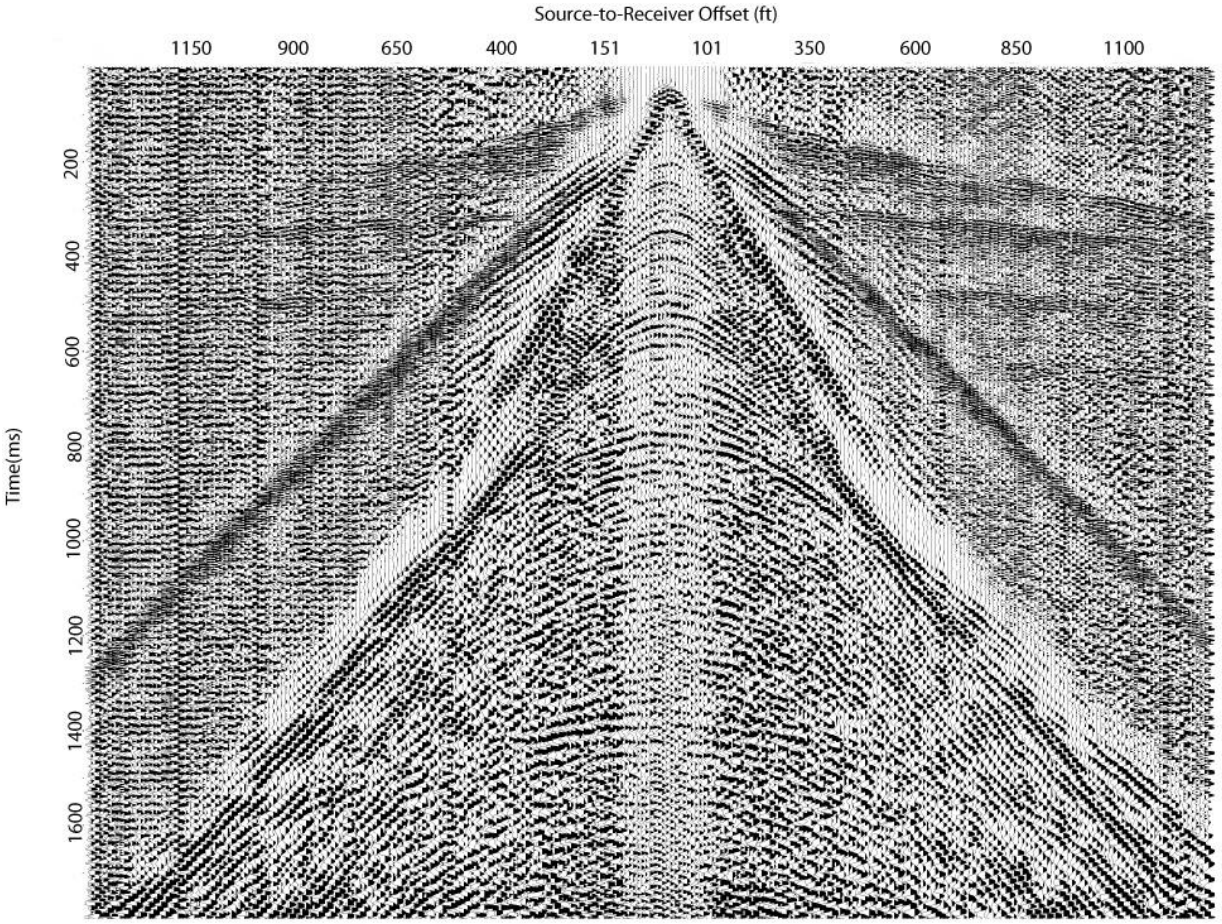


A.

Figure 16. (A) Shot gather from Line 2 with a 500 ms gain applied.

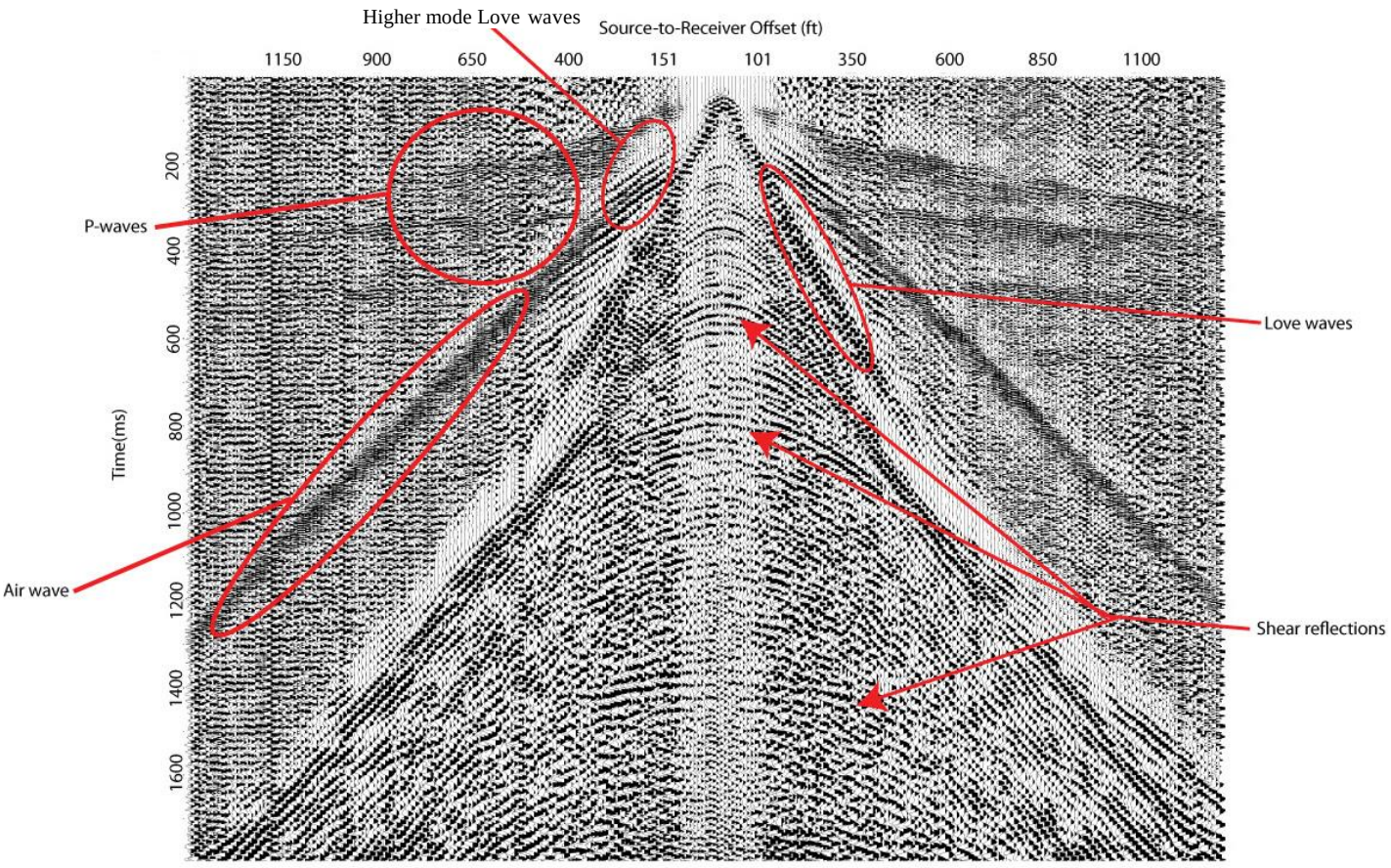


B.

Figure 17. (B) Interpreted shot gather from Line 2 with a 500 ms gain applied.

The frequency spectrum for Line 2 has noise at single frequencies, which are easy to remove with filters, while keeping the other frequencies in the signal. For example, there were power lines present on Line 2, which is the 60 Hz frequency noise in Figure 16a. The amplitude spectra for Lines 1 and 2 show noise at different frequencies on the two lines (Figure 16). Figure 17 shows an alternative plot of the amplitude spectra for both lines. Noise at different frequencies show up as show up as horizontal lines at single frequencies on these plots, as well as noise that is randomly throughout the data. Both lines 1 and 2 have a dominant frequency of

~35 Hz with minimum and maximum usable frequencies of about 22-65 Hz respectively. With velocities as low as 500-600 ft/s, this dataset has a potential vertical resolution of about 5 ft.

The presence of high-amplitude dispersive Love waves is evident on both lines (Figure 18). It can be challenging to determine where a reflection ends and a Love wave begins (Figure19), and to separate true reflections from coherent noise when dispersive Love waves are present (Miller et al., 2001).

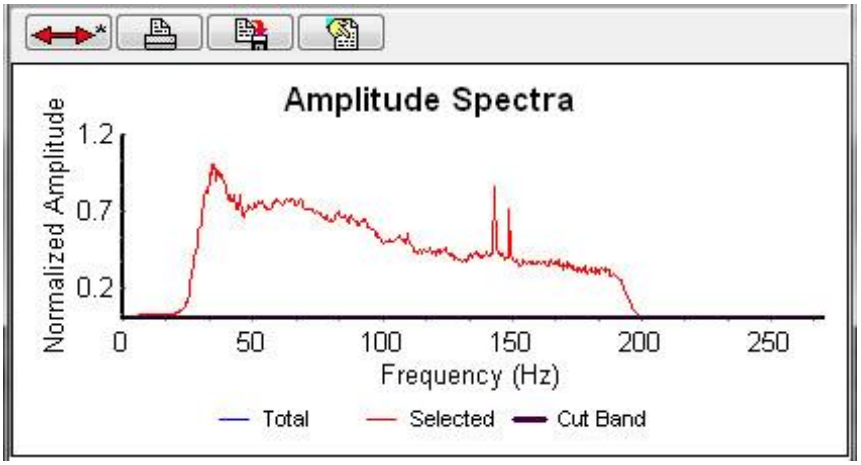


A.

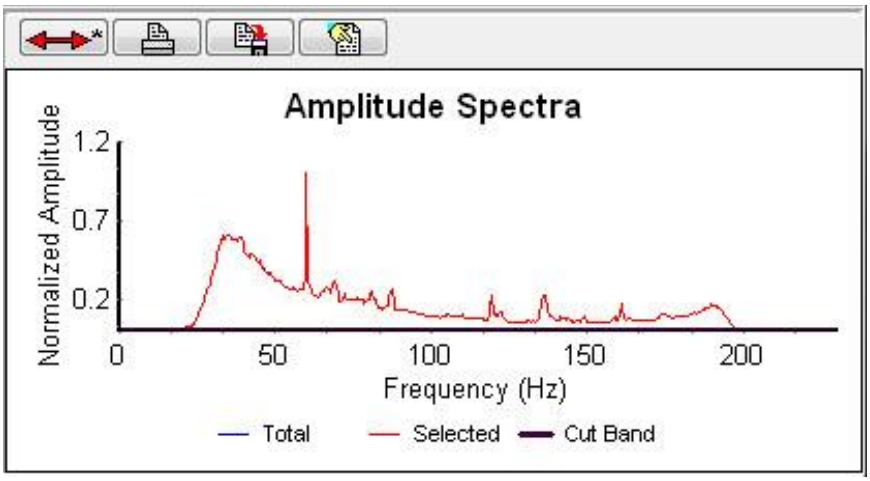


B.

Figure 18. (A) Amplitude spectra for Line 1. Spectra shows noise spikes near 150 Hz. (B) Amplitude spectra for Line 2. Spectra shows power line noise at 60 Hz

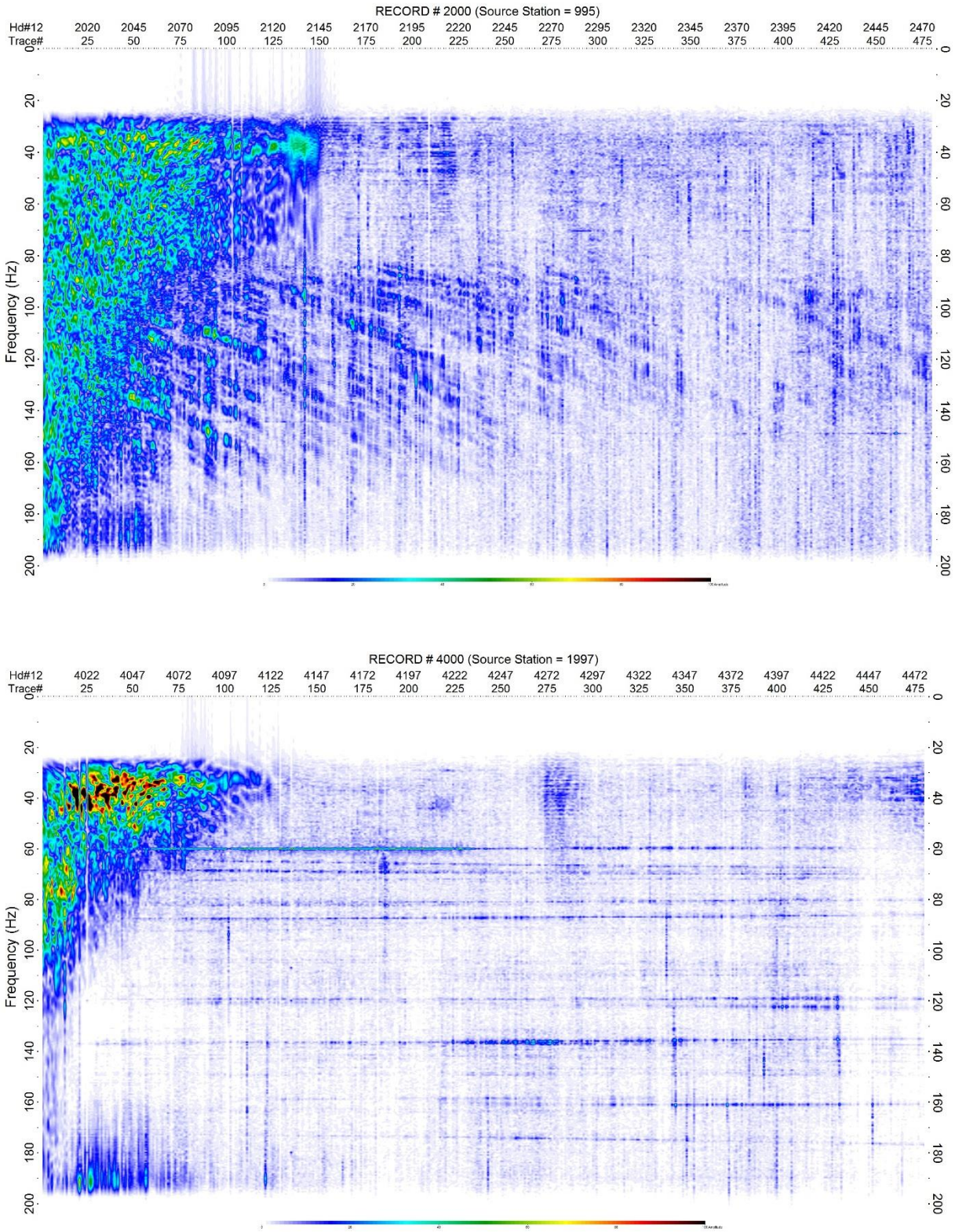


Figure 19. Alternate amplitude spectrums of Line 1 (top) and Line 2 (bottom). Line 1 contains much more random noise that is more difficult to remove than the noise at certain frequencies in Line 2.

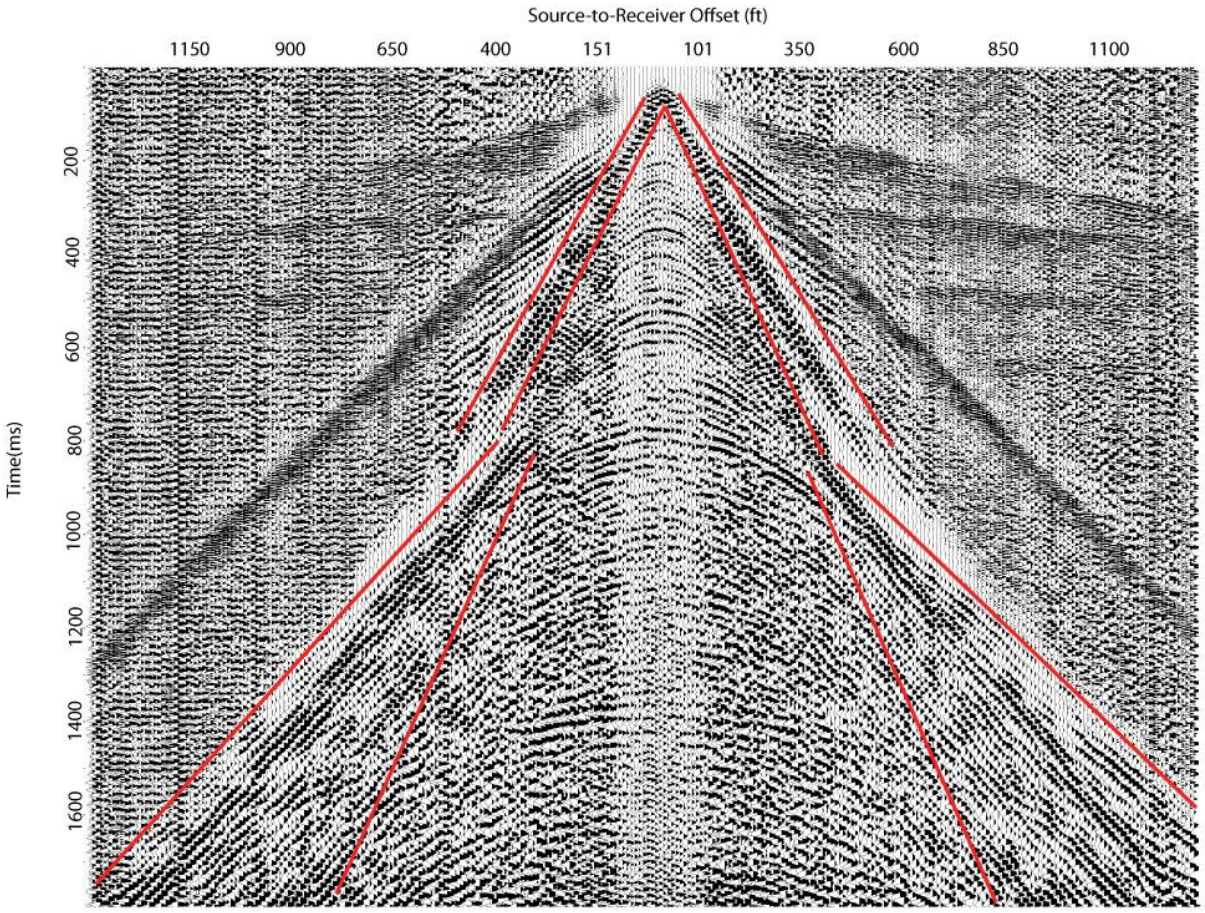


Figure 20. Shot record from Line 2 where Love waves are clearly visible in between the red lines.

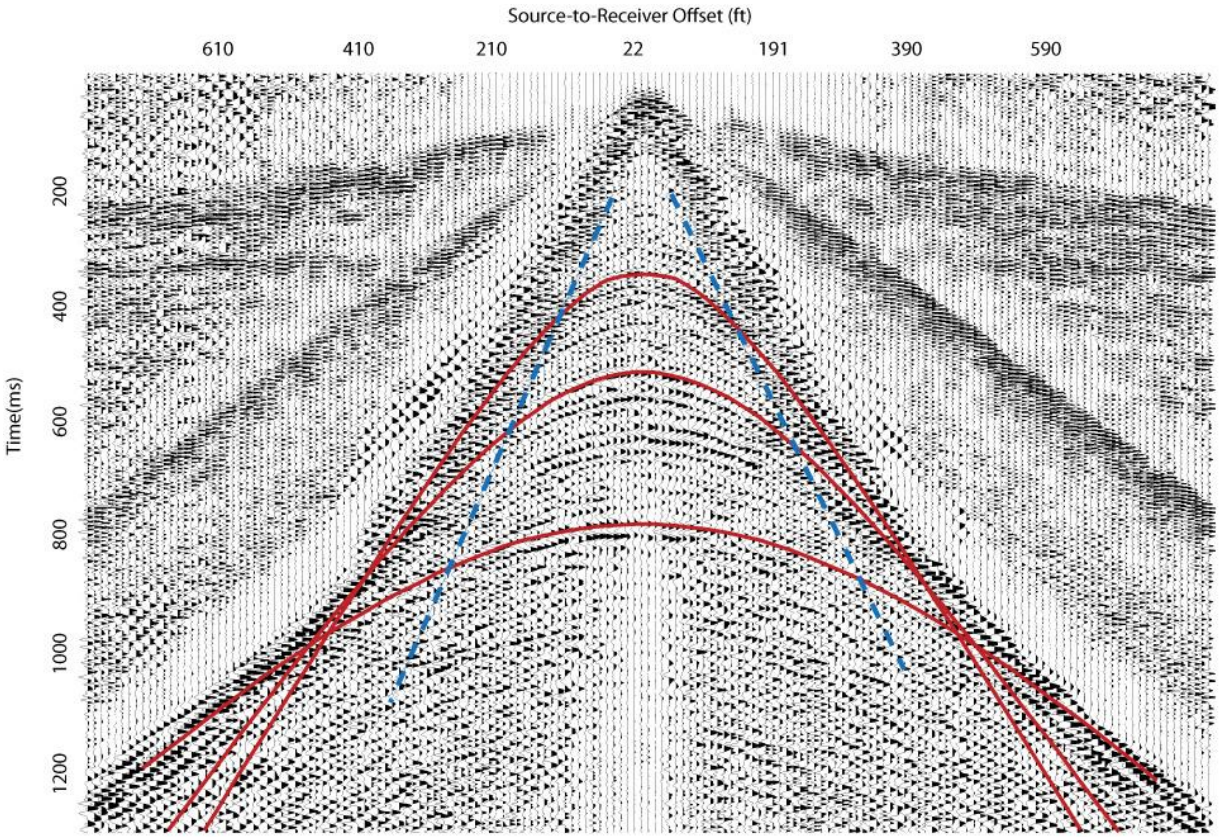


Figure 21. Zoomed in shot gather from Line 2 showing curves fit to reflections. Dashed blue lines indicate where it becomes difficult to distinguish reflections from Love waves.

First-arrival muting was used to mute everything arriving before the noise cone, including first arrivals, refractions, direct wave, P-wave reflections and Love waves. There must be a low velocity layer for Love waves to propagate with a higher velocity layer beneath it (Kelly, 1983). Careful attention was paid to mute as much of the Love waves as possible so that reflections could be clearly identified. The muted records used only 100 traces of the 480 traces recorded to minimize Love-wave data included in the stacked section (Figure 20). Near-offset mutes were also applied to the first five traces on either side of the source from 900 to 1800 ms on Line 2 data. These near-offset traces were especially noisy on many Line 2 records due to their proximity to the vibrator.

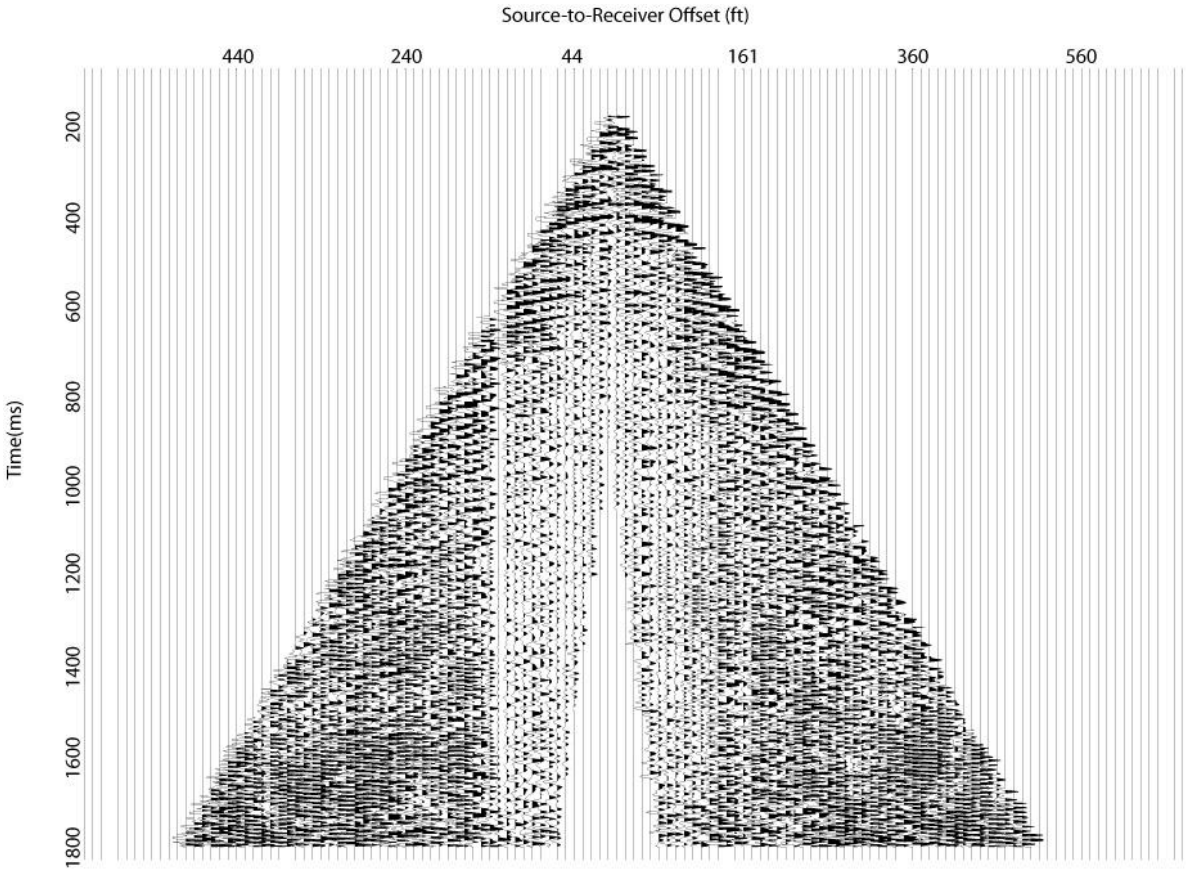


Figure 22. Shot record from Line 2 showing muted data. All linear Love-wave energy has been removed in order to prevent Love-waves from stacking into the final stacked section. Near-offset mutes from 900 to 1800 ms have also been applied to remove excessive noise.

Velocity analysis used groups of 25 CMP's to pick velocities. 11 velocity values were used ranging from 500 to 1000 ft/s in increments of 100 ft/s, and 1000 to 2000 ft/s in increments of 200 ft/s. Normal moveout (NMO) corrections were applied to CMP gathers, after scaling and frequency filtering (Figure 21). Surface-consistent correlation statics and residual correlation statics were then applied to the data (Figure 22). Once static corrections were made, velocity analysis was undertaken again, adjustments made and gathers were CMP stacked.

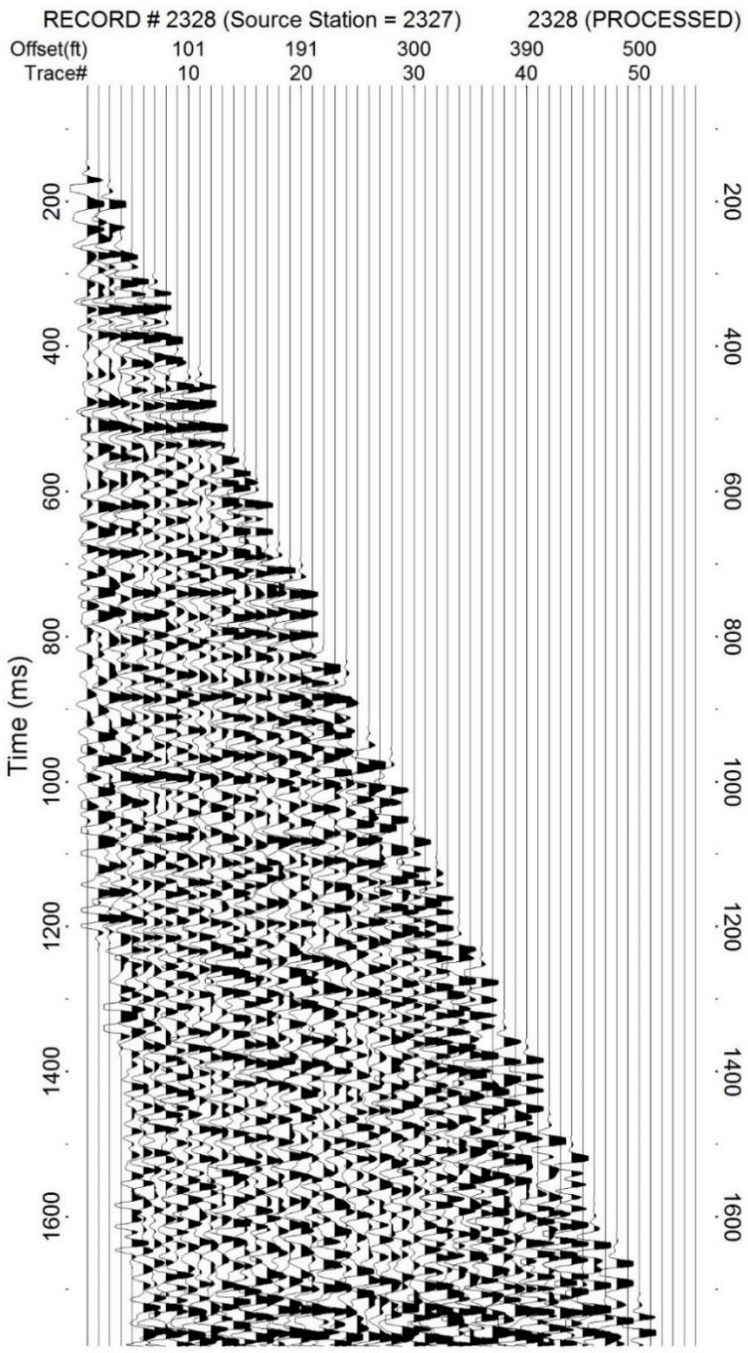


Figure 23. An NMO corrected CMP gather from Line 2 with scaling and frequency filtering applied.

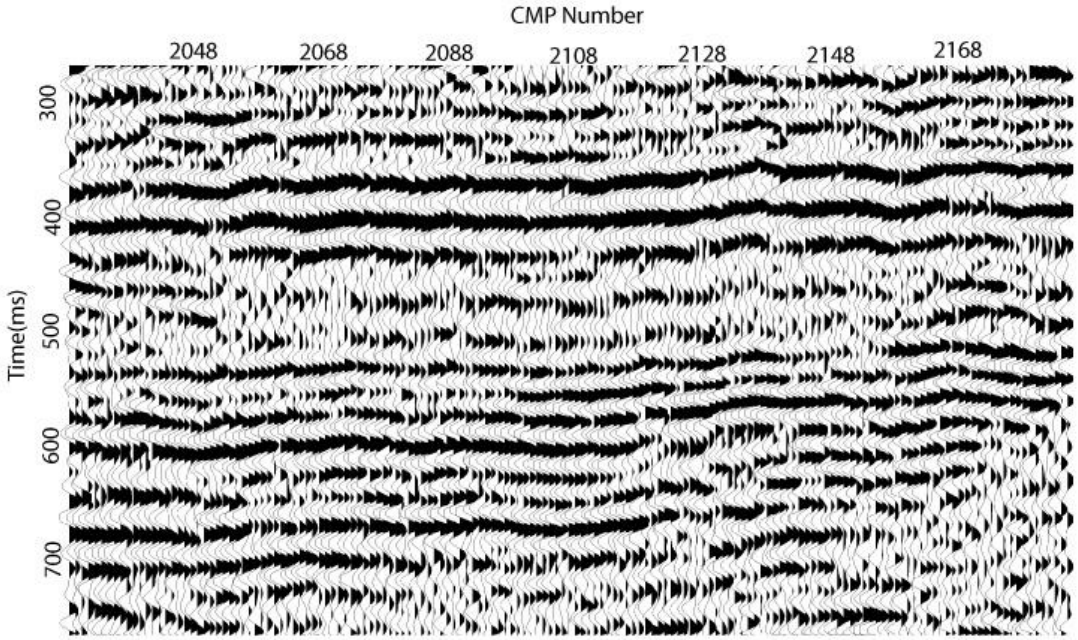


A.

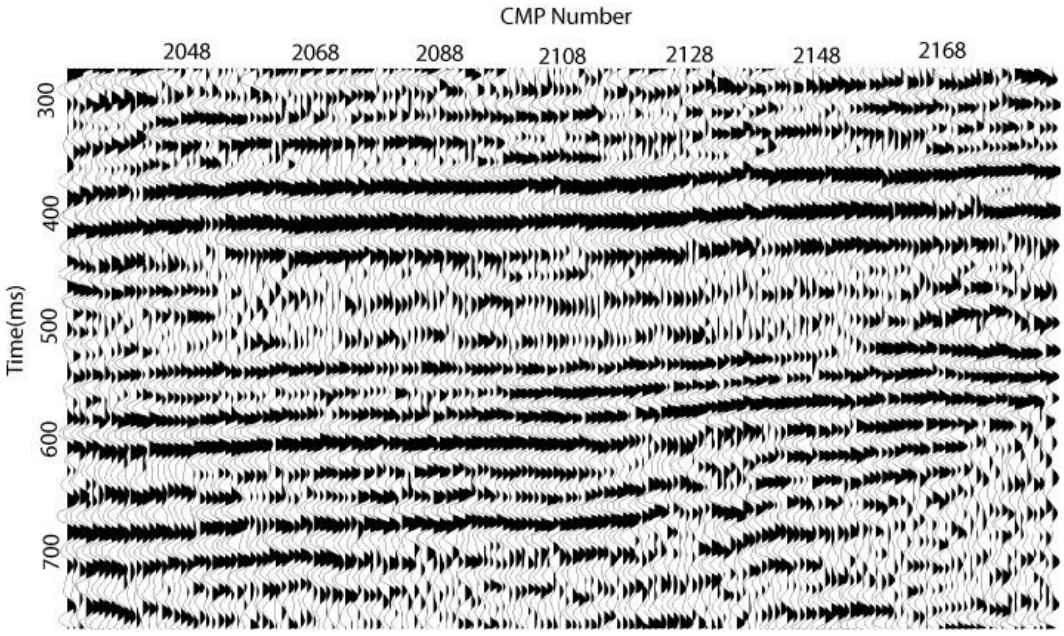


B.

Figure 24. A portion of a Line 2 CMP stack showing nature of reflectors before statics (A), and nature of reflectors after statics (B).

The CMP stacked sections were migrated to correct any dipping beds and geometric distortion caused by faulting or other subsurface variations. For high-resolution reflection data that have low near-surface velocities, migration may have a negligible effect on the appearance of reflections (Black et al., 1994). For this data set, migration did not seem to affect shallower reflections much if at all, but improved coherency of deeper reflections and spatial accuracy (Figure 23, 24). The migrated stacked sections were also time-to-depth converted. A portion of the depth converted section from Line 2 is shown for comparison to time sections (Figure 25).

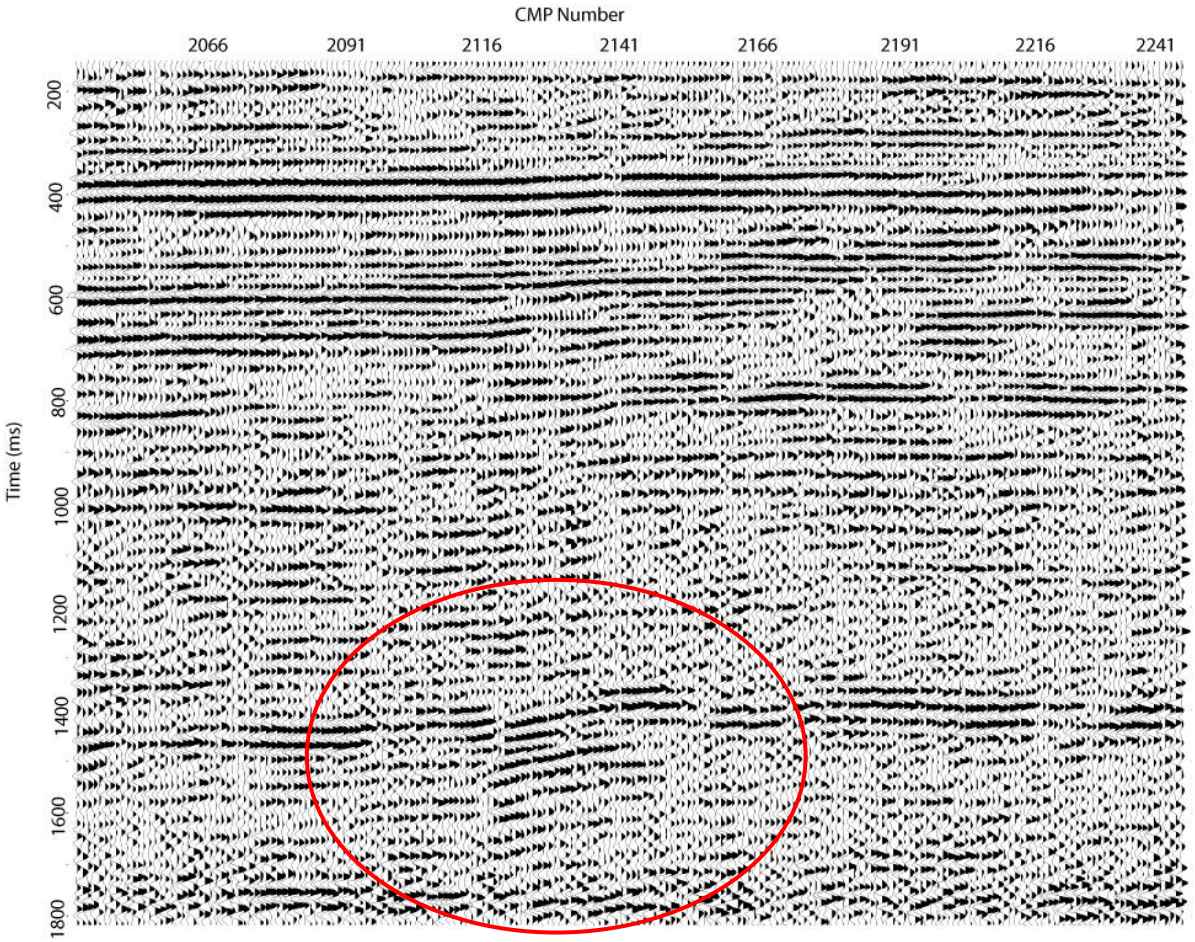


Figure 25. Portion of Line 2 stacked time section before migration. Diffraction hyperbola can be seen in the red circle.

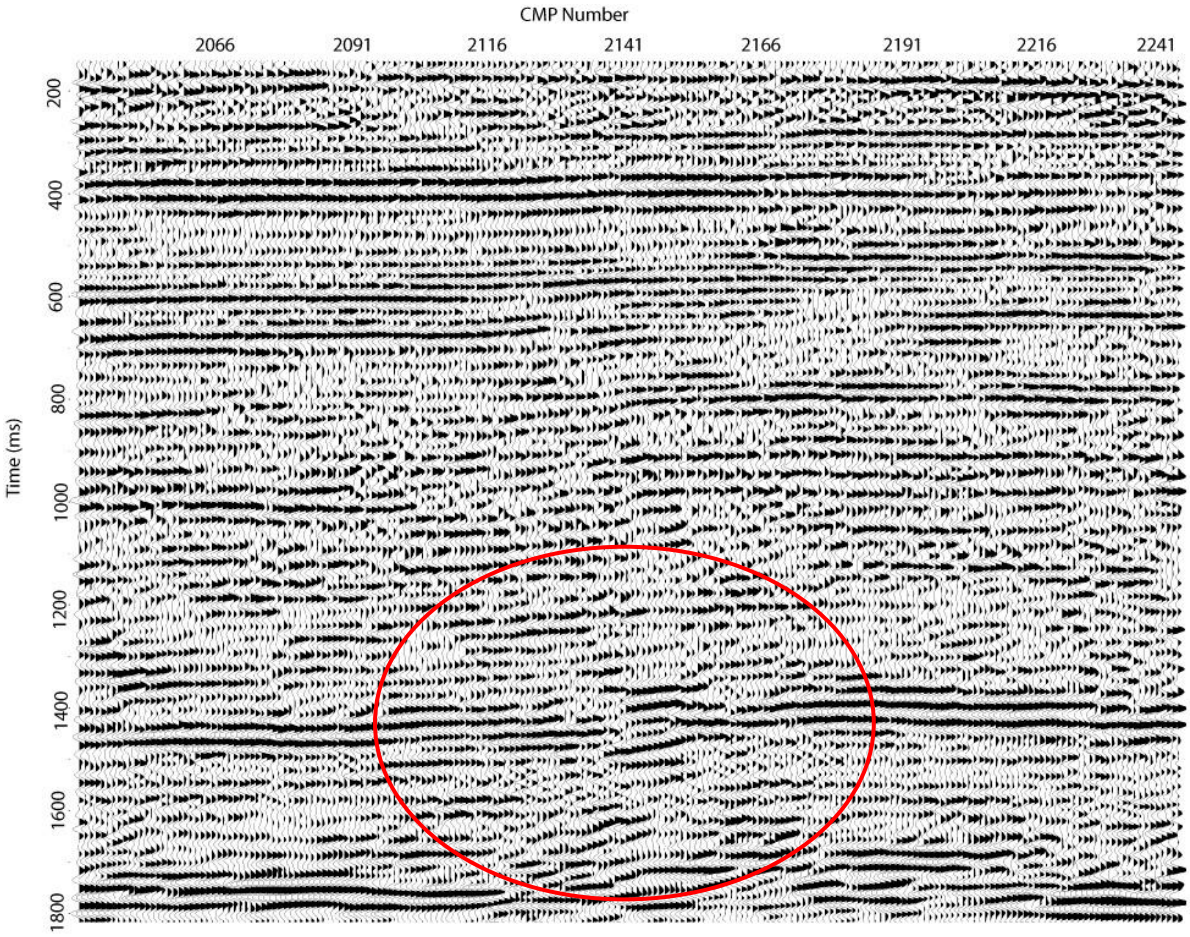


Figure 26. Portion of Line 2 stacked time section after migration. Diffraction hyperbole are removed and deeper reflectors are enhanced.

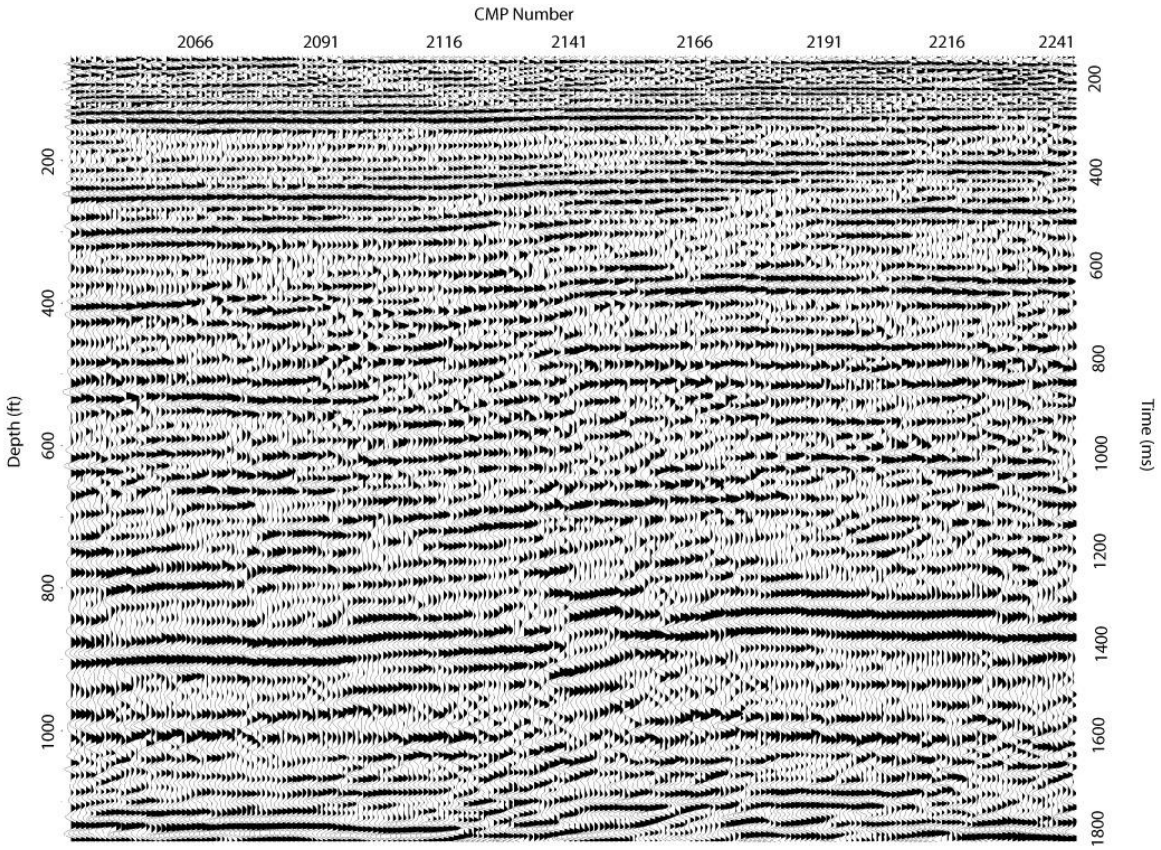


Figure 27. Portion of Line 2 depth section.

For display purposes the final stack results are split into 2 sections per line due to the length of the lines. The orientations of the lines are roughly SW to NE, so they are split into a SW named portion and NE named portion (Figure 26). The NE portion of Line 1 is shown first (Figure 27), followed by the SW portion (Figure 28). Reflections in the Line 1 stacked sections lack coherency across the entire section and data quality is relatively poor. Structures are difficult to identify due to the poor quality of the data. The NE portion of Line 2 (Figure 29), followed by the SW portion (Figure 30). The data quality of Line 2 is better than that of Line 1, and many reflections are coherent events across the section. Structural features, such as faults and folds are also evident in the Line 2 stacked sections.

On Line 1 depths of around 1,000 ft were obtained (Figure 31, 32), while on Line 2 depths of around 1,100 ft were obtained (Figure 33, 34).

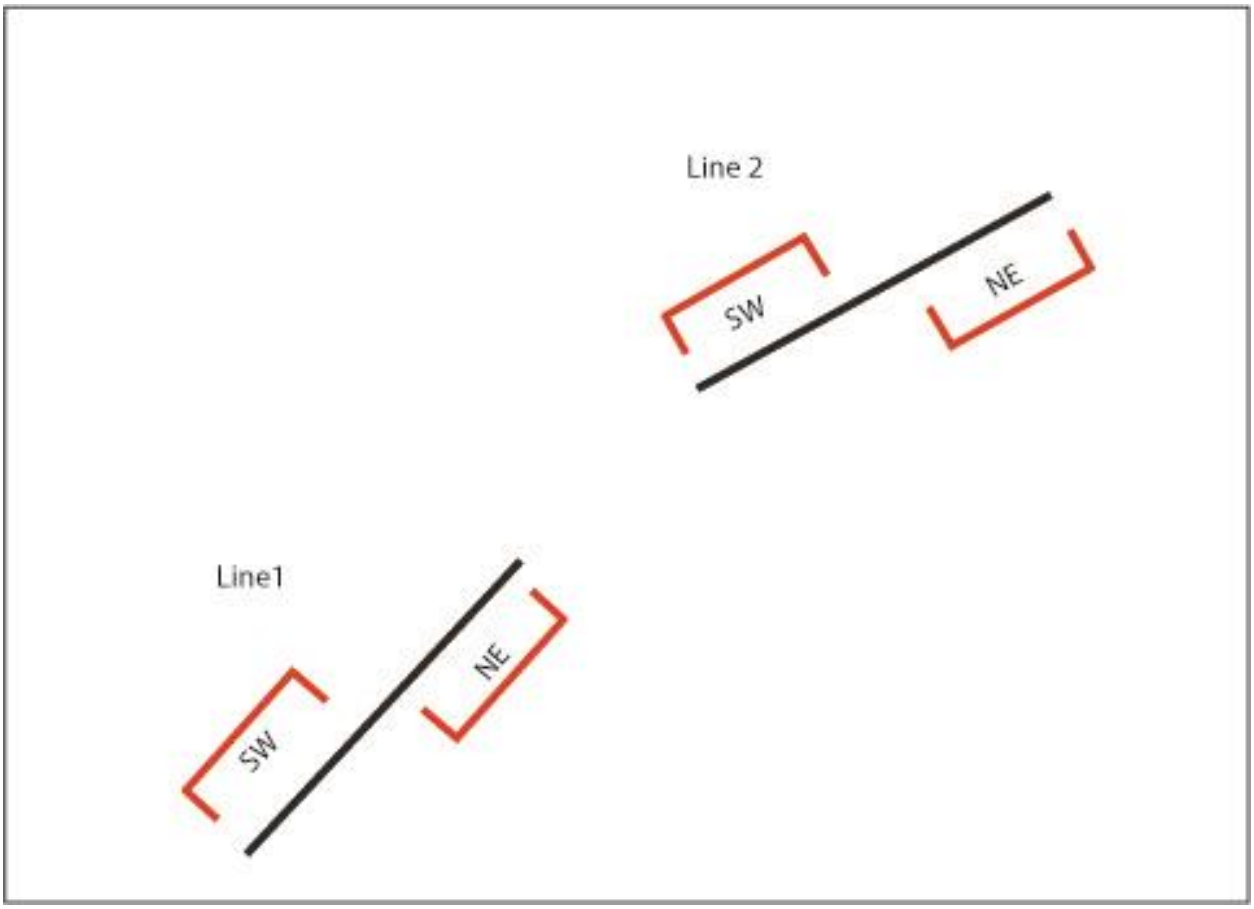


Figure 28. Diagram of how Lines 1 and 2 are split up for display purposes into SW and NE sections.

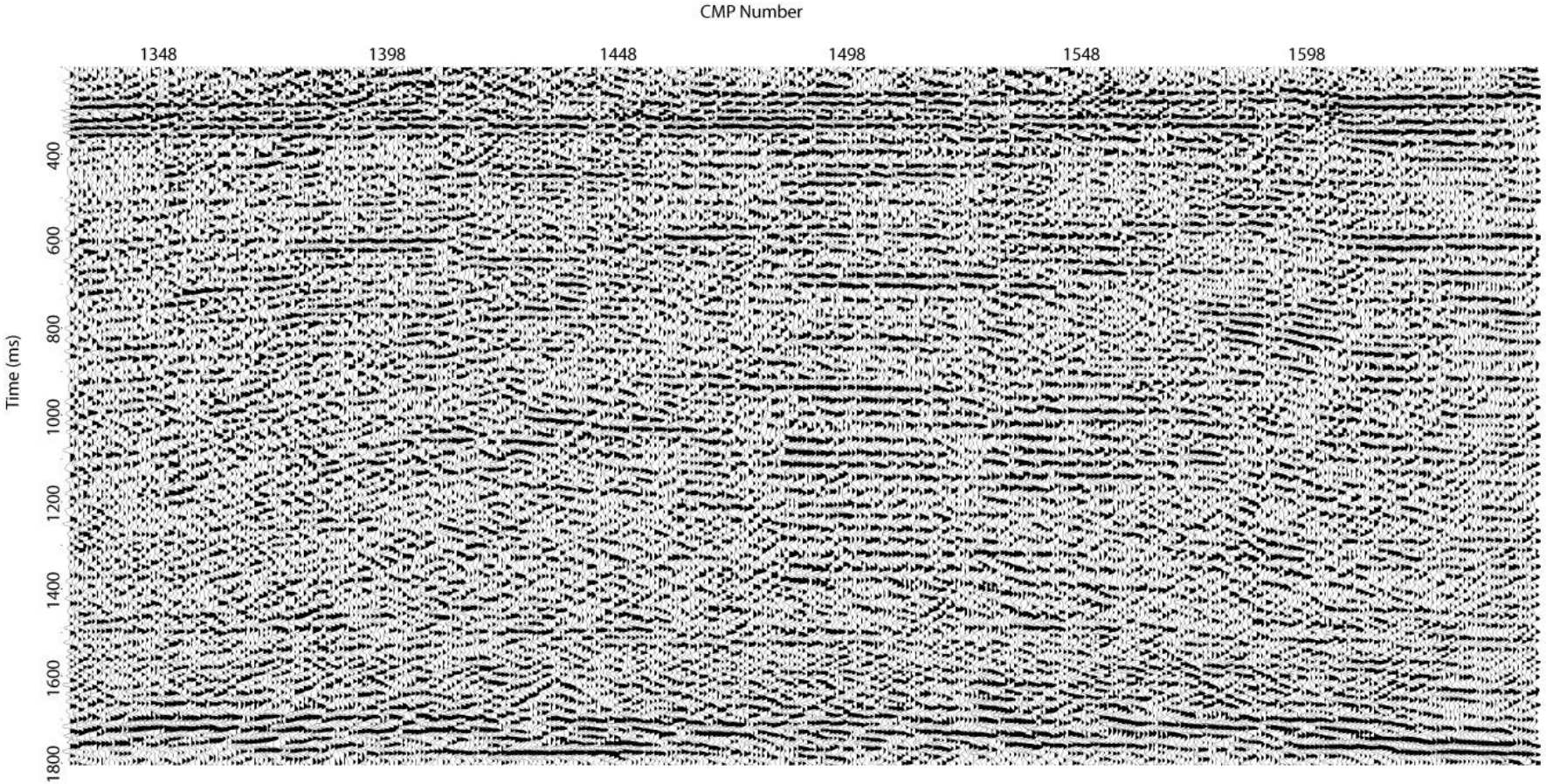


Figure 29. NE portion of Line 1 stacked migrated time section.

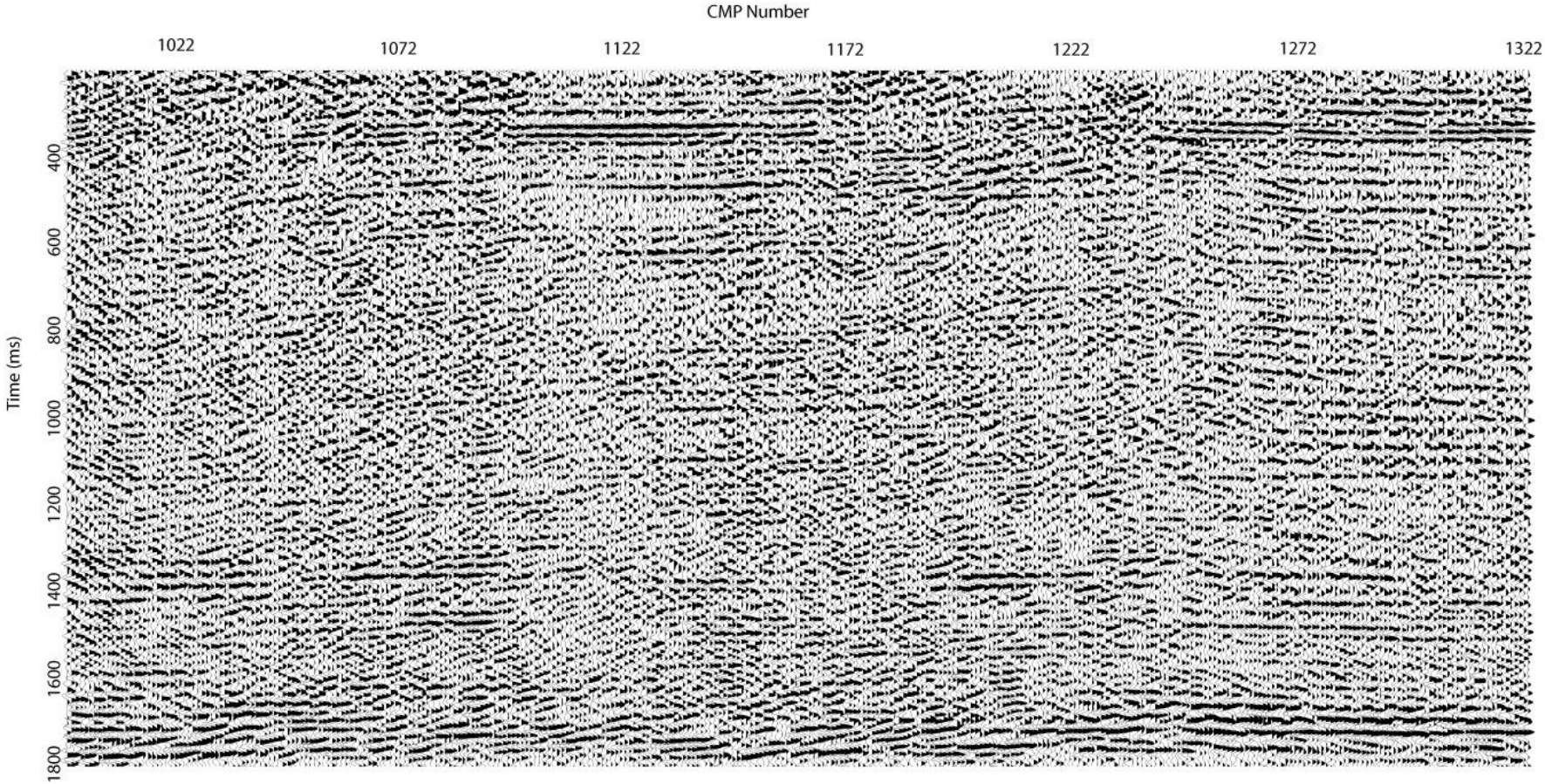


Figure 30. SW portion of Line 1 migrated time section

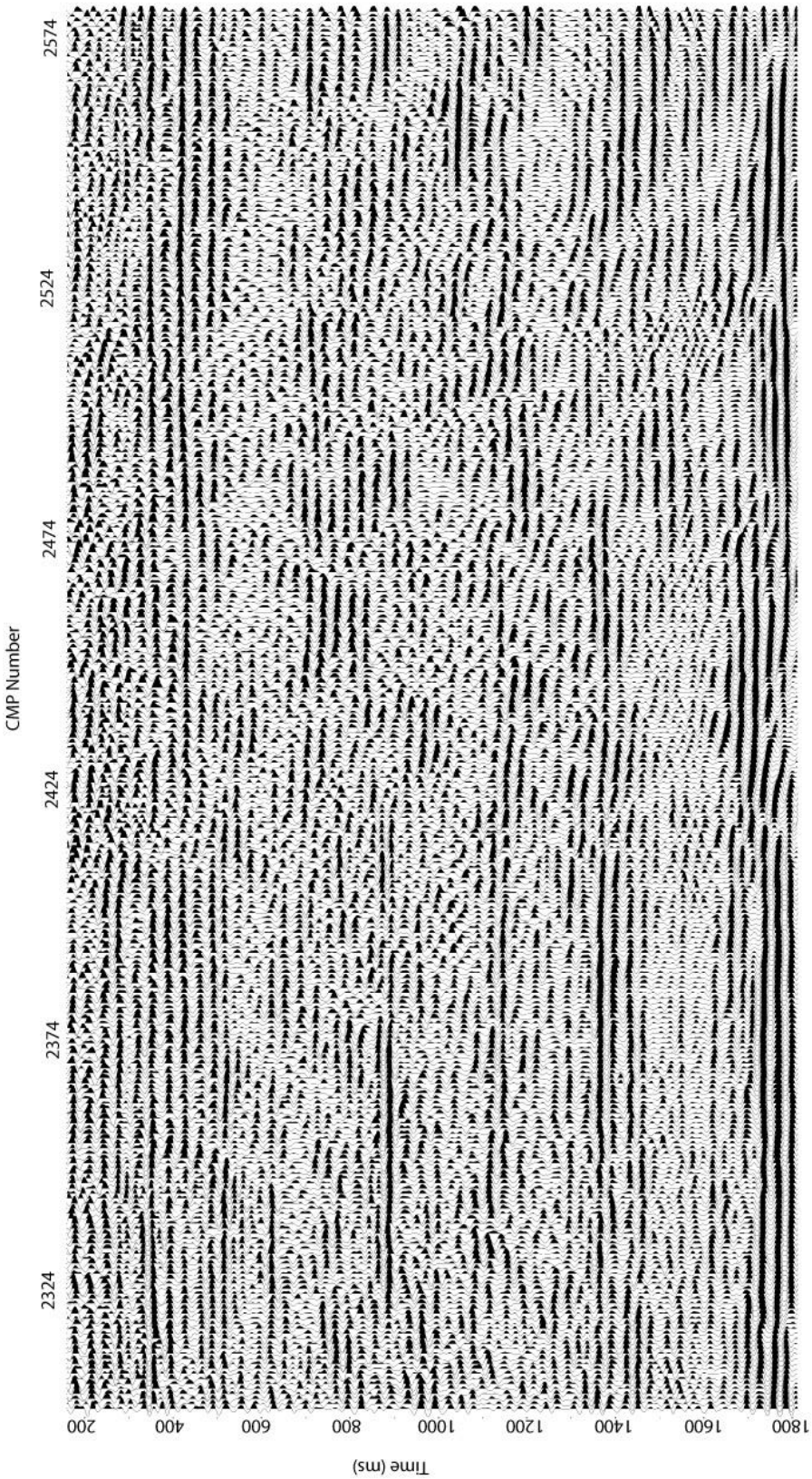


Figure 31. NE portion of Line 2 migrated time section

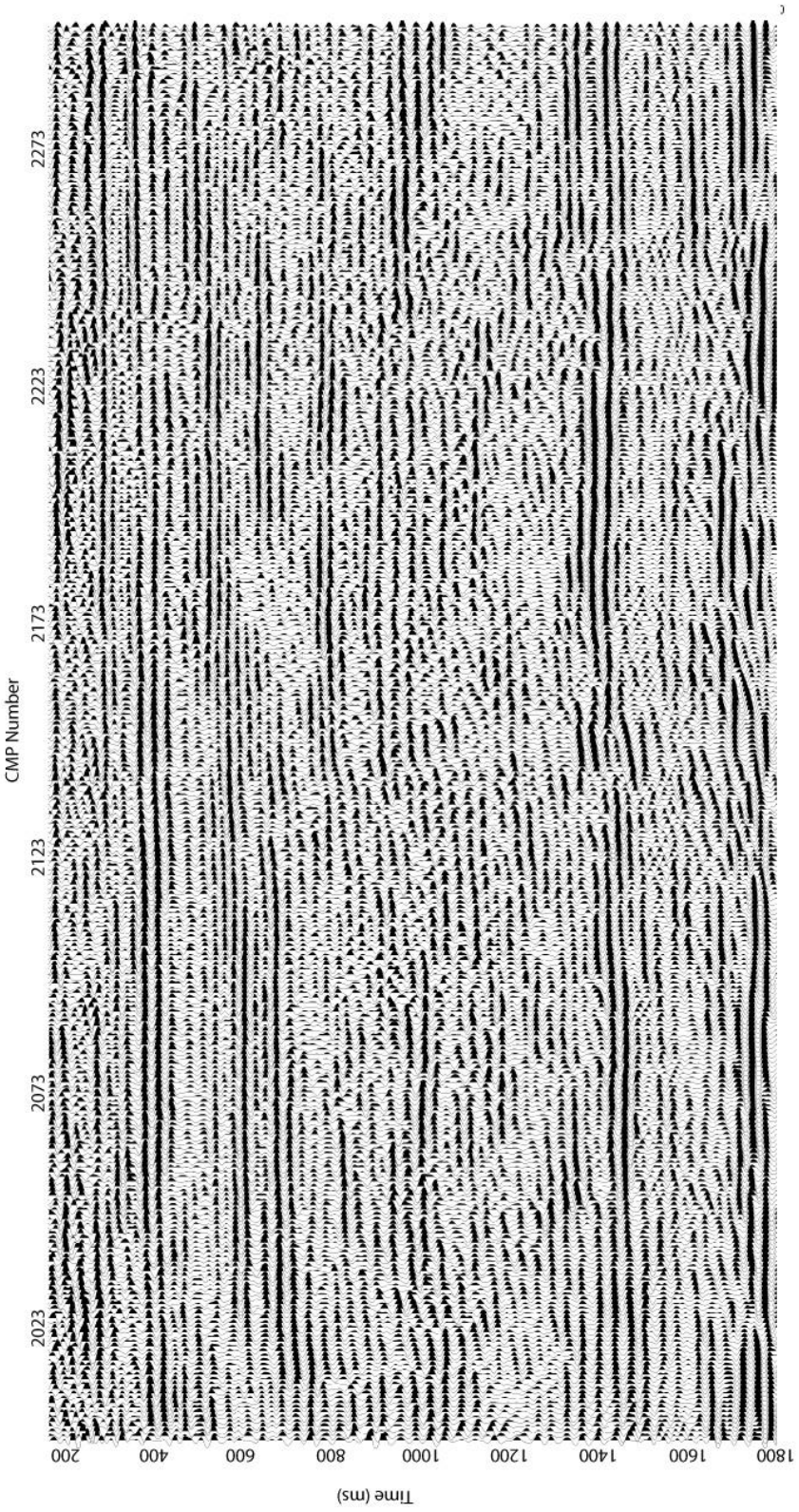


Figure 32. SW portion of Line 2 migrated time section.

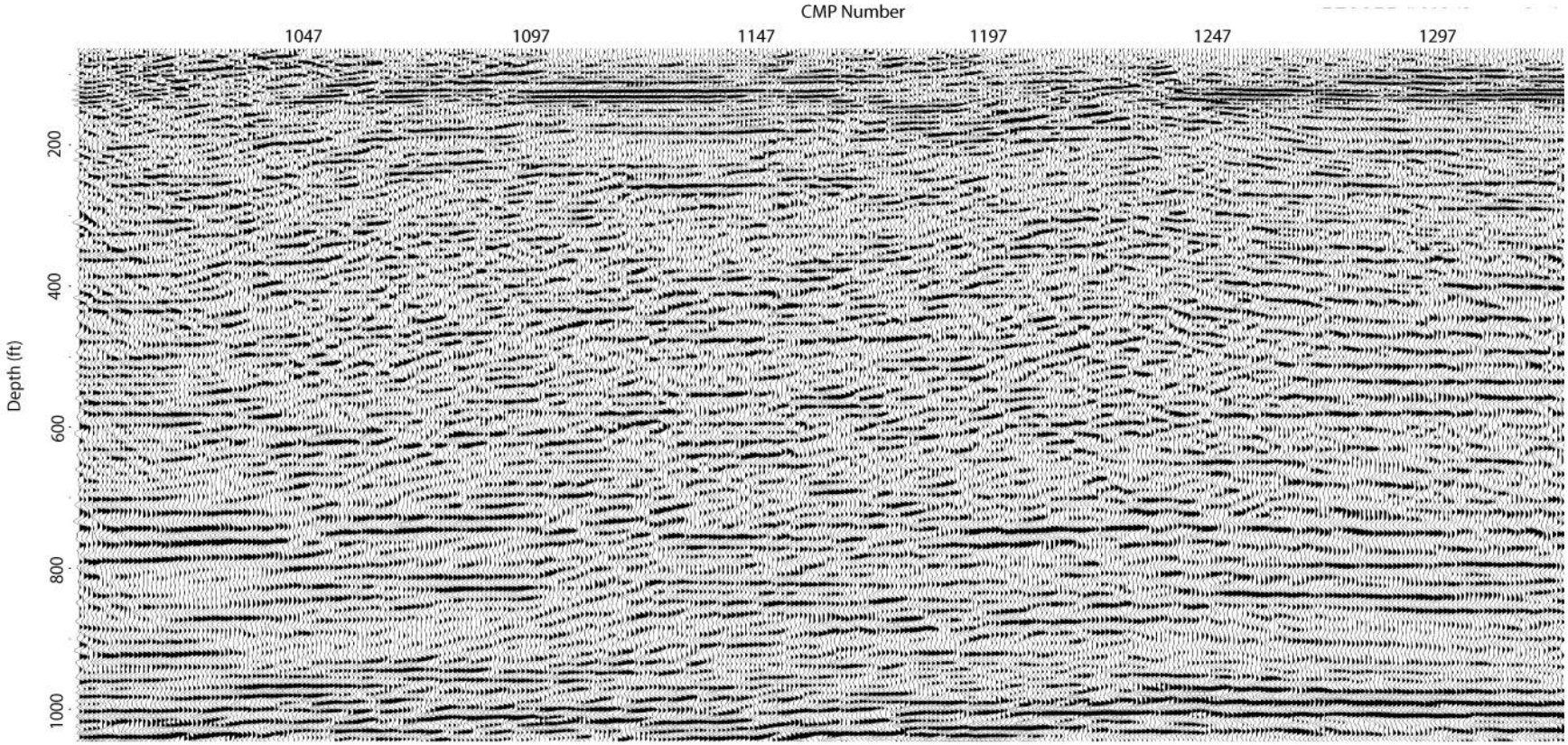


Figure 33. NE portion of Line 1 depth section.

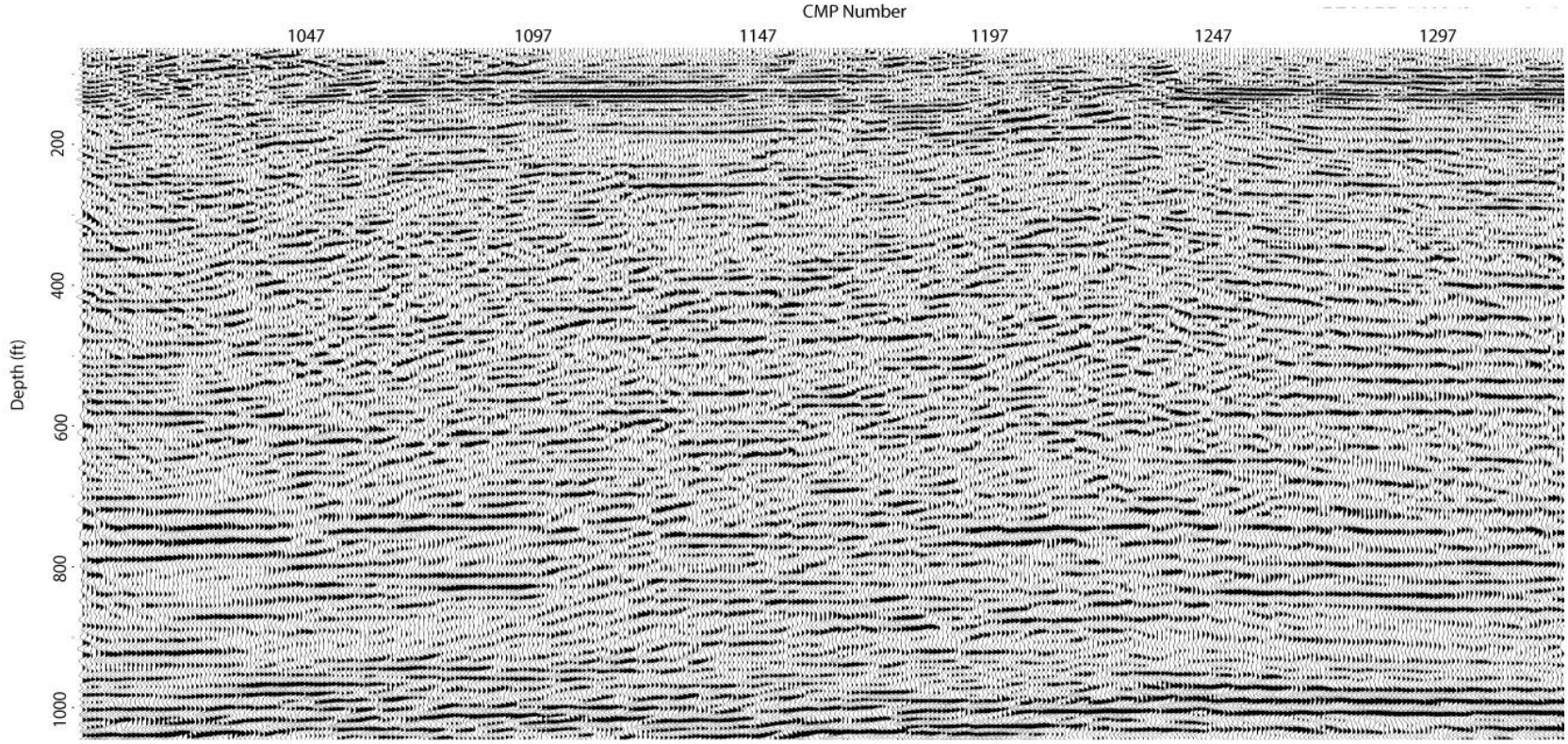


Figure 34. SW portion of Line 1 depth section

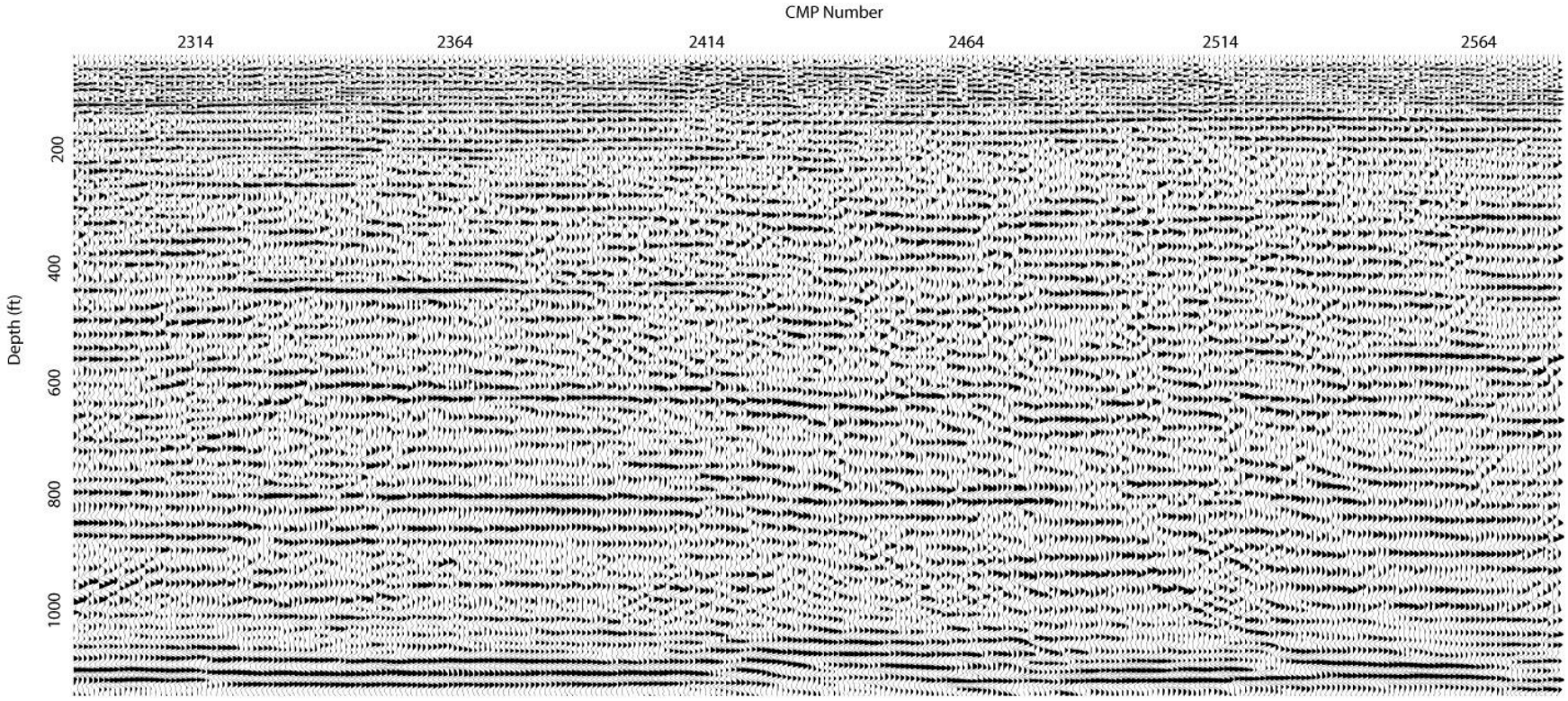


Figure 35. NE portion of Line 2 depth section

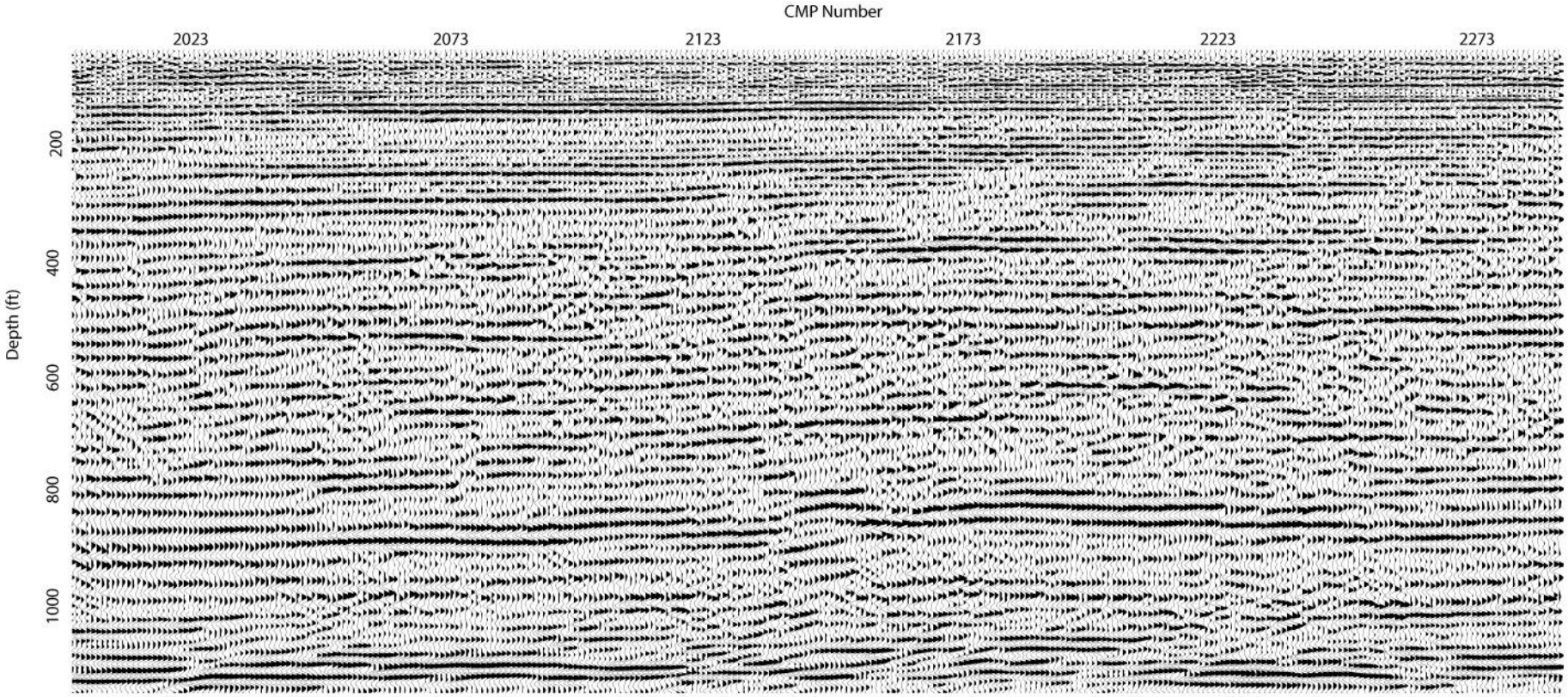


Figure 36. SW portion of Line 2 depth section

Line 2 data in general possessed a higher signal-to-noise ratio and more coherency than in Line 1. Therefore, Line 2 was most interpretable and was interpreted first. Line 1 was interpreted based on reflections highlighted on the Line 2 interpreted sections. Line 1 interpretations show a shallow reflection highlighted in blue, a reflection highlighted in yellow, and a reflection highlighted in red that are both seen in Line 2 (Figure 35, 36). The reflection highlighted in purple gives an extra example of a fairly continuous reflection across the section. The reflection highlighted in green on the Line 2 sections is not distinguishable on Line 1. Due to the nature of the data from Line 1 these were the only reflections that could be picked with confidence. Slight offsets are noticeable on the right side of the NW portion of the Line 1 section. Otherwise reflectors in the deeper parts of the section are decent but are not as coherent as reflections on Line 2.

A fault is interpreted on Line 2 based on reflections that show significant offset (Figure 37, 38). All four of the highlighted reflectors can be traced across both sections of the Line. While the red, green and yellow reflections possess offset, the shallowest blue reflector does not possess any offset, indicating that this fault may no longer be active.

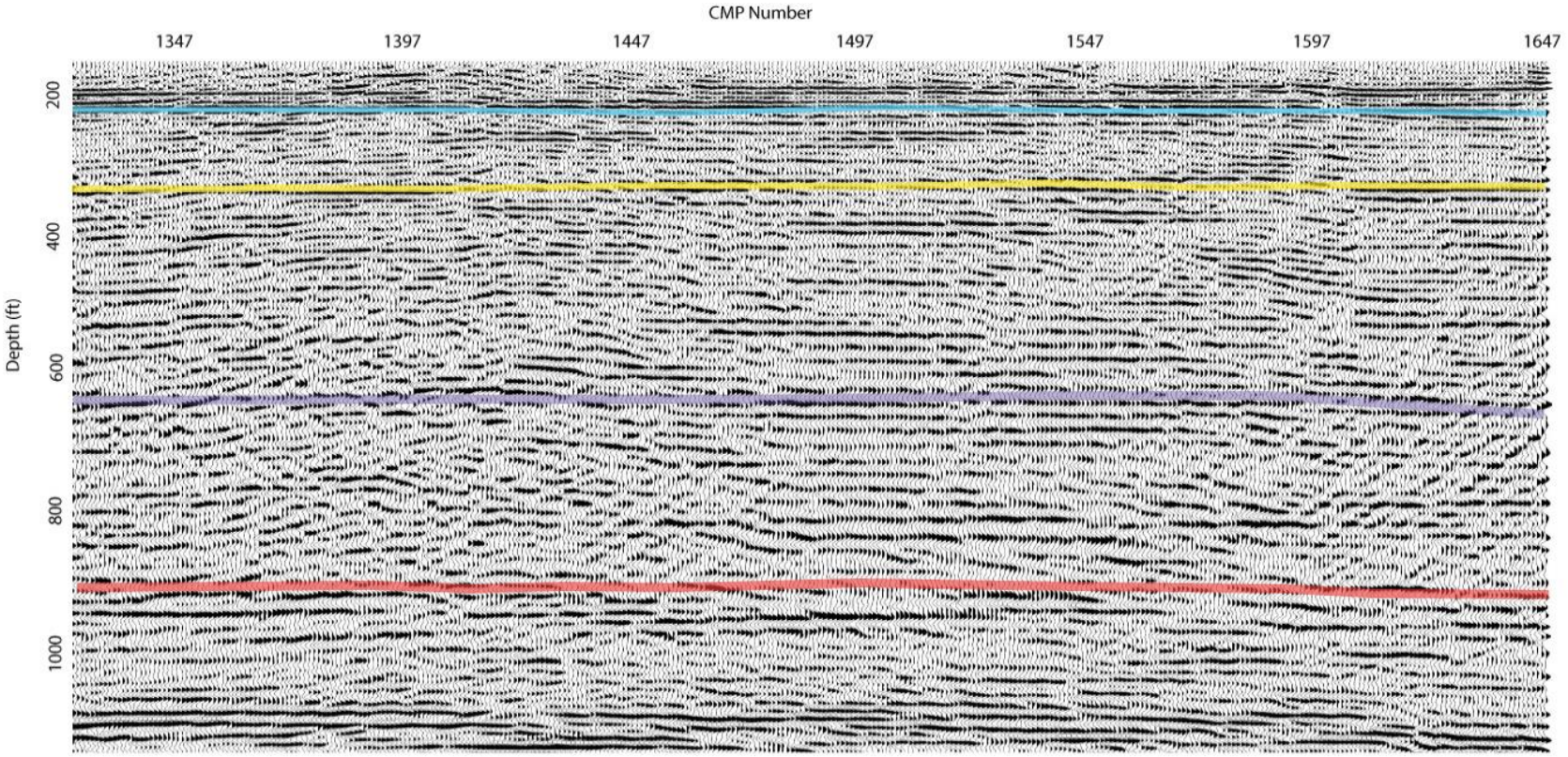


Figure 37. Line 1 NE portion of depth section interpreted.

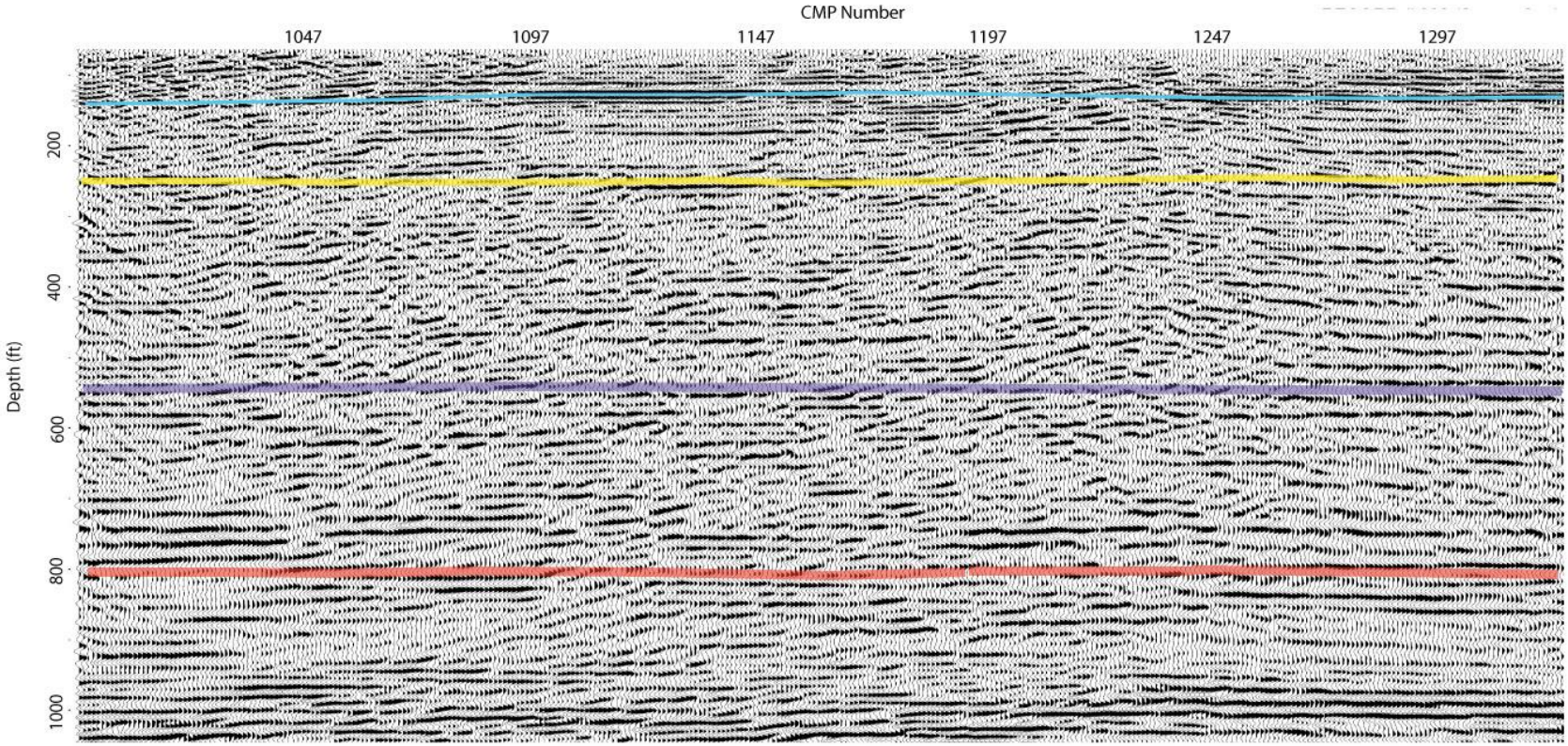


Figure 38. SW portion of Line 1 depth section interpreted

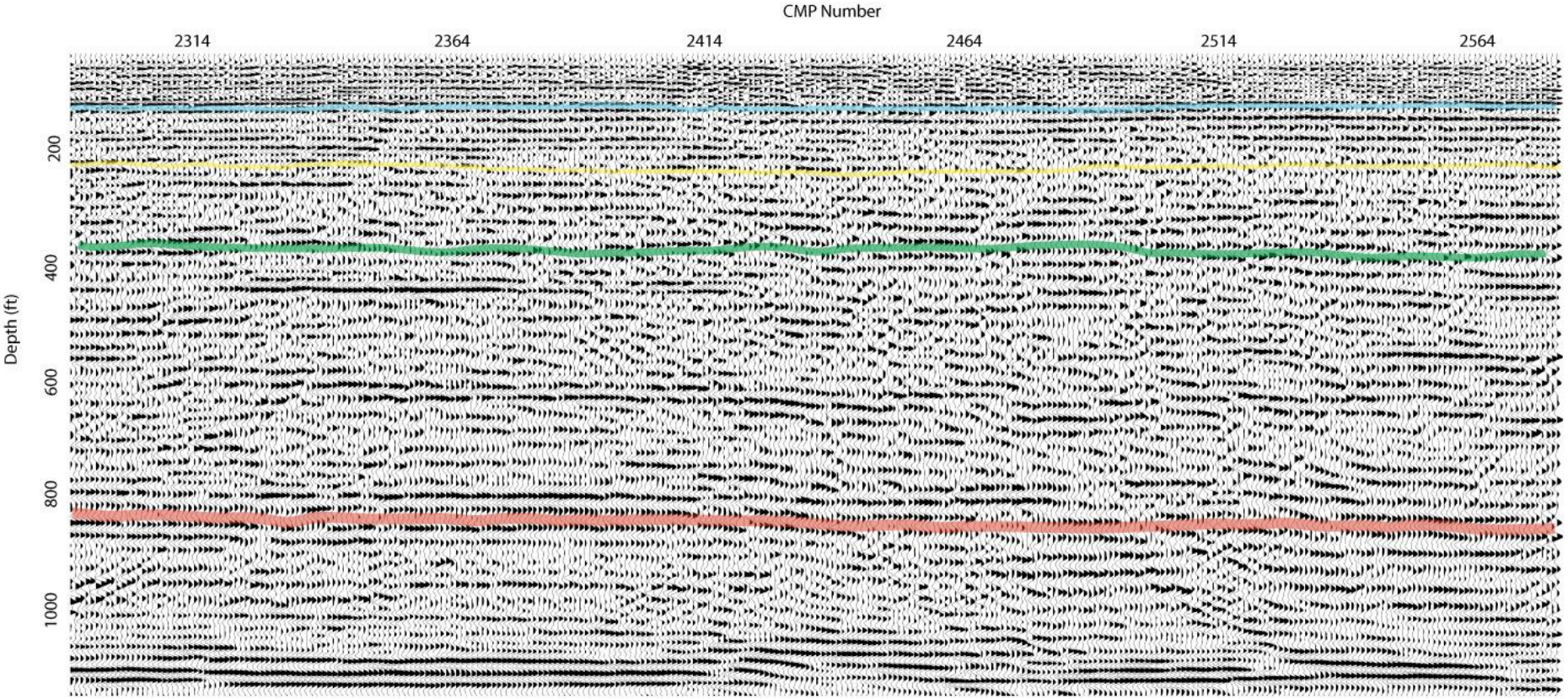


Figure 39. NE portion of Line 2 depth section interpreted

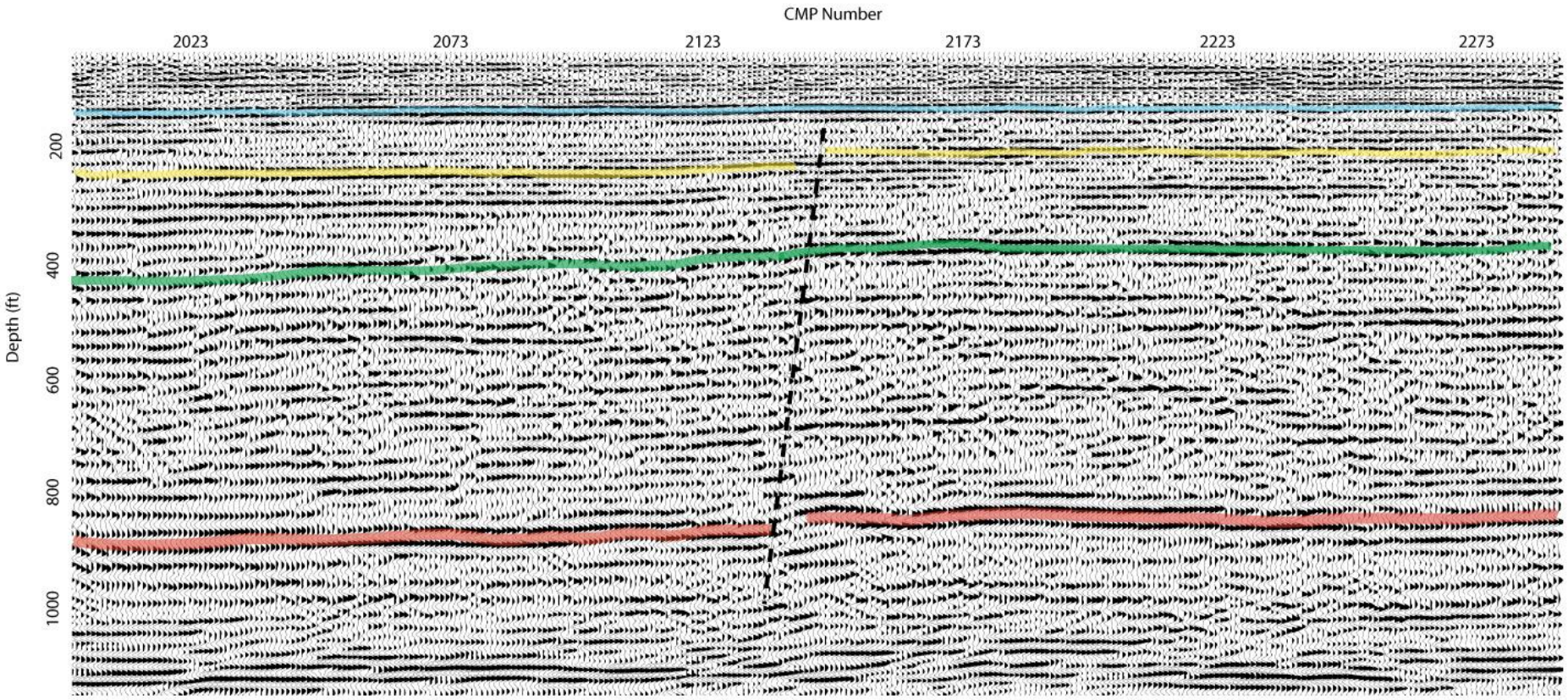


Figure 40. SW portion of Line 2 depth section interpreted

## 2.5 Shear-wave processing pitfalls

As previously stated, more caution must be taken to avoid processing pitfalls with S-wave data than with P-wave data. This dataset possessed many of the difficulties and potential for most pitfalls associated with S-wave processing. One of the more challenging issues in the data was the presence of dispersive Love waves with a thick section of unlithified sediments. Dispersion occurs when vertical velocity variations exist and each unique frequency component of a surface wave will have a different propagation, or phase velocity (Nazarian and Stokoe, 1985; Park et al., 1999). In addition, Love-waves have a velocity of $0.9V_S$, making the masking of reflections by hyperbolic Love-waves another pitfall possibility. Love waves can appear hyperbolic on shot records due to interference of linear components and dispersive arrivals (Kelly, 1983) (Figure 39). This study provides a real-world example of the hyperbolic appearance of Love waves on shot gathers (Figure 40).

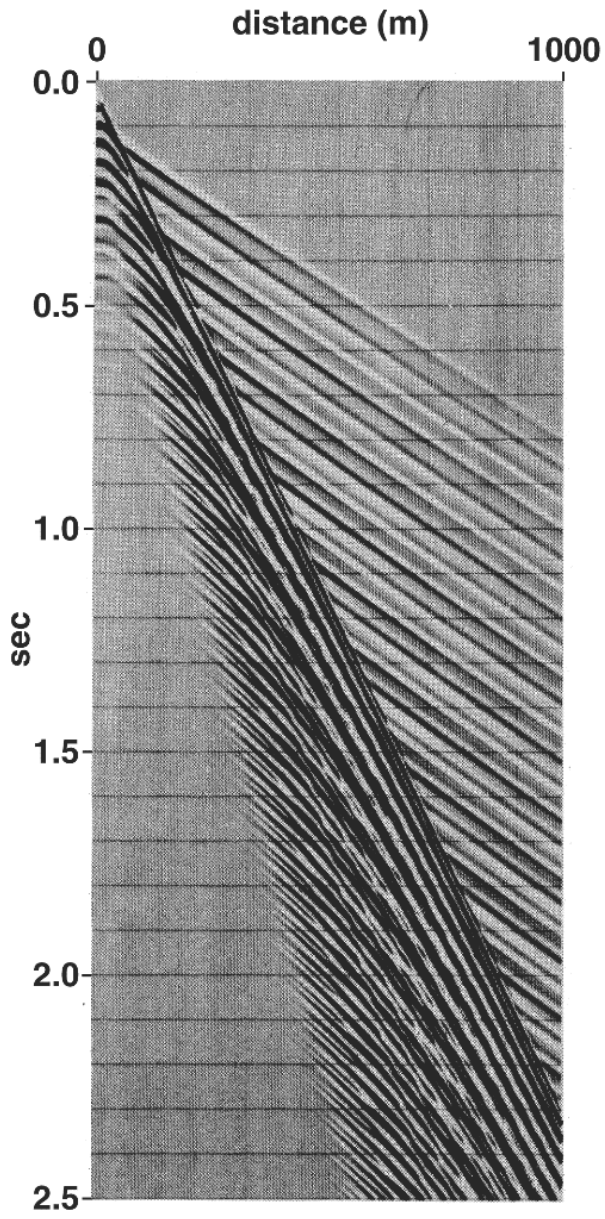


Figure 41. A synthetic seismogram showing only dispersive Love waves. (Modified from Kelly, 1983).

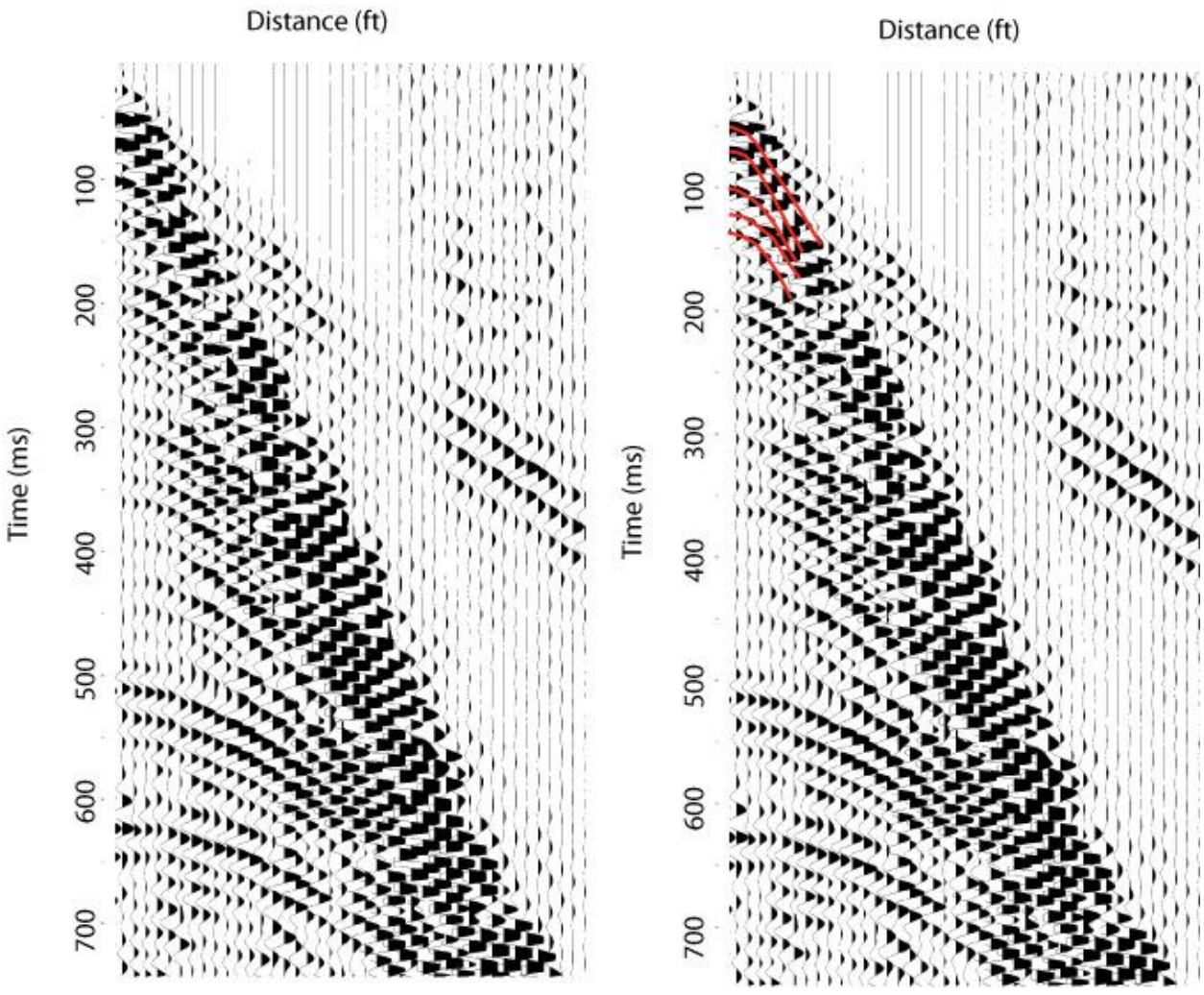


Figure 42. Shot record from Line 2 zoomed in to show Love-waves and reflections. From Figure 27, it is easy to compare the synthetic seismogram showing only Love waves to this example showing Love-waves and reflections. Possible hyperbolic Love-waves are shown in red.

To demonstrate the potential detrimental effects of not properly handling love waves during processing, these data were re-muted to include Love-waves and re-stacked. Love-waves can stack coherently and be easily misinterpreted as reflections (Figure 41). High amplitude, low frequency coherent events are clearly seen from the beginning of the record down to about 150 ms. To avoid stacking this coherent noise into the final section, all data were muted beginning at 175 ms.

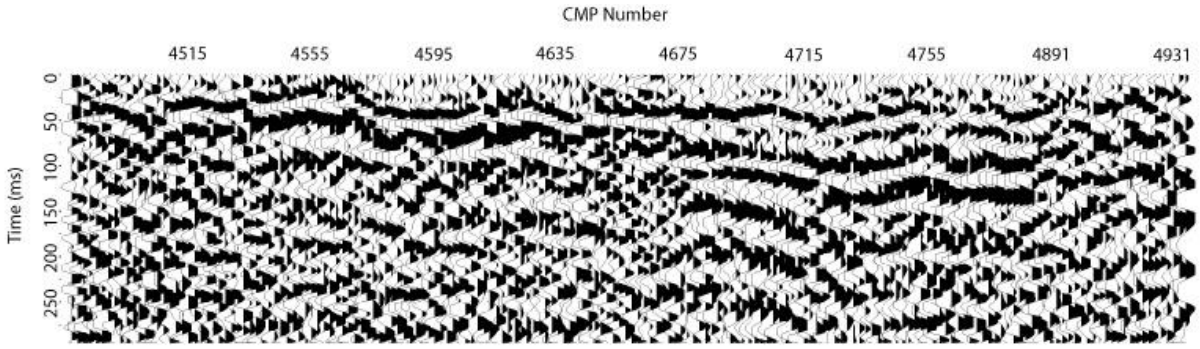


Figure 43. A section of Line 2 with the Love-waves unmuted. A brute stack shows high-amplitude, low-frequency coherent events from the top of the record to about 150 ms. These are most likely Love-waves.

Though it was possible to acquire relatively broad bandwidth data at this site, usually a challenge in S-wave surveys, a number of noise factors including high-voltage power lines, highway, airplane, boat and train noise all strongly inhibit the potential of these data. This data set is characterized by low signal-to-noise ratio and a narrow bandwidth resulting from frequency filtering to remove dominant noise energy. Unfortunately frequency filtering to remove higher frequency noise resulted in a narrowing of the bandwidth to about 25-65 Hz (Figure 42). Much of the lower frequency noise in this dataset is particularly challenging to remove because it generally possesses the same frequency band as the signal (Figure 43).

Another form of noise present in the data is harmonic distortion, which occurs when the weight on the vibratory source is exceeded by the ground force (Schrodt, 1987). Coupling is an issue for shear vibrators, as it is only possible for a shear vibrator to transmit a force equal to the product of its own weight and the friction between the base plate and the ground (Garotta, 1999). Harmonic distortion can be seen on some of the shot records, and an attempt was made to remove it by muting the near-offsets (Figure 44).

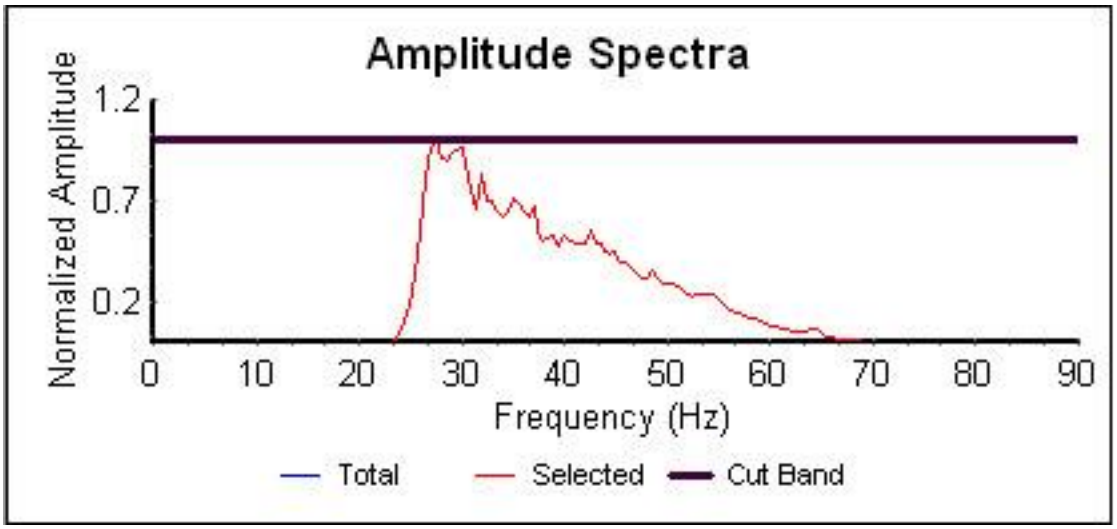


Figure 44. Frequency bandwidth for final stacked section of Line 2. Bandwidth was narrowed by filtering out noise.

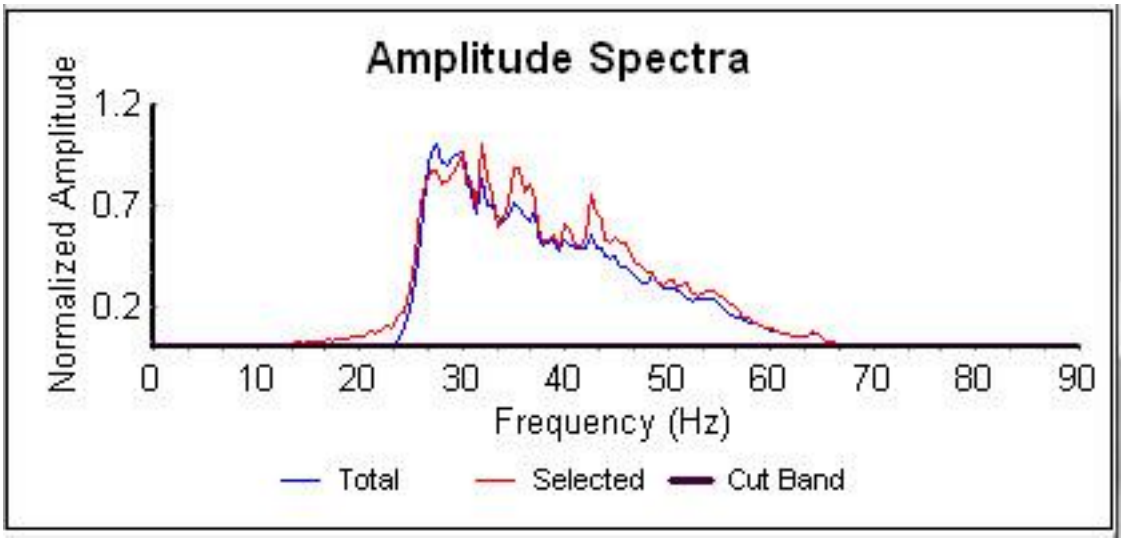


Figure 45. Total amplitude spectra of Line 2 final stacked section (blue) with a noisy area selected (red). The signal and noise have the same frequencies making it difficult to impossible to remove all noise.

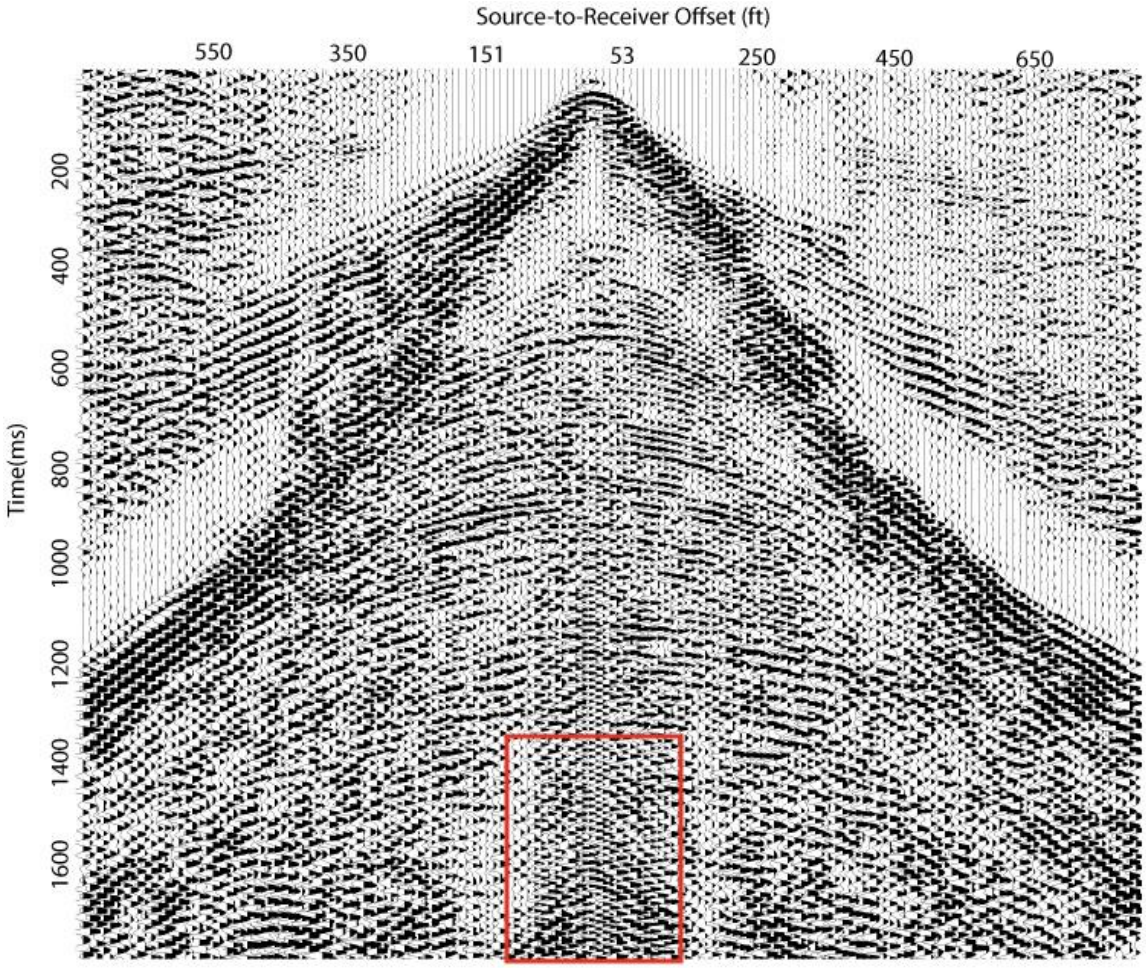


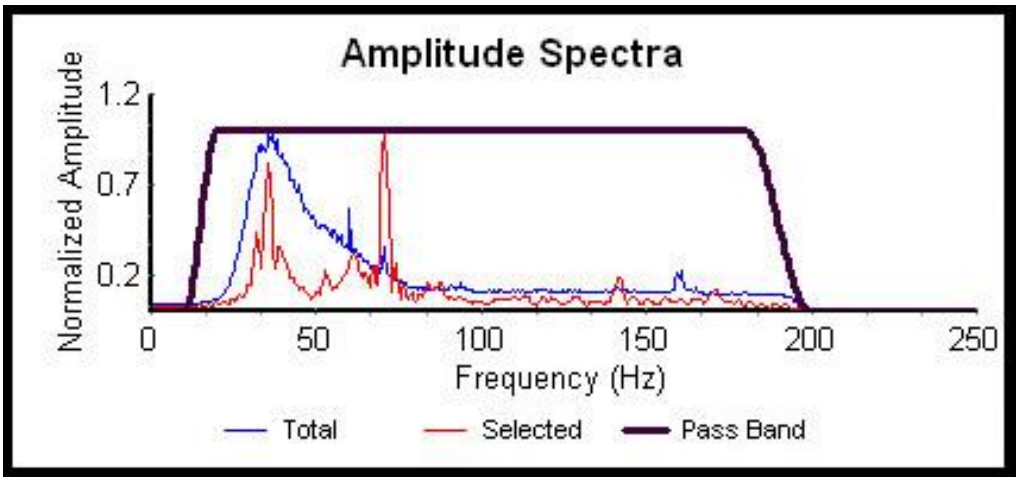


Figure 46. Shot gather from Line 2 showing harmonic distortion within the red box. The amplitude spectra for the box is shown also. The black line represents the sweep frequencies of 20-200 Hz, the blue line represents the total frequency content and the red line indicates the frequency content within the red box.

## Chapter 3: Extended Correlation

Based on the retrieved literature, extended Vibroseis correlation has only been used for crustal-scale profiling applications where the reprocessing of exploration scale data was necessary to significantly deepen the interpretable reflection potential (Okaya and Jarchow, 1989). As best it can be determined it has not been used with near-surface data of any kind. Okaya and Jarchow (1989) describe two methods for extending Vibroseis data. The first is the fixed bandwidth method, whereby the correlation operator is shortened, allowing a correspondingly longer record to be produced through crosscorrelation (Okaya and Jarchow, 1989). The second method, and the one best suited for this study, is self-truncating extended correlation (Figure 45). Self-truncating extended correlation uses as much of the operator length as possible by allowing it to truncate on its own. This allows for the use of as much of the correlation operator as possible when correlating deeper reflections (Okaya and Jarchow, 1989). This method is best for this study because bandwidth is better preserved as the correlation operator gradually diminishes with extra correlation time. Prior to the extended listen time bandwidth is maintained, as in standard correlation, so this method can theoretically be applied without sacrificing resolution within the original listening time (Okaya and Jarchow, 1989).

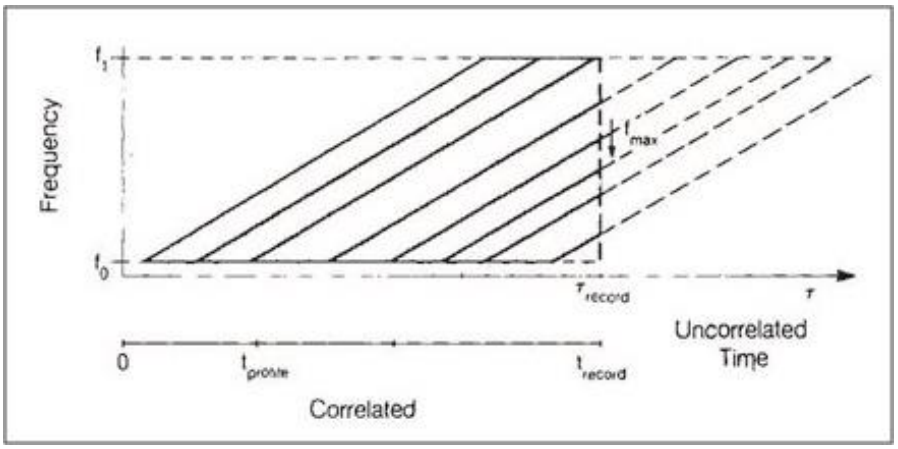


Figure 47. The self-truncating extended correlation method. (Modified from Okaya and Jarchow, 1989).

To extract existing signal with self-truncating extended correlation, diminishing portions of the correlation sweep are necessary for times greater than $t_{Profile}$ (the original record length in time) (Figure 45) (Okaya and Jarchow, 1989). The wavelets associated with deeper reflections not in the original records that are added on, have a frequency content that drops in a predictable manner (Okaya and Jarchow, 1989). Therefore, wavelets that are correlated beyond the original listen time are broader in time and have more pronounced side lobes (Okaya and Jarchow, 1989).

The raw data were acquired with a 10 s upsweep of 20-200 Hz, with a 12 s listen time. With conventional correlation this provided about a 1.8 s record. The record is 1.8 s instead of 2 s because the seismograph was recording for 200 ms before the sweep began when the data were collected, therefore, during correlation the data had to be shifted down. Reflections on correlated records are clearly visible near the bottom of the 1.8 s record, suggesting more reflections could have been recorded, and with use of extended correlation they might be interpretable (Figure 46). Through the use of self-truncating extended correlation, the original record was extended by 1 s from 1.8 s to a length of 2.8 s (Figure 47). Poor signal-to-noise conditions characterize this dataset before extended correlation, and at later traveltimes, this can cause deeper reflections to

be weak or lacking. Extended correlation on this dataset does bring out later reflections, but many are weak and lack coherency trace to trace.

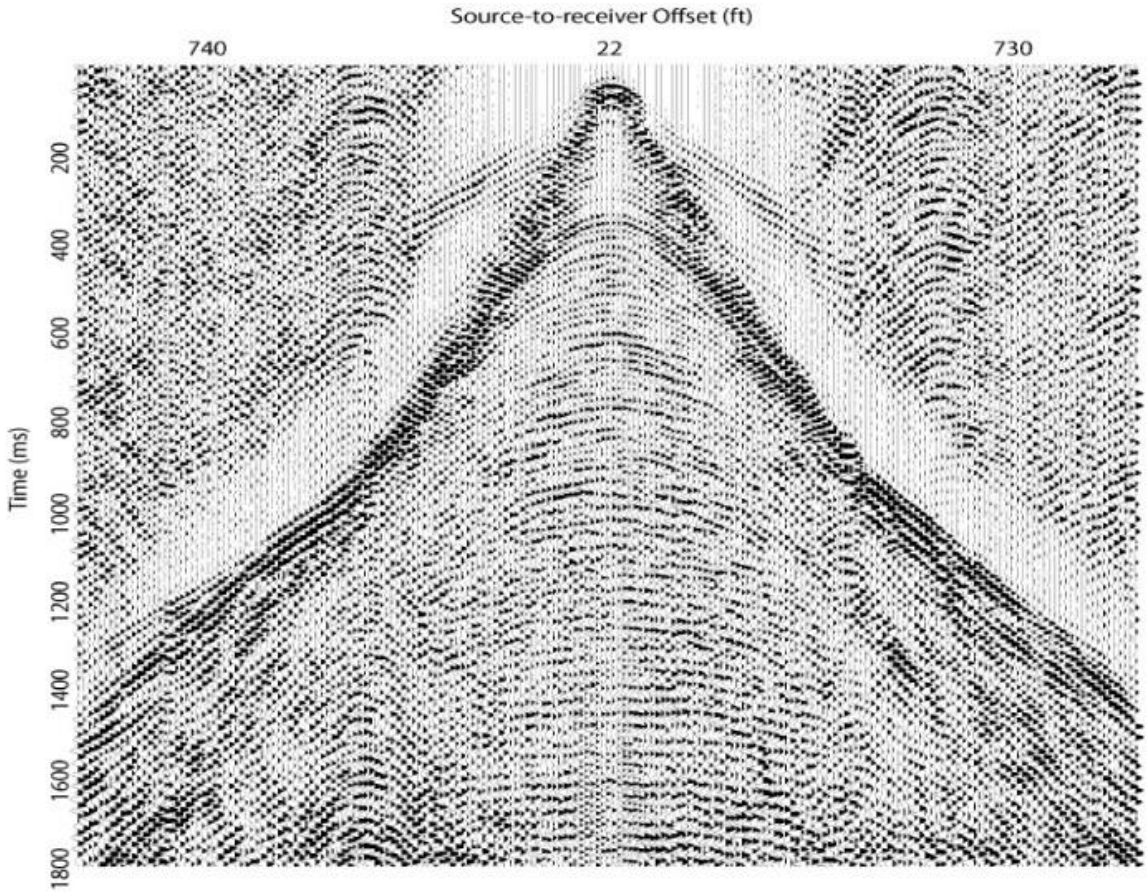


Figure 48. Shot record from Line 2 correlated using standard Vibroseis correlation. Reflections are visible at the bottom of the record, indicating more reflections could be imaged if data were extended.

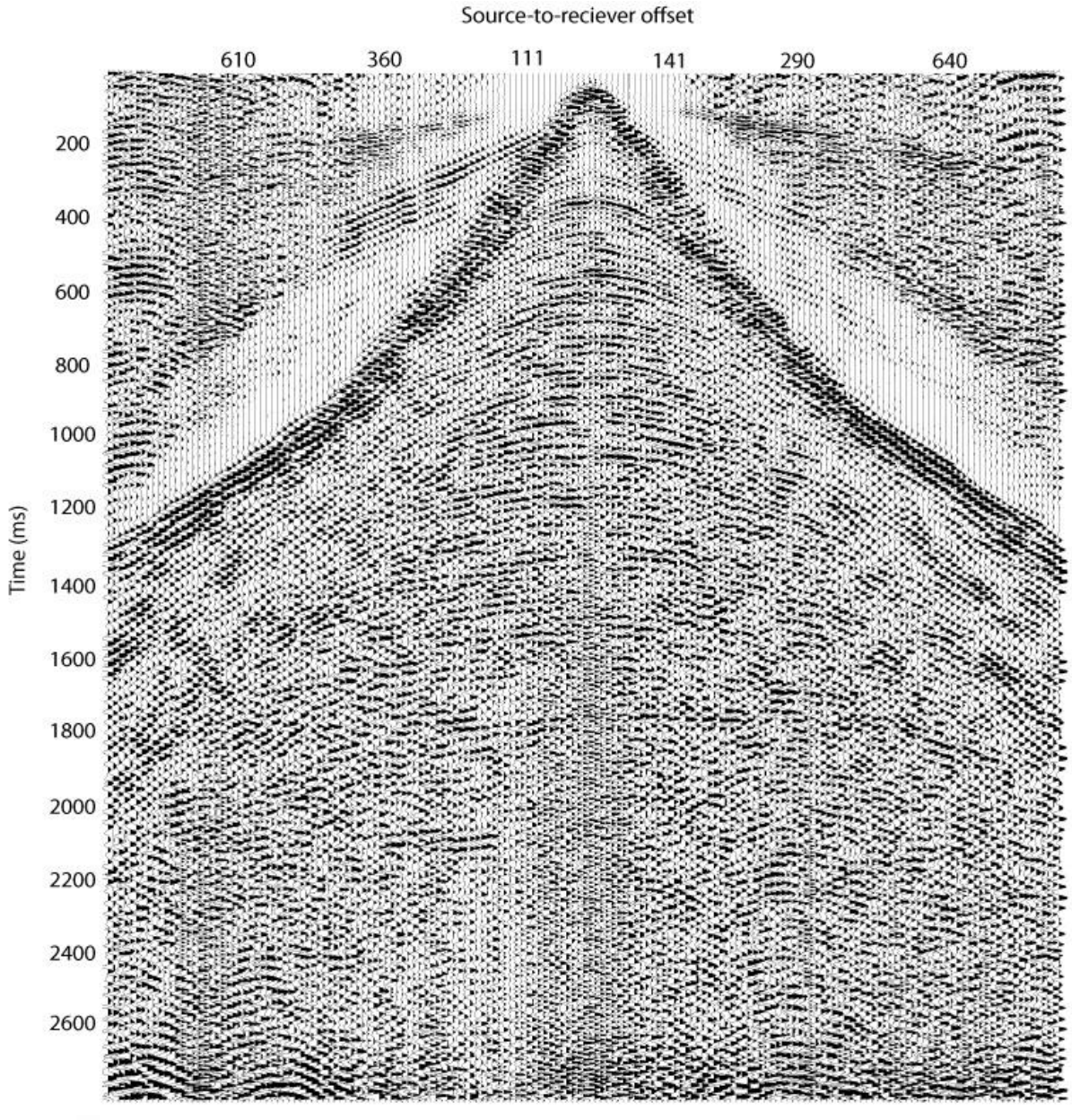


Figure 49. Shot gather from Line 2 extended using self-truncating extended correction. Reflections are visible down to approximately 2400 ms.

### 3.1 Line 1 Extended Correlation

Line 1 is characterized by a poor signal-to-noise ratio with standard correlation. Noise was difficult to impossible to remove and the resulting CMP stacked section suffered greatly from reduced signal-to-noise ratio. In some portions of the section, reflections were weak and lacked coherency in many places or not were discernable at all due to noise (Figure 46). Data possessed low signal-to-noise ratios making it very difficult to identify any structure that might exist in portions of the section. The Line 1 extended data was processed with the exact same flow as the original data, with the exception of correlation. Theoretically, the first 1.8 seconds of data should look the same as the non-extended data, however, that does not always seem to be the case. One possible reason for this could be that more noise is in the extended portion of the data that must be filtered out, causing important information to be lost in the upper 1.8 seconds of data as well.

When extended Vibroseis correlation was performed on Line 1, the character of the reflections in the deeper part of the section, 1.8 – 2.8 s, appears different from the character of the reflections in the shallower data. The extended data showed higher amplitude and more coherent reflections than are seen in the first 1.8 s of the data along parts of the line (Figure 47). The deeper reflections are more visible in the extended portion of the section. The final stacked sections are divided into four sections per line for display purposes (Figures 48, 49, 50, and 51).

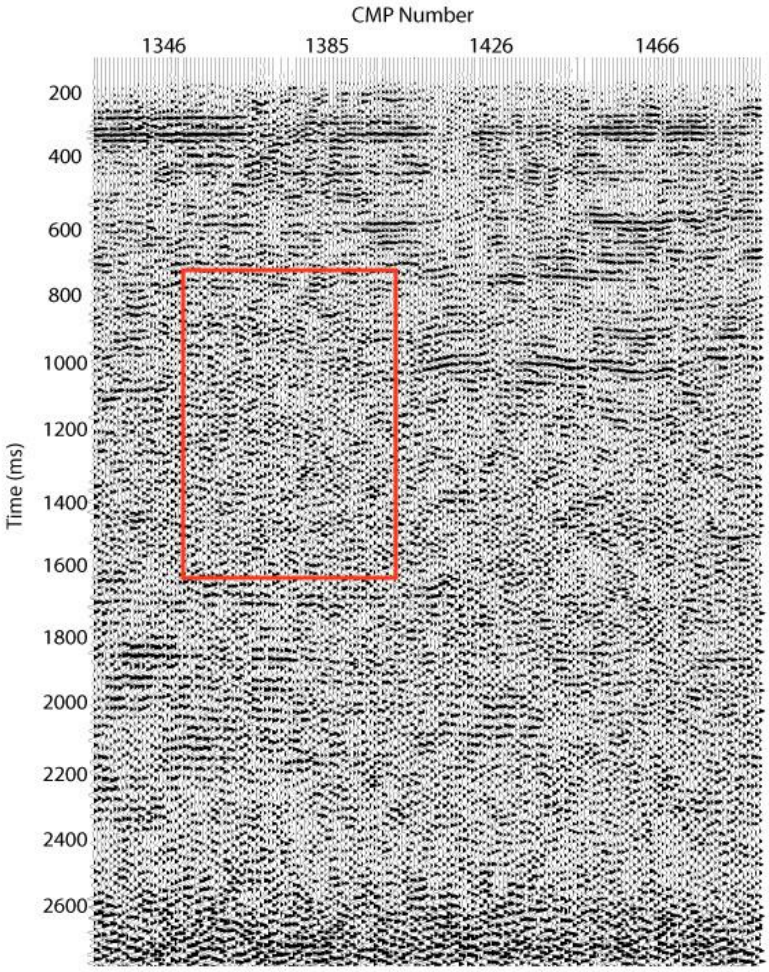


Figure 50. Section of Line 1 extended correlation data showing low coherency and how reflections are not discernible due to noise.

The quality of the extended data from Line 1 is still poor and noise is still present, however deeper reflections are clearly visible. Most of the deeper reflectors though are still lacking coherency across the section, which is likely due to the inability to remove noise.

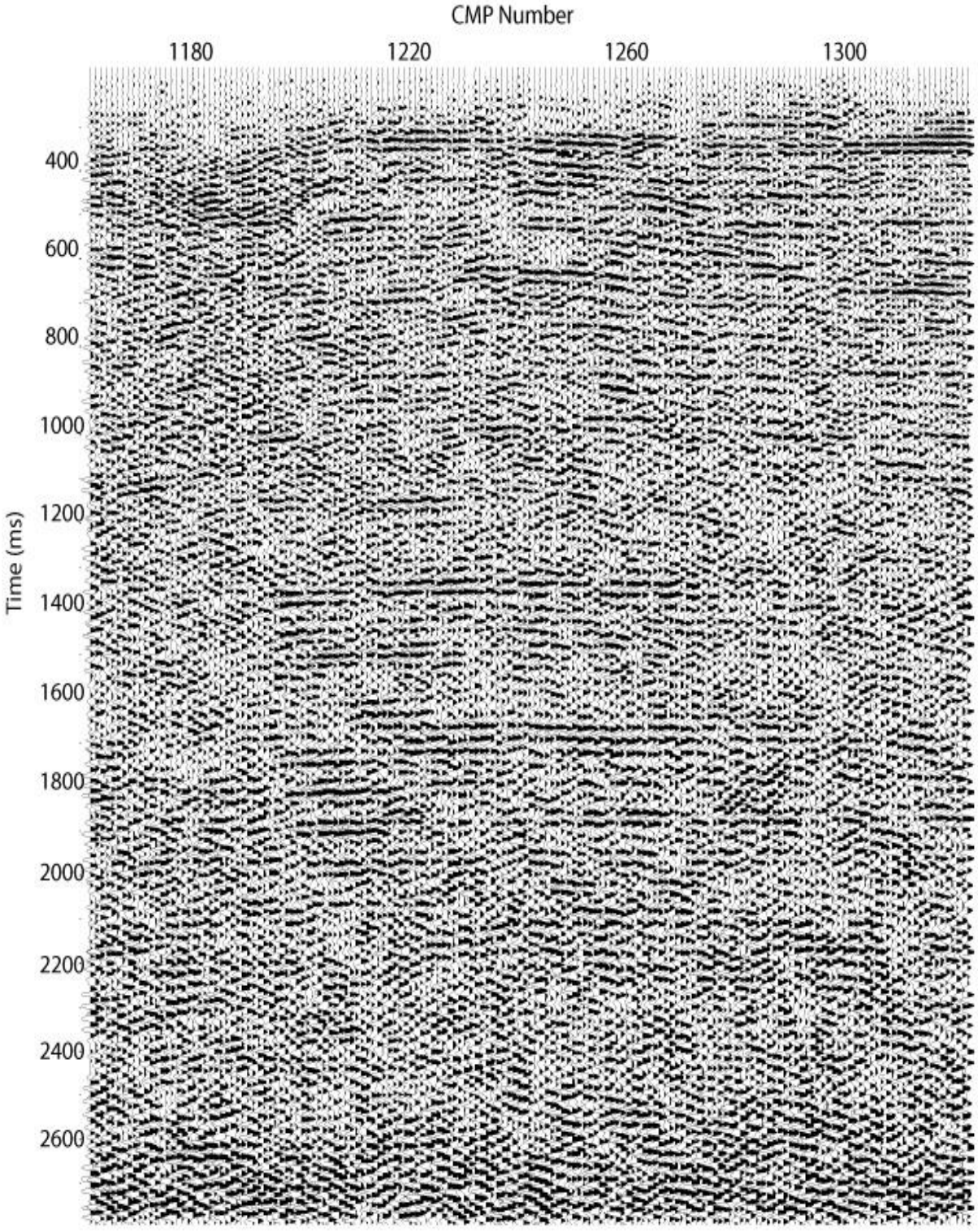


Figure 51. Section of the Line 1 extended correlation section. Reflectors below about 1300 ms have stronger amplitudes and are more coherent than reflectors in the top portion of the section.

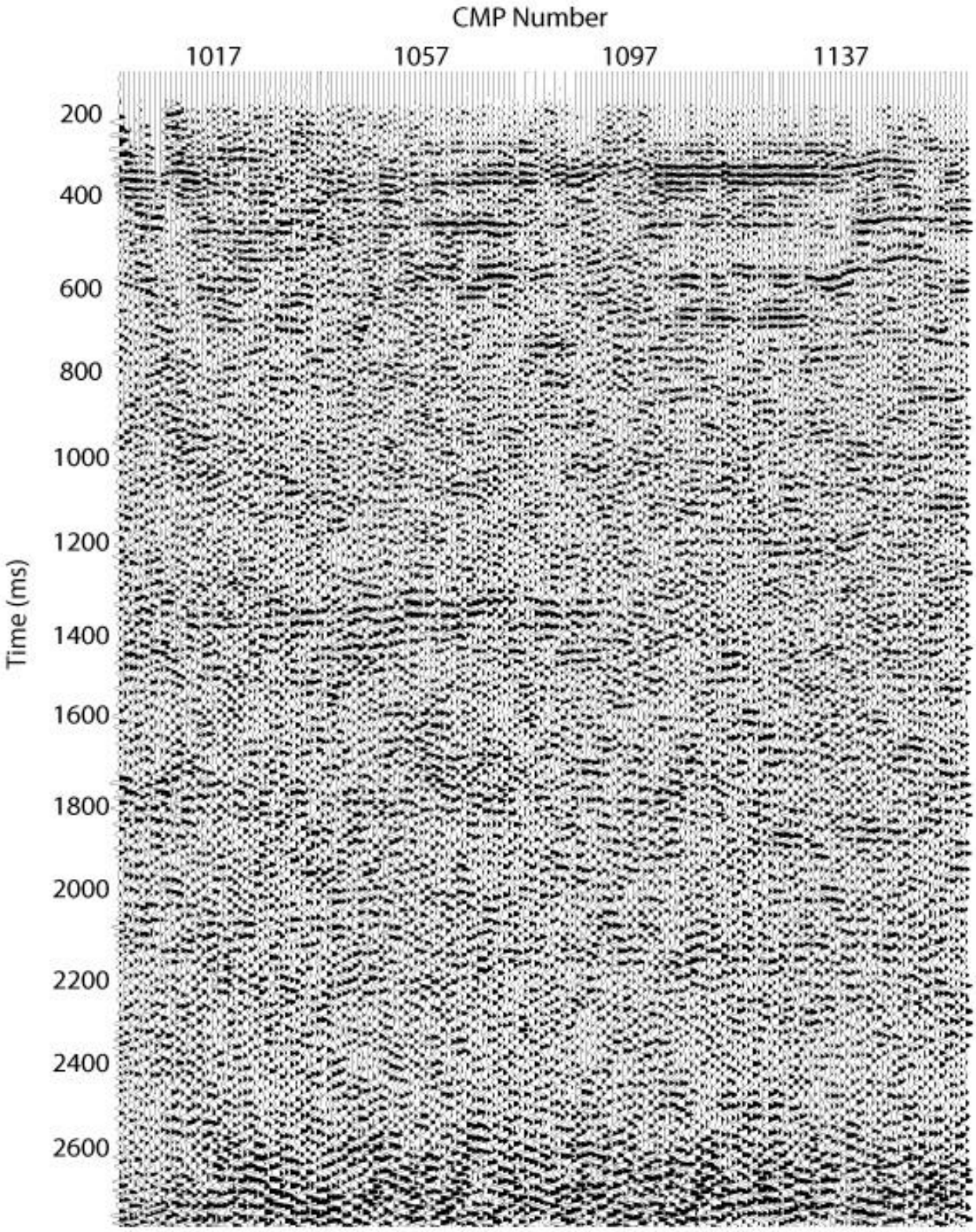


Figure 52. Section 1 of Line 1 extended correlation stacked section. Noise is still present in the data and reflectors are incoherent.

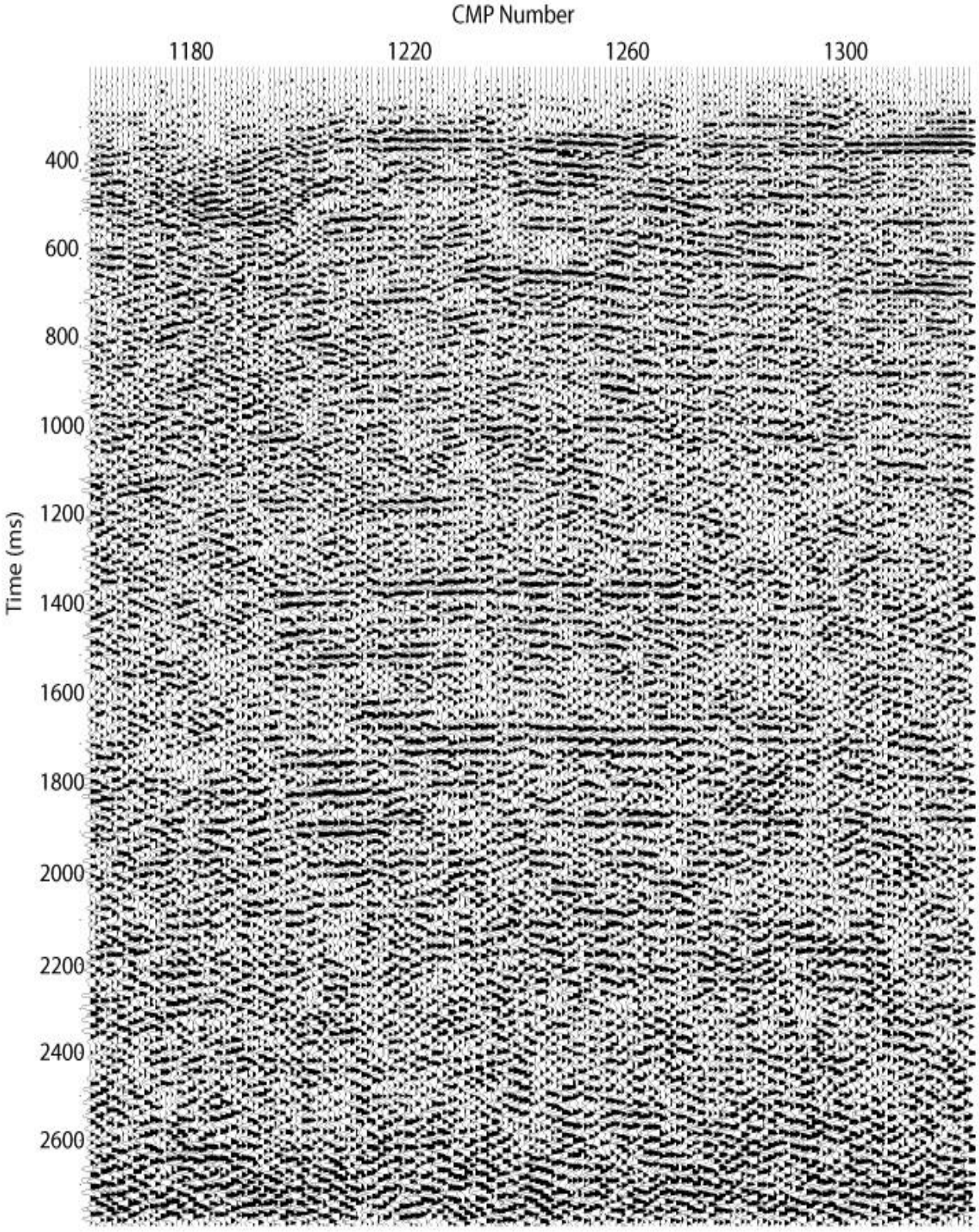


Figure 53. Section 2 of Line 1 extended correlation stacked section.

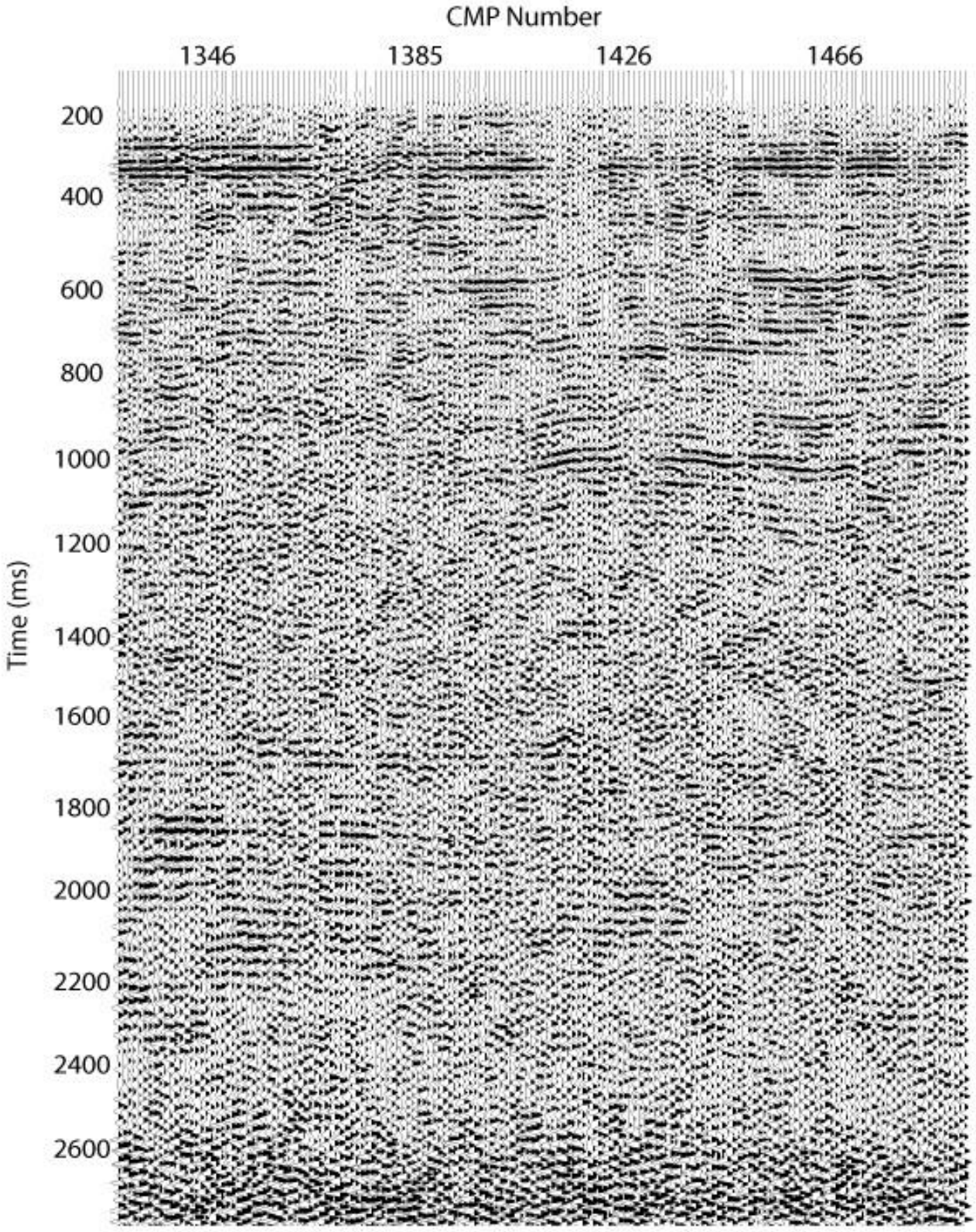


Figure 54. Section 3 of Line 1 extended correlation stacked section.

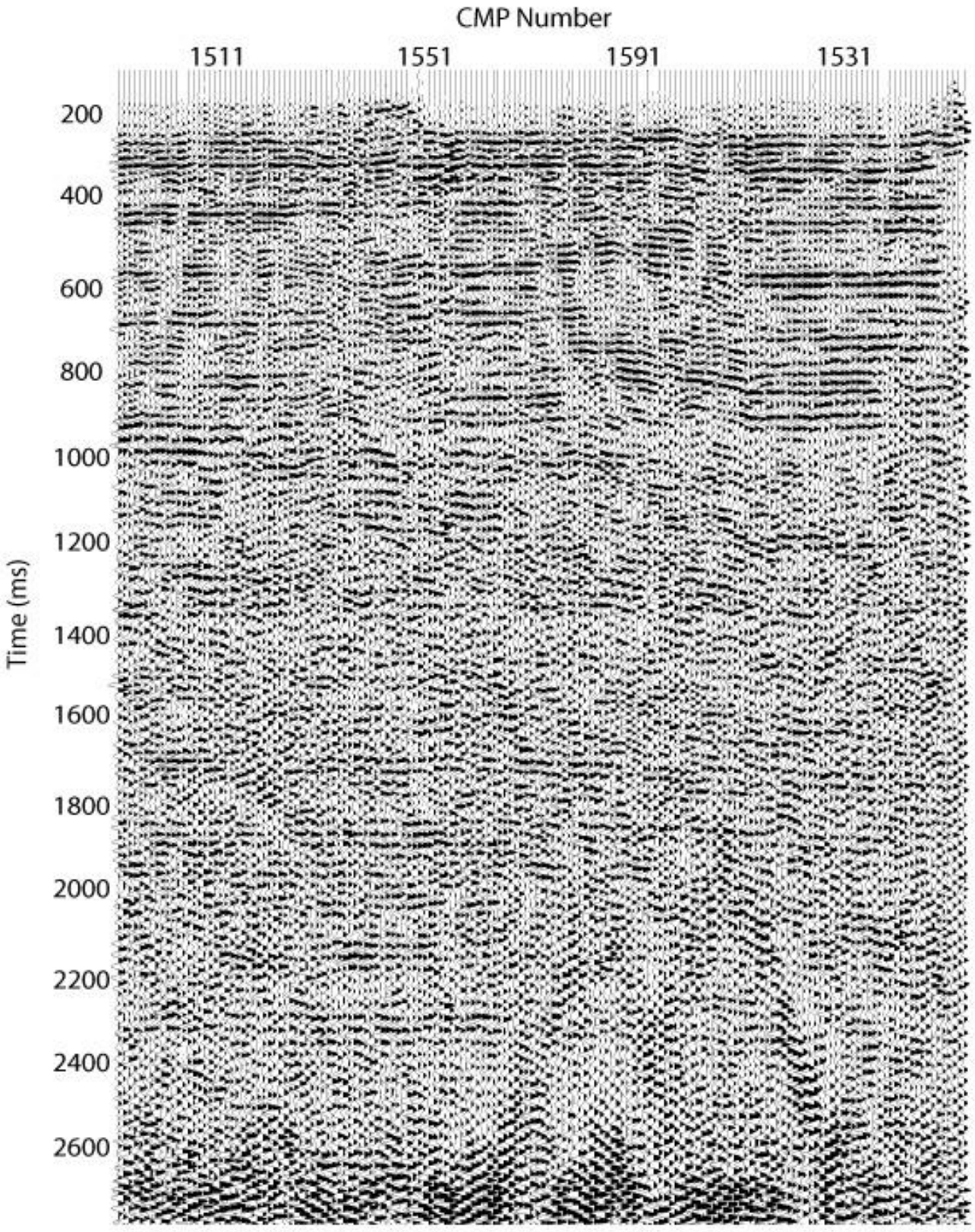


Figure 55. Section 4 of Line 1 extended correlation stacked section.

### 3.2 Line 2 Extended Correlation

Line 2 has a better signal-to-noise ratio than Line 1 on the conventionally correlated data. However, the data quality of Line 2 deteriorates when the data are extended. The extended data for Line 2 was processed with the same processing flow as the Line 2 standard correlation data, with the exception of the actual correlation process and some frequency filtering, enabling the upper 1.8 s of data to remain as close as possible to the conventionally processed 1.8 s. A range of frequencies had to be filtered as there were more noise in the later part of the record. Shot gathers contain higher frequency noise in the lower portions of the records (Figure 52), that when filtered out does not consistently reveal reflections deeper in the data (Figure 53).

The final stacked sections are divided into four sections per line for display purposes (Figures 54, 55, 56, and 57). The extended data possesses reflections at depth that are low amplitude and lack coherency.

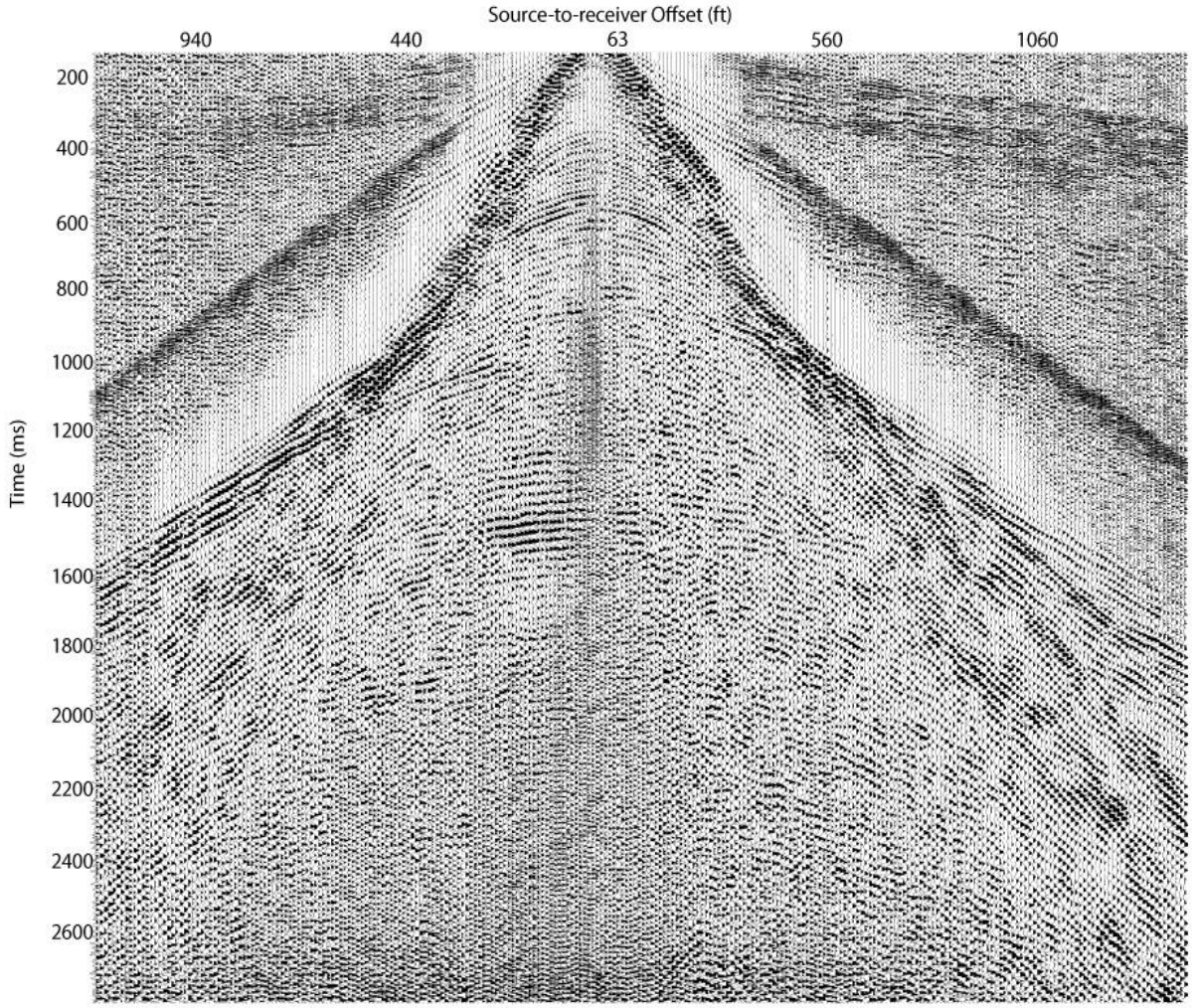


Figure 56. Shot gather from Line 2 using the self-truncating extended correlation method. The lower half of the shot gather is dominated by high-frequency noise.

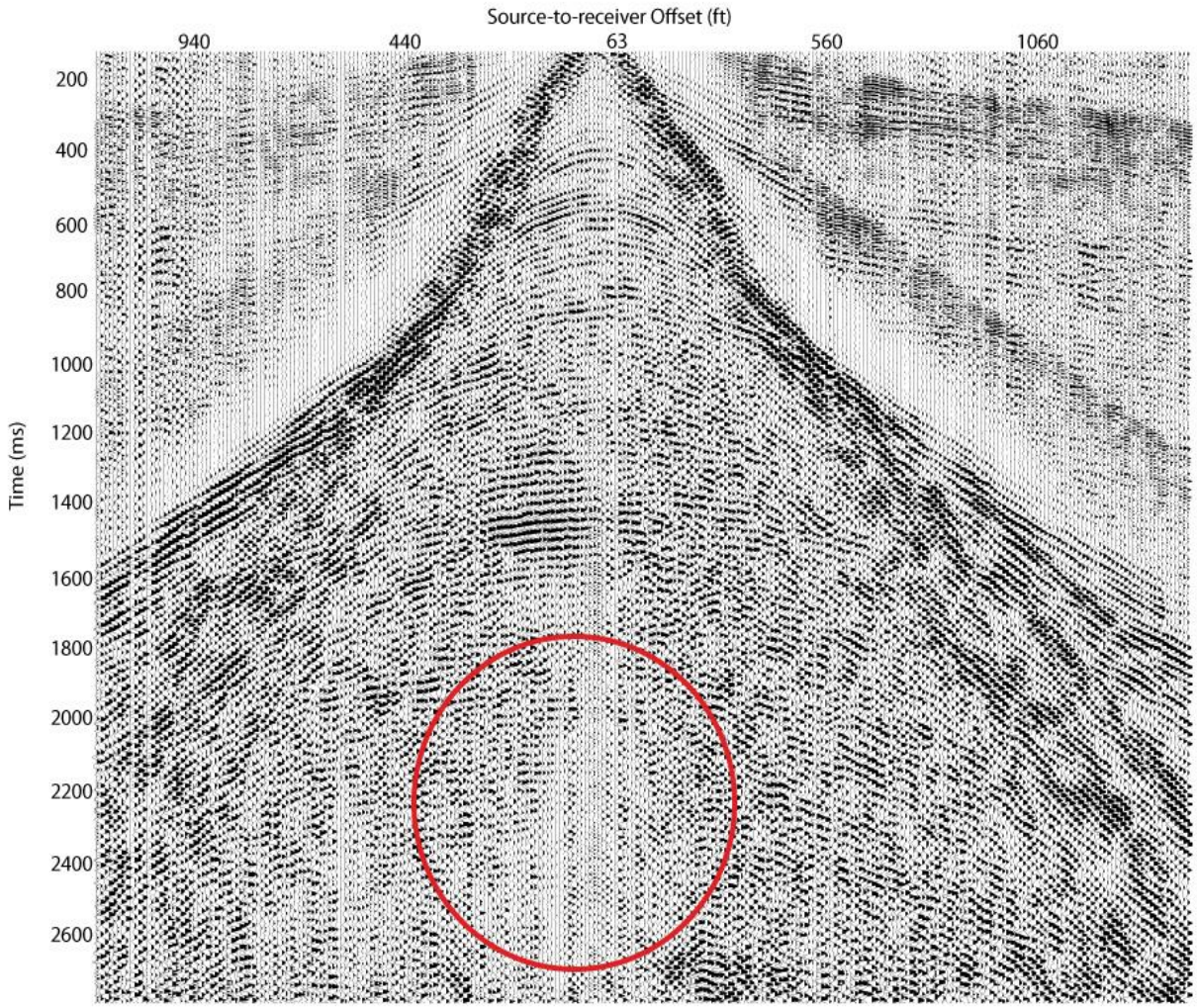


Figure 57. Shot gather from Figure 37 with high-frequency noise removed. Red circle shows area where deeper data are lost due to noise removal and poor signal-to-noise ratio causing reflections to be weak.

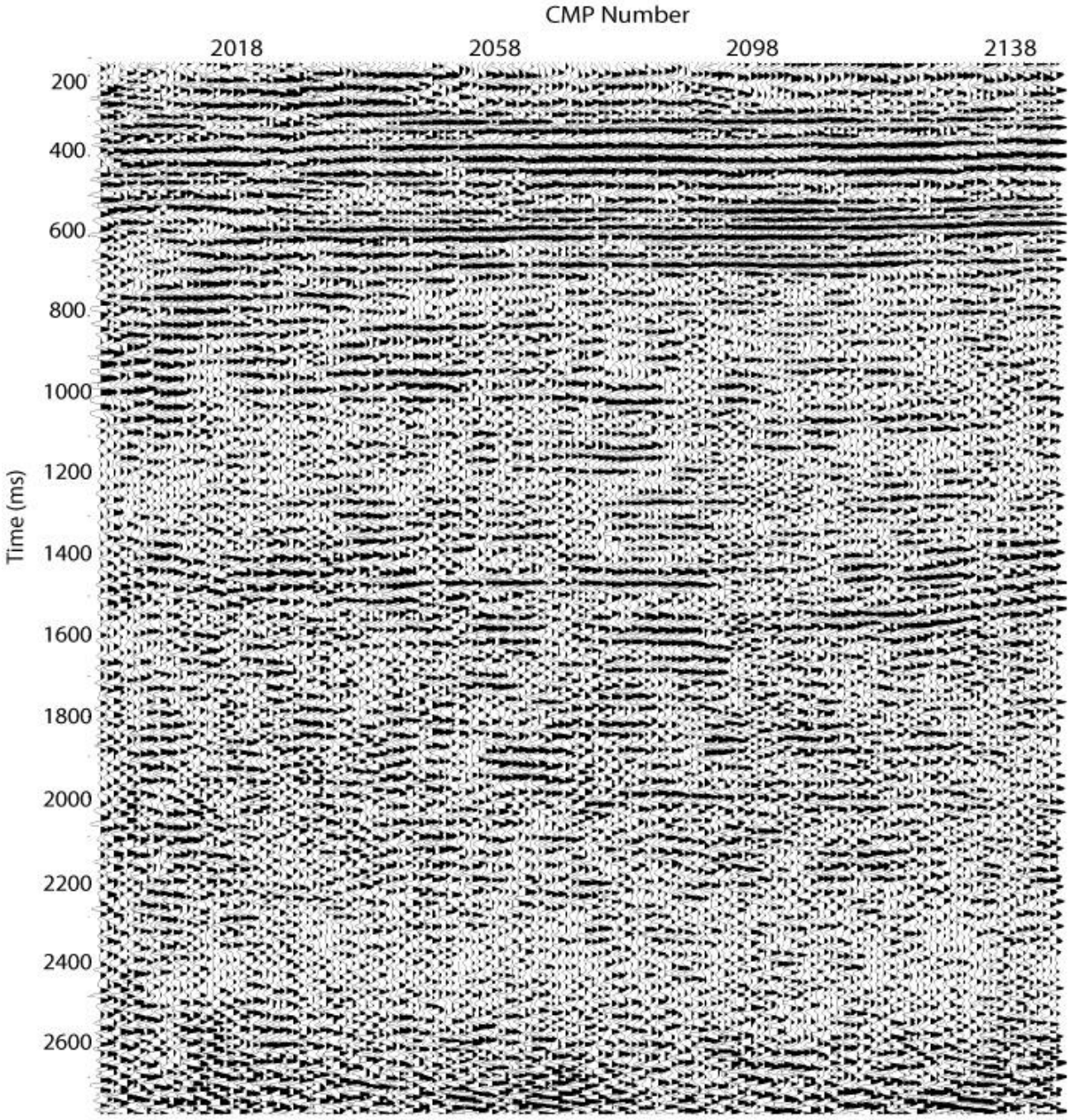


Figure 58. Section 1 of Line 2 extended correlation stack.

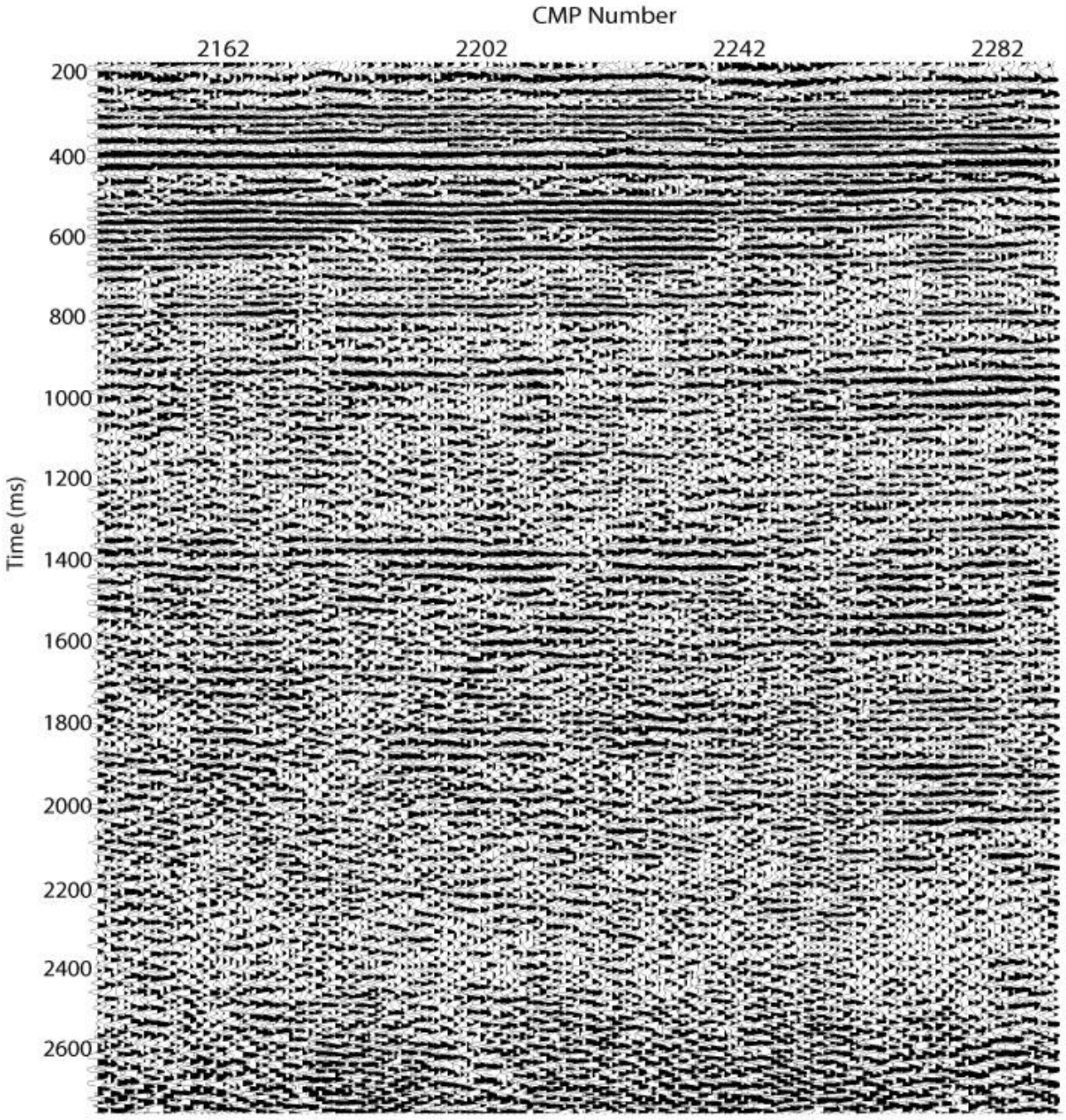


Figure 59. Section 2 of Line 2 extended correlation stack.

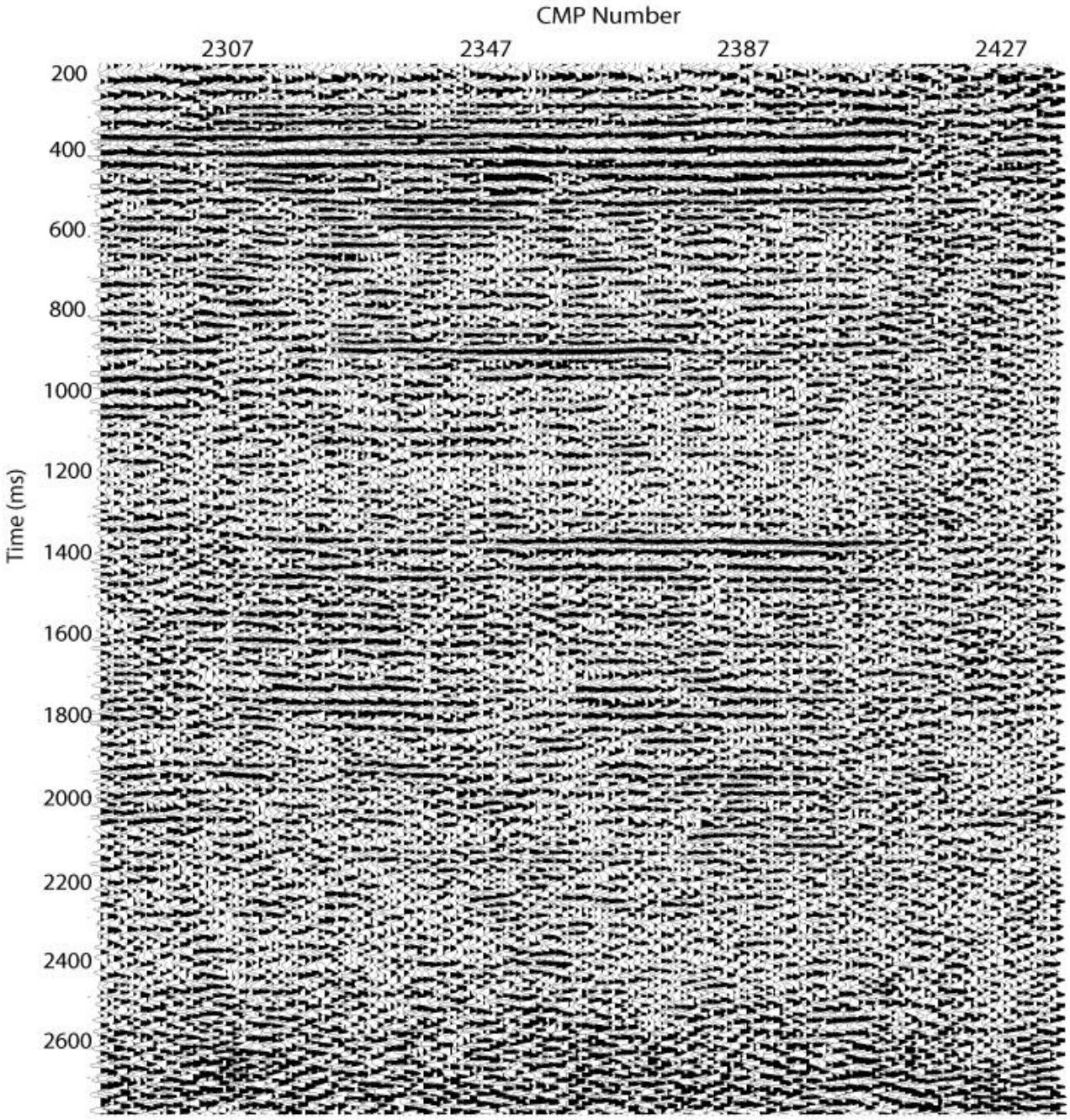


Figure 60. Section 3 of Line 2 extended correlation stack.

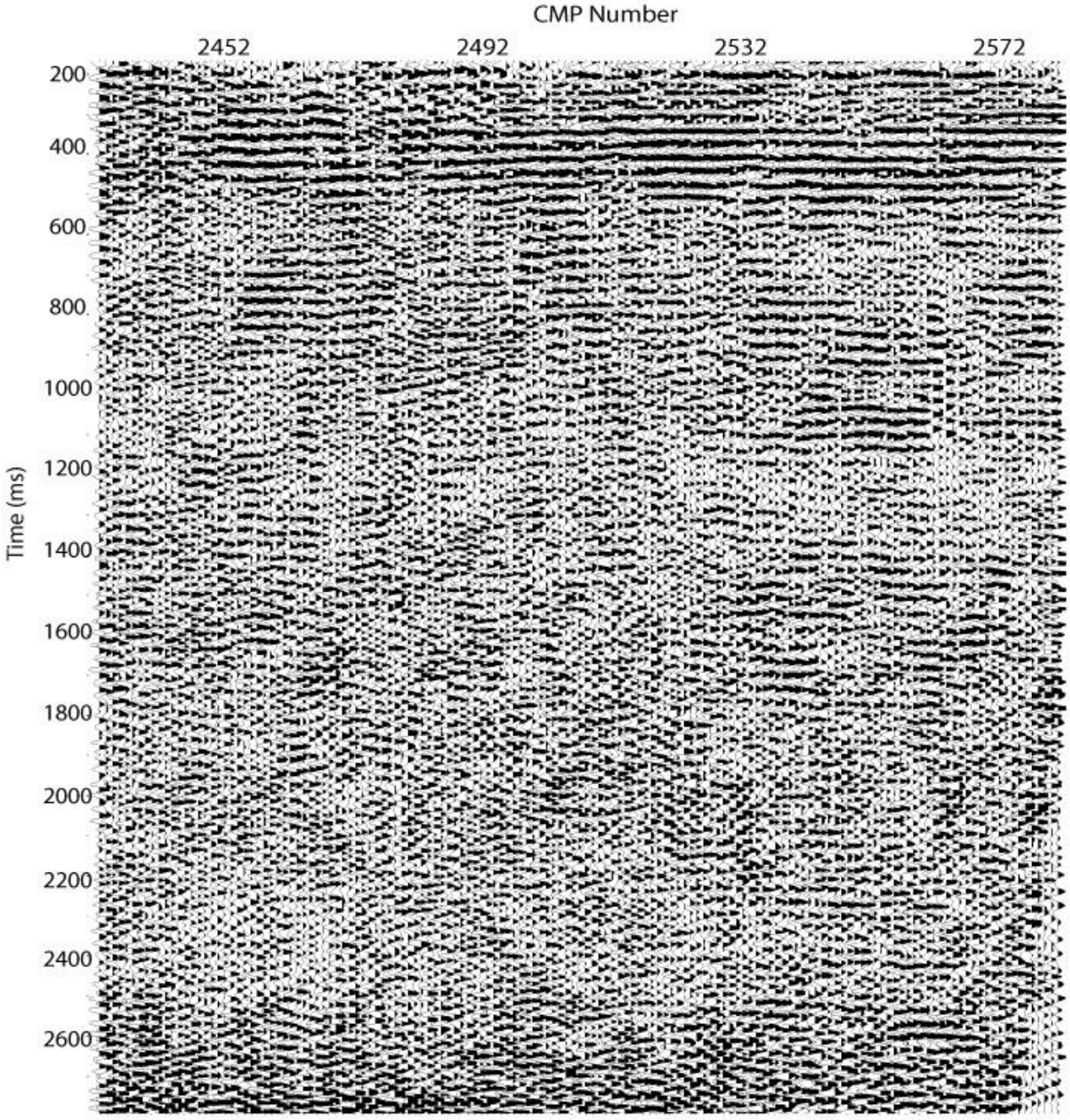


Figure 61. Section 4 of Line 2 extended correlation stack.

## Chapter 4: Inversion of Love waves for surface statics

The MASW (multi-channel analysis of surface waves) is a common method used to obtain S-wave velocity information about shallow materials at depths of generally less than 100 feet (e.g. Miller, 1999; Park, 2013). The MASW method most commonly employs Rayleigh waves (SV polarized surfaced waves) to construct a 1-D $V_S$ profile (Park et al., 1999; Xia et al., 1999). SH polarized Love waves are rarely used in the same fashion. Recently the utility of inverting Love waves through the use of MALW (multi-channel analysis of Love waves) to obtain $V_S$ profiles has been noted (Safani et al, 2006; Xia et al., 2010; Xia et al., 2009). Furthermore, only one example of Love waves being inverted and subsequently used for static corrections on exploration-depth surveys exists in the literature (Mari, 1984).

S-wave data in this study are SH polarized, making recorded surface waves SH polarized Love waves. In this study Love waves were successfully inverted to produce a $V_S$ section, which was then used for surface elevation static corrections. Data was processed by first applying geometry to the uncorrelated field records. Uncorrelated field records were used to avoid introducing any noise caused by the correlation process. Data were then vertically stacked with data from only one side of the split spread used as input into the MALW software.

Within the MALW software different offsets and spread lengths were analyzed and tested to find the optimum parameters for creating good dispersion curves. Data were then cut down to the optimum number of traces to create dispersion curves. Dispersion curves were then picked and inverted to obtain a $V_S$ section. From the $V_S$ section, average velocities were calculated to different depths depending on the model used for elevation corrections. The velocities and depths were then used to correct the reflection data for surface elevation to a flat datum.

### 4.1 Line 1 surface elevation corrections

The processing of Line 1 data for use with the MALW software followed the general flow described above. Dispersion curves from Line 1were very good quality and showed strong fundamental-mode curves as well as higher-mode curves (Figure 58). The inversion of Line 1 dispersion curves gave a $V_S$ profile that extends to a depth of 25 ft (Figure 59). On the profile an area of higher velocity exists from a depth of about 7-15 ft. The model used for inversion is a 10 layer model with 25 % depth inversion ratio (compared to a 50% depth conversion ratio standard for Rayleigh waves). The max RMS was set at 8 and the model converged after 7 iterations.

MASW data were originally collected at the site to provide a $V_S$ profile for the very near surface, however because MASW is SV data, it is not used in this study in conjunction with the SH reflection data. The MALW and MASW profiles show very different models (Figure 60). The MALW profile for Line 1 extends to a depth of only about 25 ft, while the MASW profile gives a deeper section with a depth of about 60 ft. The MALW profile shows a greater detail and more velocity variation than does the MASW profile. The MALW profile does not match well with the MASW profile and the differences in the profiles could suggest anisotropy in the near-surface.

The $V_S$ profile for Line 1 was broken up into a three layer model to be used for elevation corrections. Average velocities were calculated for the first layer (0-7 ft), the second layer (7-15 ft), and the third layer (15-25 ft), using the same software used for Love wave inversion **(**Figure 61). The surface elevation changes over the distance of Line 1 are shown in. Elevations along the line range from 4,125 ft to 4,133 ft (Figure 62). A datum was set at 4,110 ft. A new model was created to take into account these elevation changes over the distance of the line, and an elevation was chosen as a datum for corrections (Figure 63).

Surface elevation statics were then applied to the reflection data based on this model (Figure 64) and can be compared to the data without static corrections (Figure 65). The surface elevation corrections improve the section by bringing out some dipping structure in the left half of the section that was not evidenced before. This has significant implications because it could indicate the presence of another previously unidentified fault.

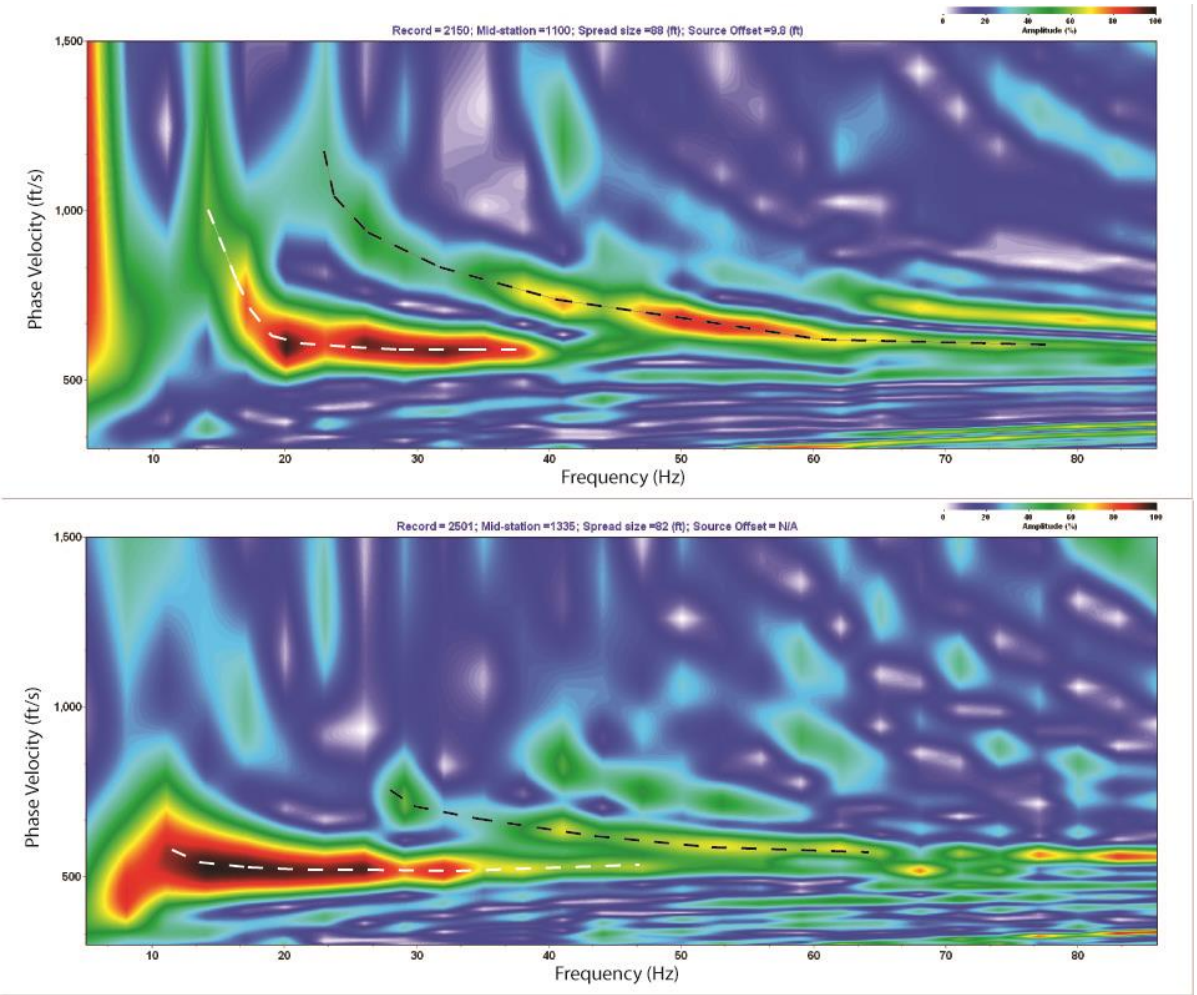


Figure 62. Dispersion curves examples from Line 1. Fundamental modes picked are shown by a dashed white line and higher modes are shown by a black dashed line. Fundamental modes are clear and easy to pick in the Line 1 data.

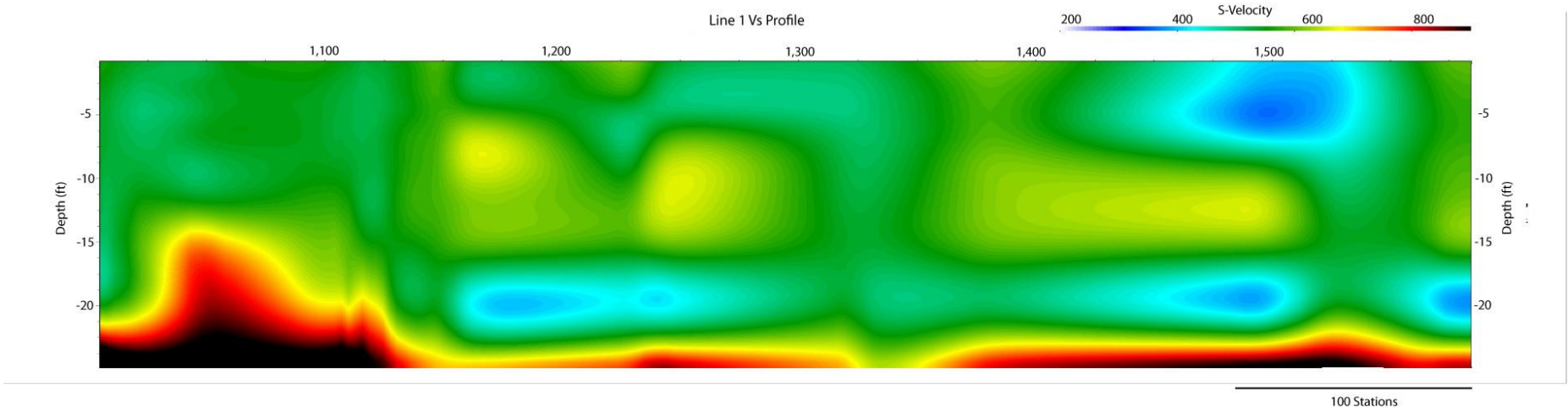


Figure 63. Line 1 $V_S$ profile from the inversion of Love waves.

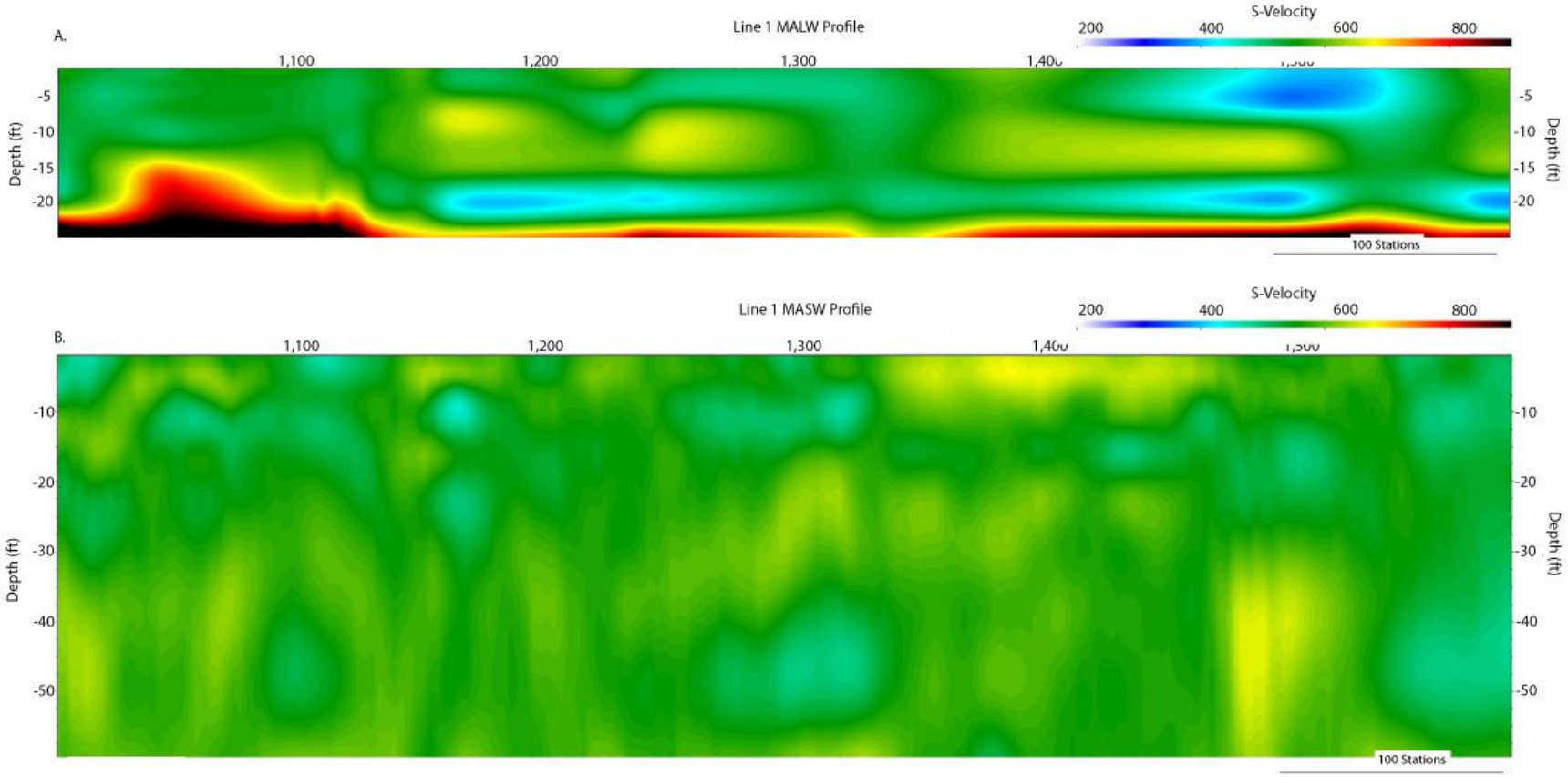


Figure 64. (A) MALW and (B) MASW comparison for Line 1.

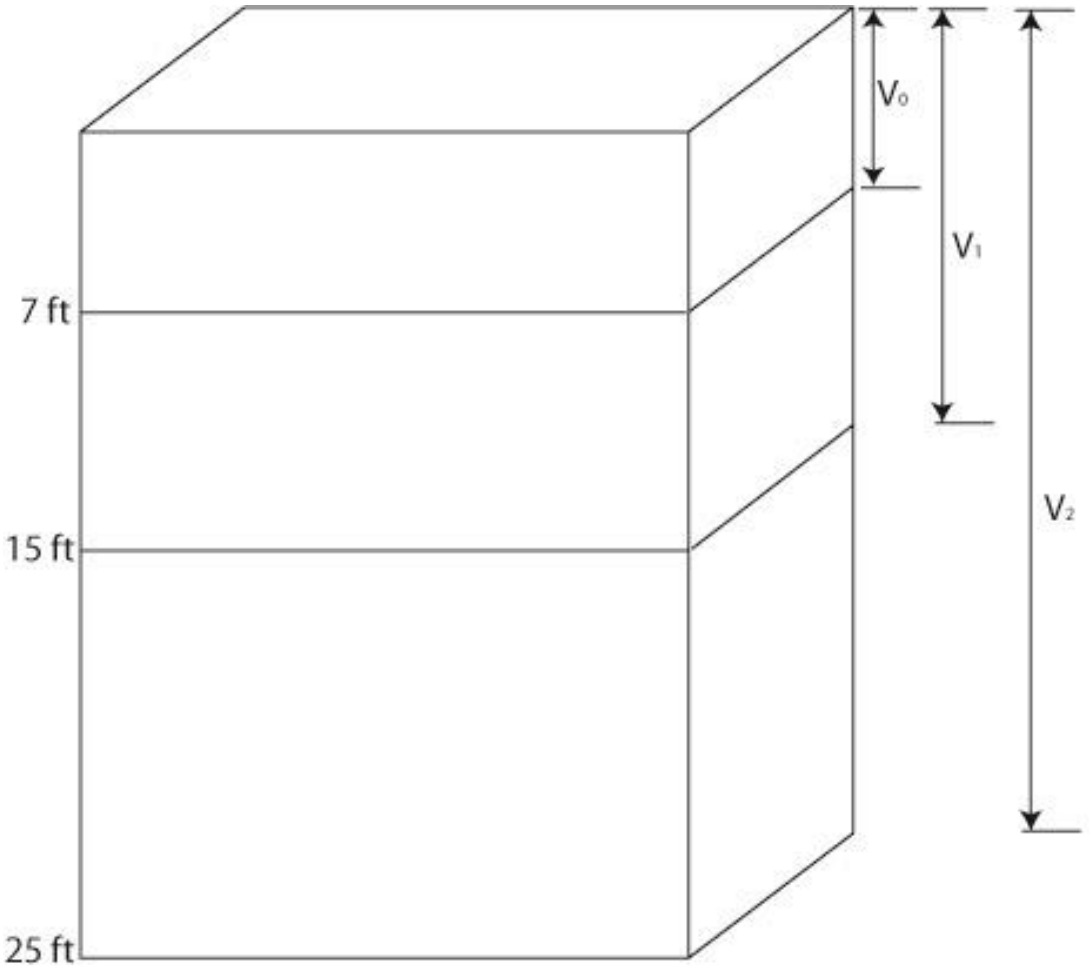


Figure 65. Three layer model for the Vs profile for Line 1. The depths and velocities shown are used for the surface elevation corrections.

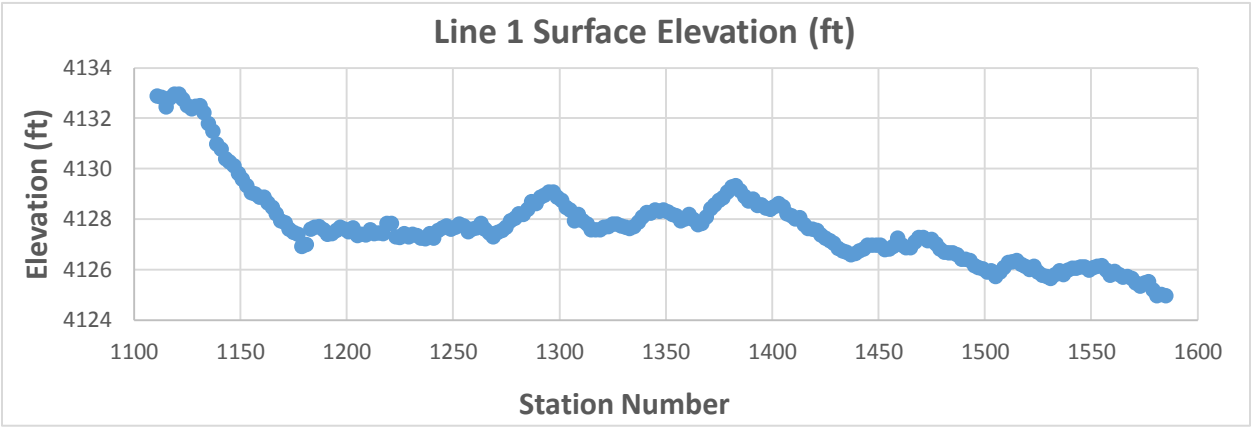


Figure 66. Surface elevations in ft from station numbers 1100 to 1585 for Line 1.

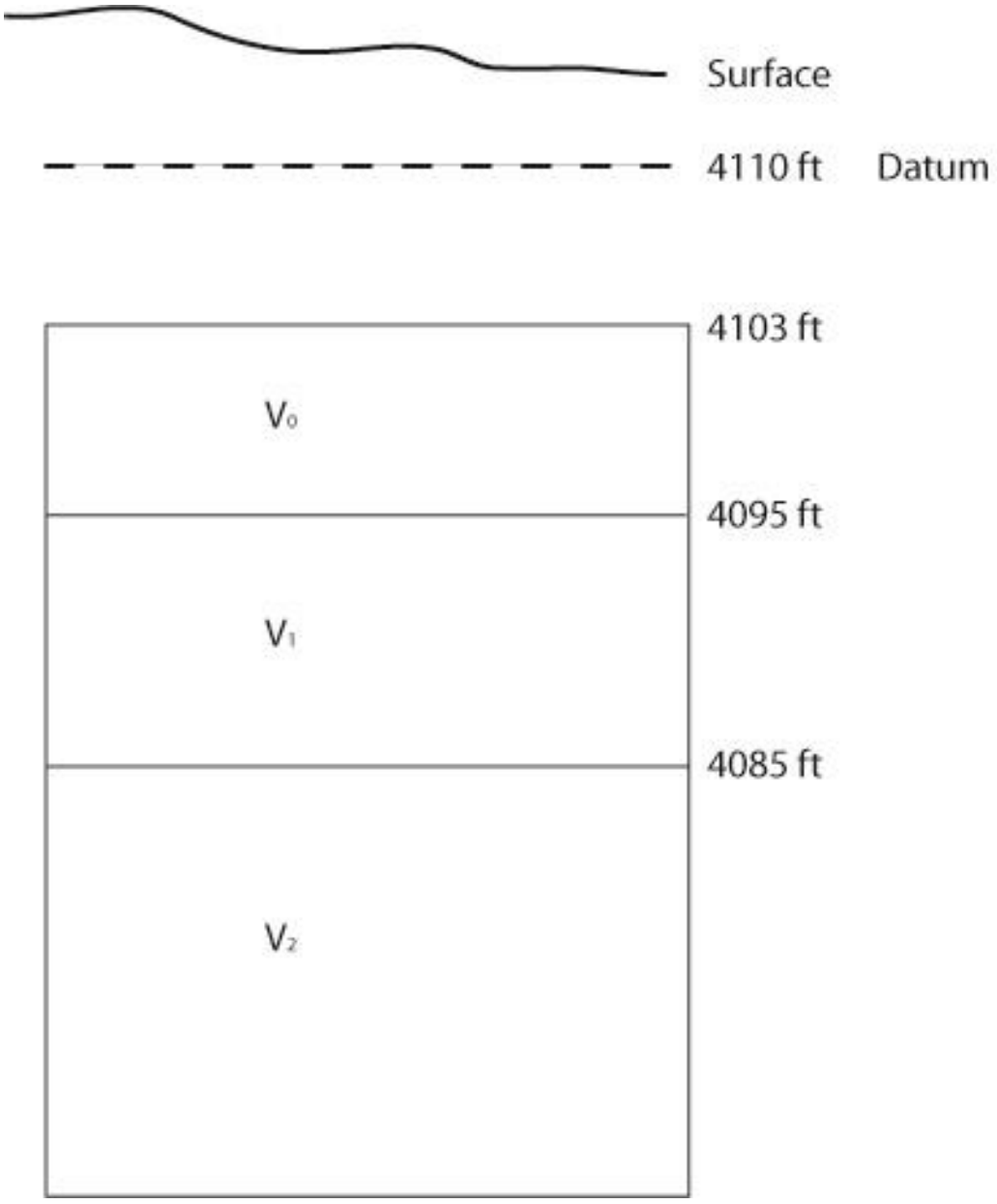


Figure 67. Surface elevation correction model for Line 1 including the true elevation, a datum and the depths of the model layers below datum.

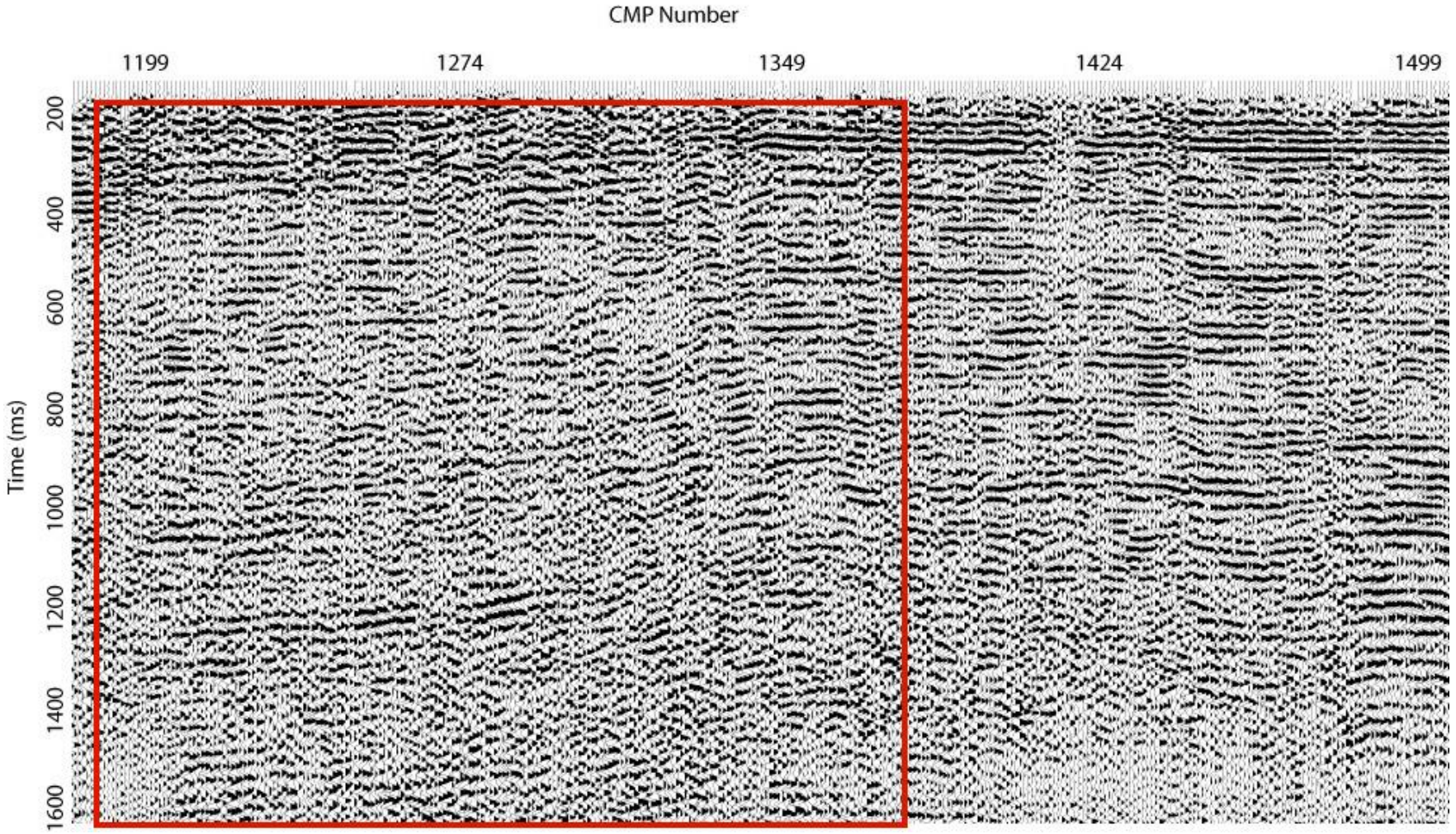


Figure 68. Line 1 with surface elevation corrections applied. Red box indicates area where changes in subsurface structure of reflections can be seen.

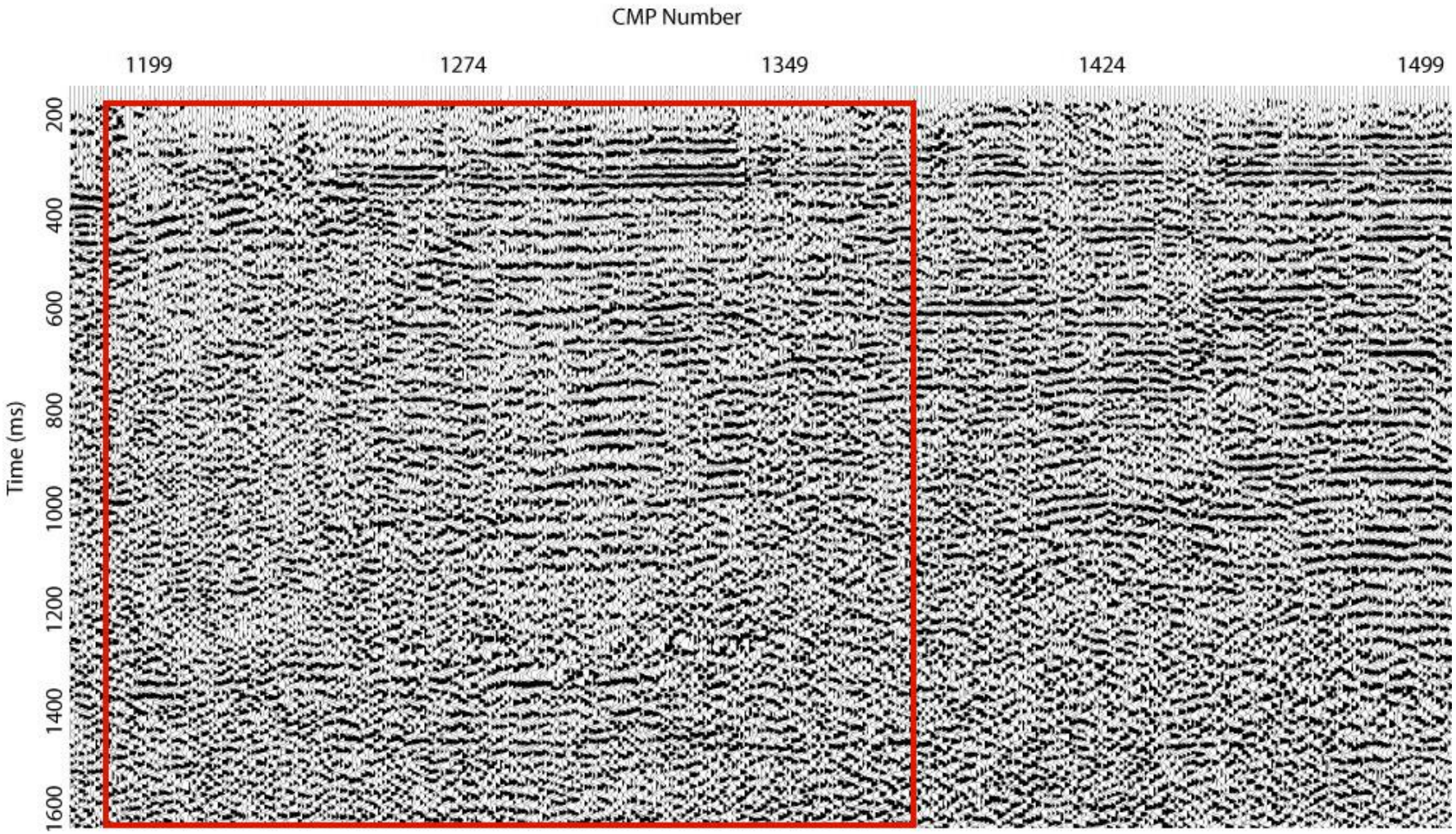


Figure 69. Line 1 with no surface elevation corrections applied. Red box shows the area where changes occurred once statics were applied.

### 4.2 Line 2 surface elevation corrections

The processing of Line 2 data for use with the MALW software followed the general flow described in the beginning Chapter 4. Dispersion curves from Line 2 were much poorer quality when compared to those of Line 1. Fundamental modes were difficult to distinguish from contamination from higher modes making delineating the fundamental mode to pick ambiguous (Figure 66). The inversion of Line 2 dispersion curves gave a $V_S$ profile that extends only to a depth of 13 ft, compared to a 25 ft depth for Line 1 (Figure 67). This is due to the poor quality of dispersion curves. The profile shows a low velocity layer from a depth of about 8ft to 11 ft. The model used for inversion is a 10 layer model with 25 % depth inversion ratio (compared to a 50% depth conversion ratio for Rayleigh waves). The max RMS was set at 8 and the model converged after 7 iterations.

The MALW and MASW profiles for Line 2 show differences as in the Line 1 data (Figure 68). The MALW profile for Line 2 extends to a depth of only about 13 ft, while the MASW profile gives a deeper section with a depth of almost 90 ft. The MALW profile again shows a greater detail and more velocity variation than does the MASW profile. The bottom of the MALW profile seems to match with a higher velocity layer in the MASW profile at about the same depth on Line 2.

The $V_S$ profile for Line 2 was broken up into a three layer model for elevation corrections. Average velocities were calculated for the first layer (0-8 ft), the second layer (8-11 ft), and the third layer (11-13 ft), using the same software used for Love wave inversion (Figure 69). The surface elevation changes over Line 2 range from 4,125 ft to 4,132 ft. The datum was set to 4,110 ft Figure 70. A new model was created to take into account these elevation changes over the line, with an elevation that was chosen as a datum for corrections (Figure 71).

Surface elevation statics were then applied to the reflection data based on this model (Figure 72) and compared to the original section with no surface elevation corrections (Figure 73). The section with surface elevation corrections applied shows that a previously interpreted unfaulted layer is actually affected by the fault. This is significant because this unfaulted layer suggests that faulting had ceased a significant amount of time ago and is a minimal threat to surface structures. However, if faulting affects recently deposited layers, especially directly underneath a dam, significant implications come with these findings.

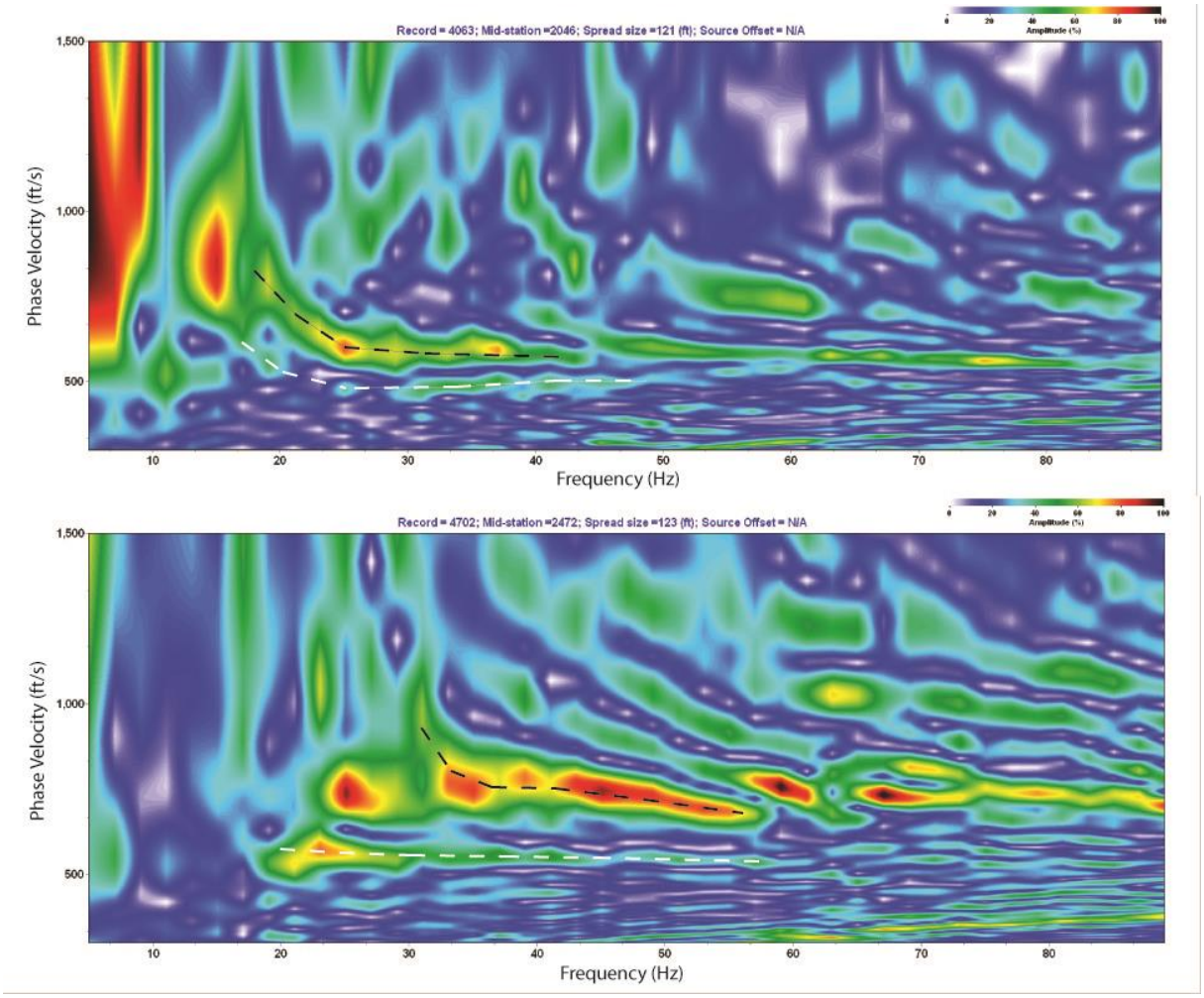


Figure 70. Dispersion curve examples from Line 2. Dispersion curves from Line 2 are difficult to interpret and fundamental modes are not easily picked. Fundamental mode is shown with a dotted white line and higher modes with a dotted black line.

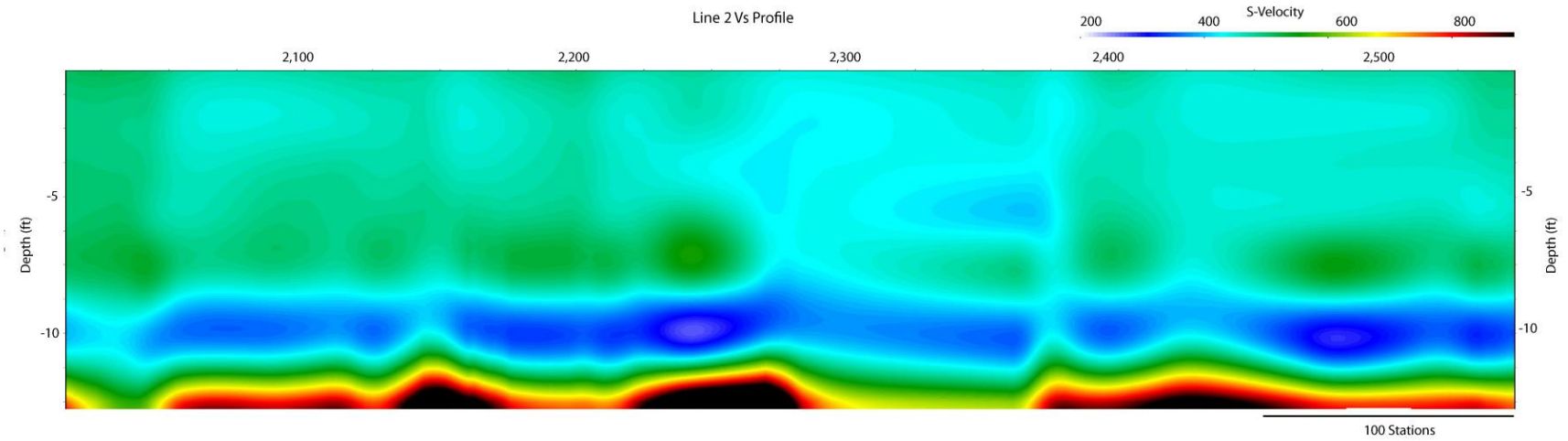


Figure 71. Vs profile from inverted Love waves for line 2.

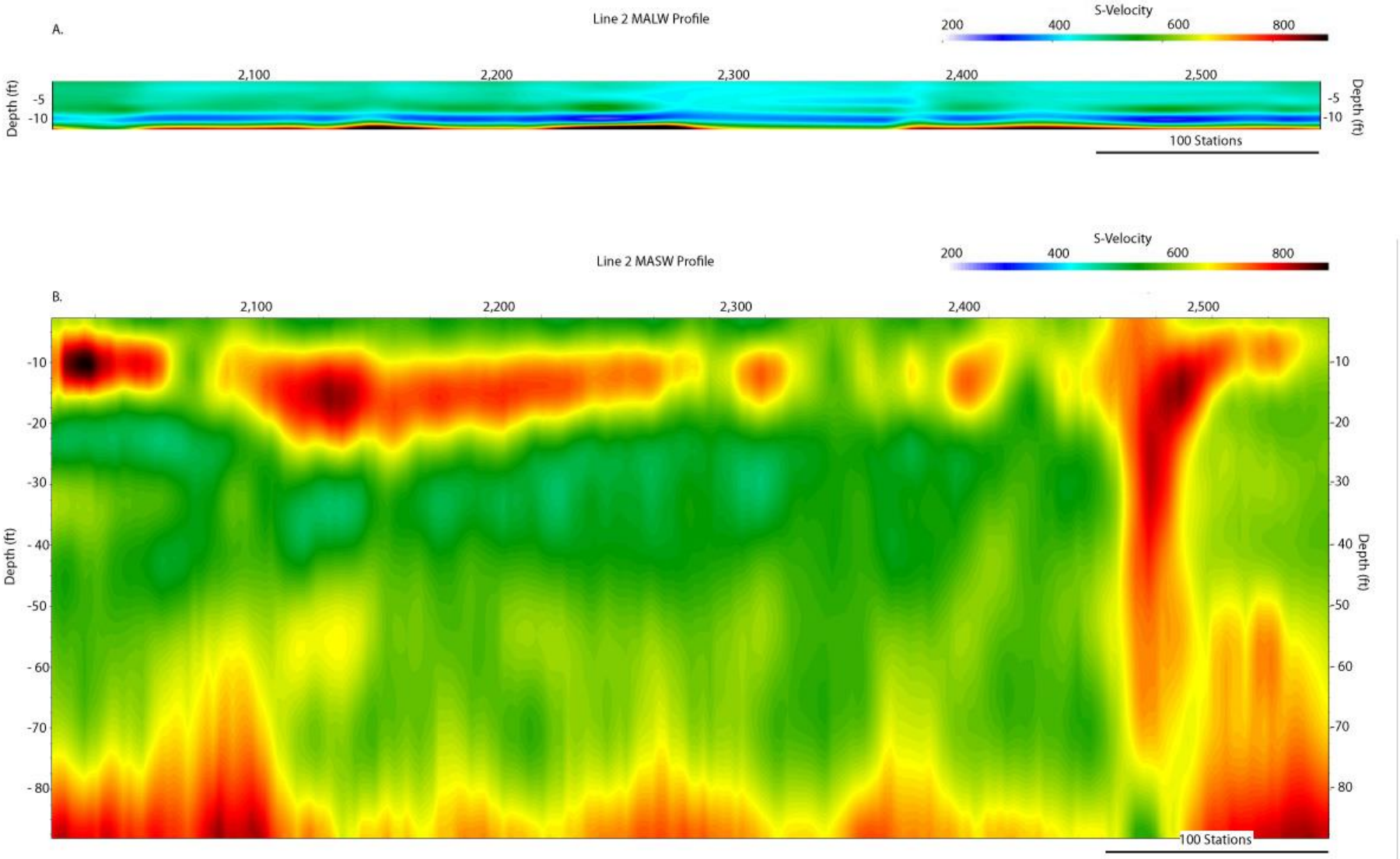


Figure 72. (A) MALW and (B) MASW comparison for Line 2.

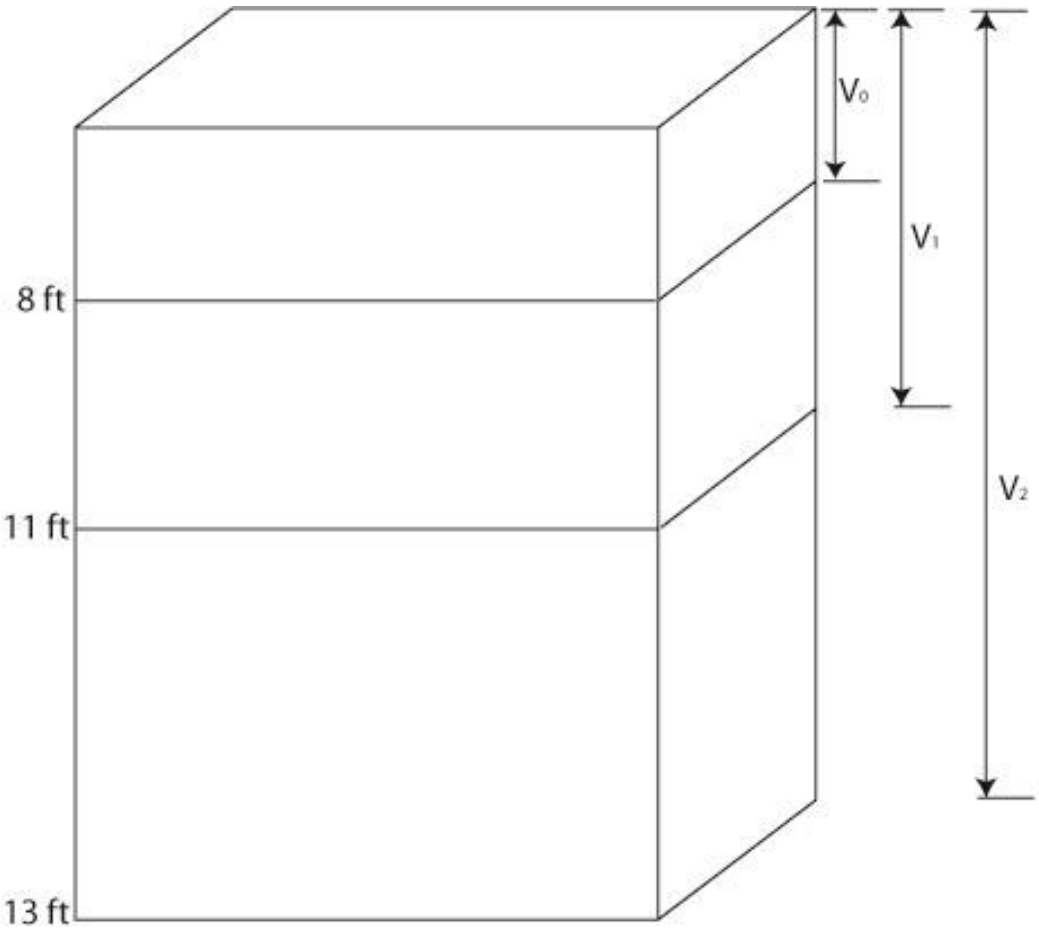


Figure 73. 3 layer model based on Vs profile from the inversion of Love waves for Line 2

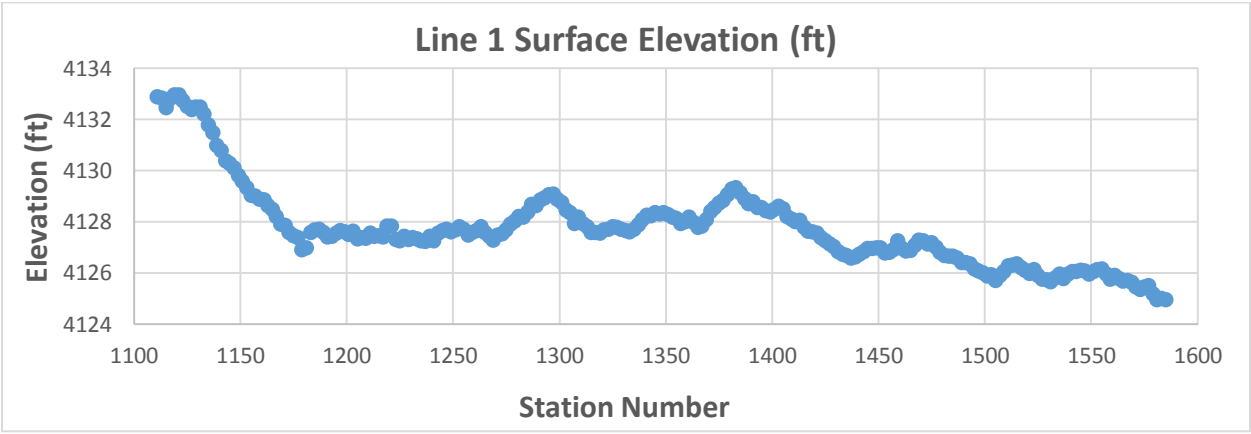


Figure 74. Line 2 surface elevations

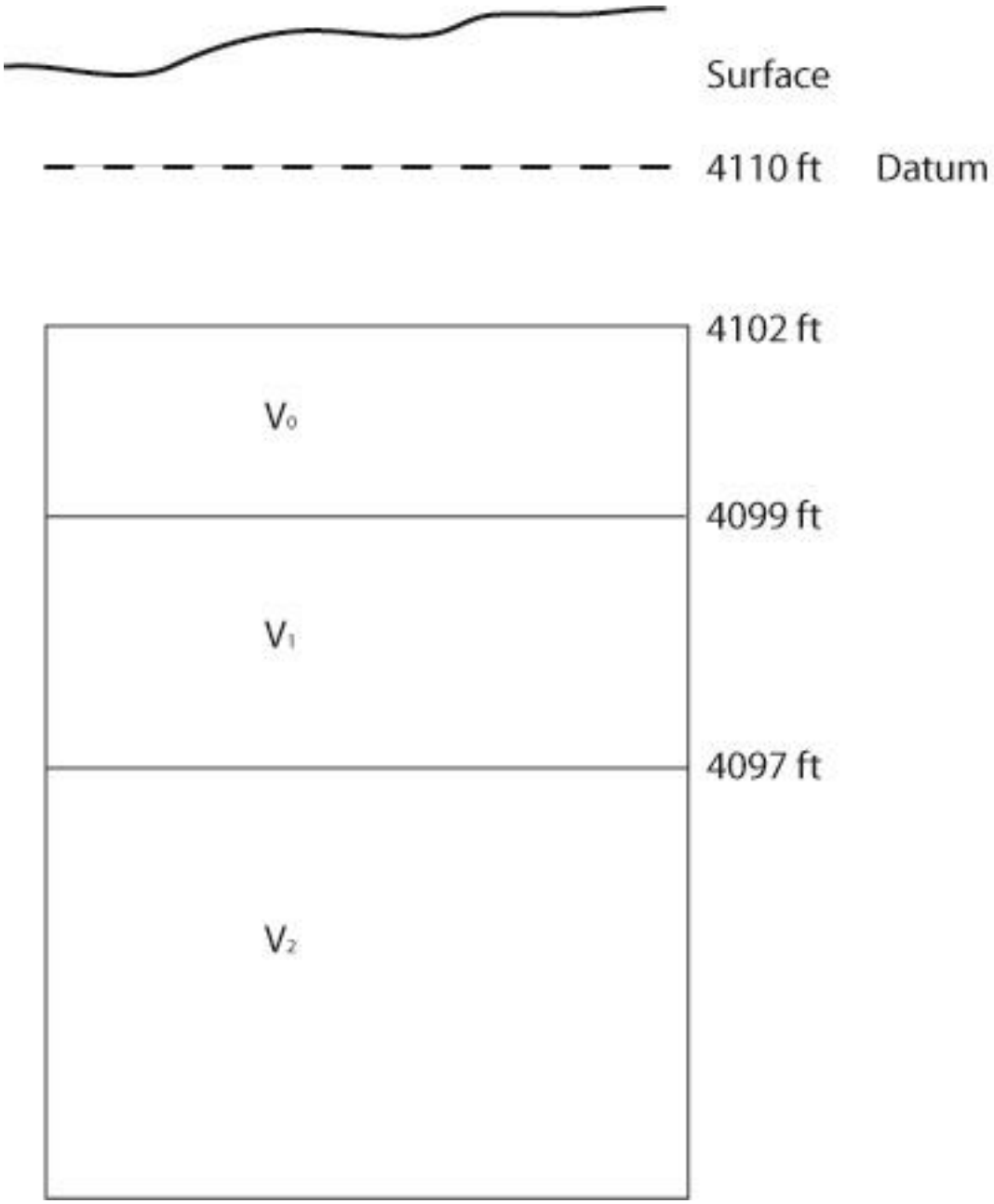


Figure 75. Surface elevation correction model for Line 2 including the true elevation, a datum and the depths of the model layers below datum.

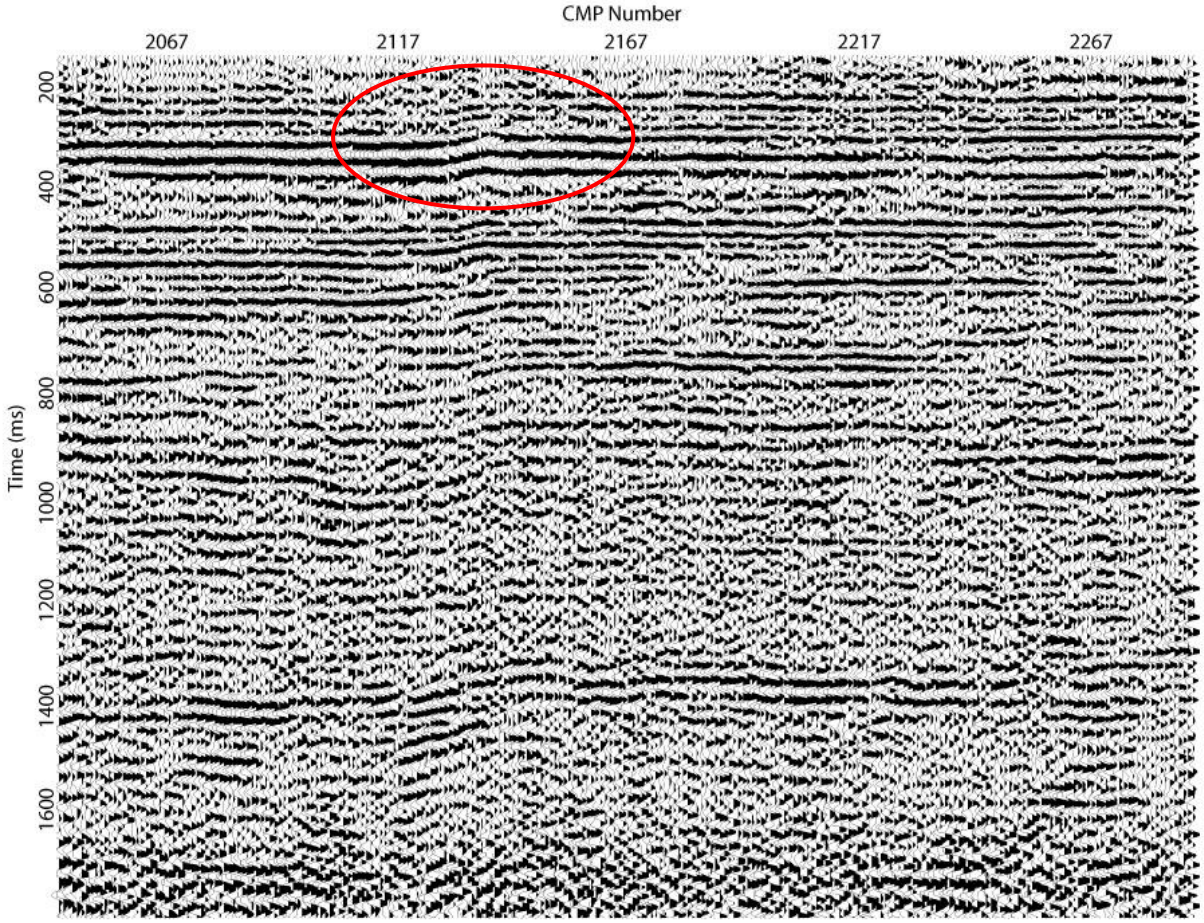


Figure 76. A portion of the Line 2 stacked section that has been corrected for surface elevation statics. A previously unfaulted layer is shown in the red circle.

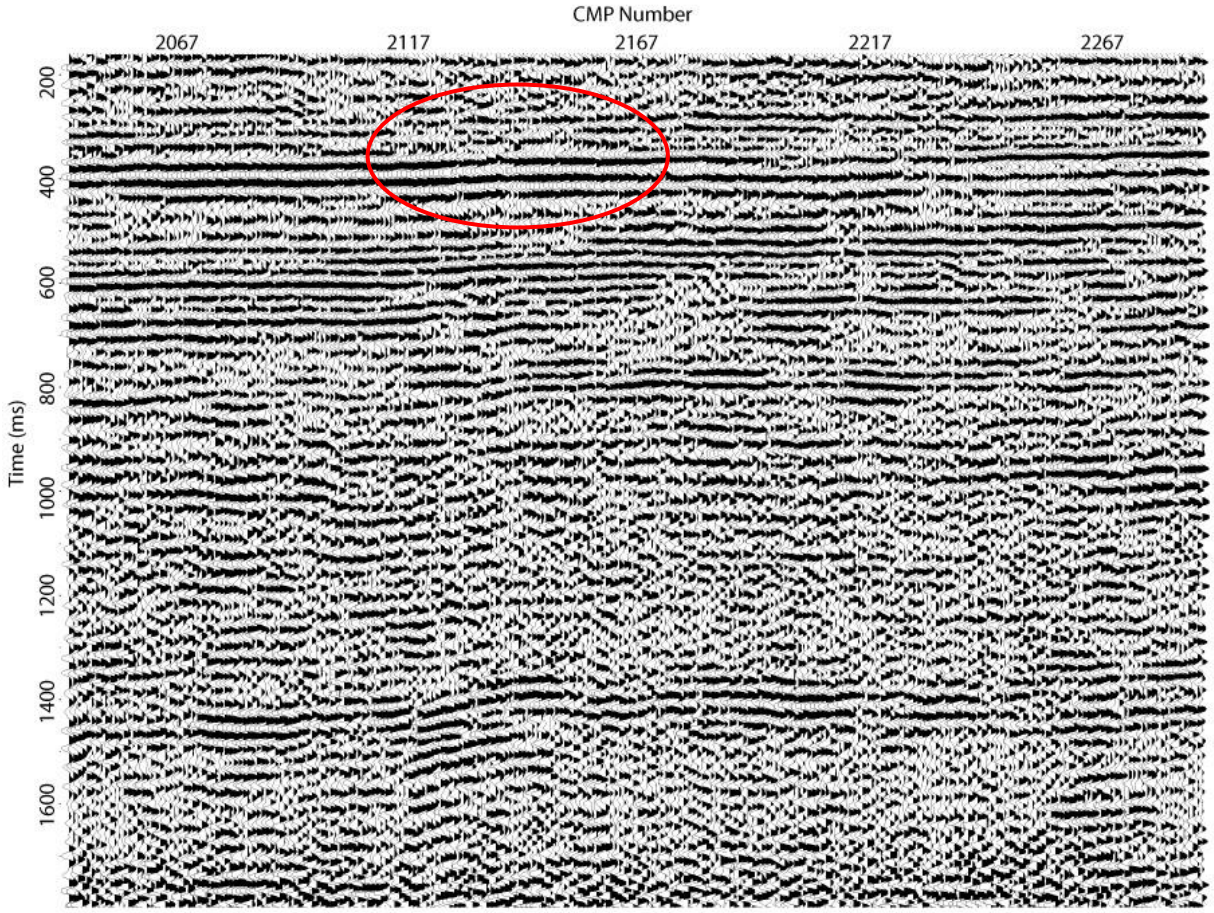


Figure 77. Original stacked section with no surface elevation corrections applied. The red circle shows the layer that appeared flat before corrections.

## Chapter 5: Geologic Interpretation

The study site is located in the Great Basin on the eastern margin of the Great Salt Lake. Around 17.5 million years ago, with the formation of the San Andreas Fault, the Great Basin began to form (Hintze, 2005). As the San Andreas grew in length, the Great Basin grew in width. The spreading of the Great Basin contributed to the formation of the roughly north-south oriented reverse Wasatch fault, which is the most significant fault in the state of Utah. As the basin spread, earthquakes were induced along the Wasatch Fault.

The Great Basin is characterized by a basin and range topography, where mountain ranges are separated by valleys that are eventually filled with erosional debris from the mountains (Hintze, 2005). Many of the valleys in the Great Basin specifically are also covered with a layer of lacustrine deposits from the ancient Lake Bonneville, which covered much of the Great Basin region in prehistoric times. Lake Bonneville existed from about 32,000 years ago to 14,000 years ago. The Great Salt Lake is a remnant of the ancient Lake Bonneville. The near-surface sediments are comprised of over 3,000 ft of valley fill deposits (Figure 76) (Hintze, 2005). The seismic sections in this study do not image below the sediments. All sediments imaged are of Pliocene-Miocene age, or younger than about 23 million years old (Figure 76) (Hintze, 2005).

Detailed geologic information below depths of about 200 ft for this area is not available and sediments can only be identified generically to depths of 3000 ft. General descriptions of sediments present in the upper 200 ft are provided by the U. S. Bureau of Reclamation (Figure 77).

## OGDEN AREA ROCK COLUMN

| Age | Formation | Thickness in feet | Lithology and fossils |
|---|---|---|---|
| Quaternary | Alluvium, soil | 0-100 | also Lake Bonneville deposits |
| Pliocene–Miocene | valley-fill deposits | 3,000 | present in the subsurface under the Ogden and Great Salt Lake valleys |

Figure 78. Ogden area representative rock column. S-wave sections extend to depths of ~1100 ft into Pliocene-Miocene aged valley-fill deposits (Modified from Hintze, 2005).

**General Geologic Legend**

| | |
|---|---|
| ***Qbs*** QUATERNARY BEACH SAND DEPOSITS: Divided into two units. A younger (Qbs1) unit is though to represent beach or near-shore deposits comtemporaneous with more recent levels of the Great Salt Lake. An older (Qbs2) unit is though to be beach or near-shore deposits representing a stage near the end of Lake Bonneville and prior to the Great Salt Lake. | ***Qbc*** QUATERNARY BONNEVILLE CLAY DEPOSITS: Divided into three units. A younger (Qbc1) unit is thought to represent near-shore deposits contemporaneous with more recent levels of the Great Salt Lake. An older (Qbc2) unit is though to be lacustrine (lake deposits) representing a stage near the end of Lake Bonneville and prior to the Great Salt Lake. An undifferentiated unit (Qbcu) in included in areas of the foundation where it is unclear where to divide the younger (Qbc1) unit from the older (Qbc2) unit. |
| ***Qbs1*** Deposit laboratory gradations average 44.7 percent fines, 54.2 percent sand, and 3.2 percent gravel with a liquid limit of 28.5 percent and a plasticity index of 10.6 percent. This average gradation would be classified as Clayey Sand following the Unified Soil Classification System (USCS). | ***Qbc1*** Deposit laboratory gradations average 92.9 percent fines, 6.7 percent sand, and no gravel with a liquid limit of 43.4 percent. This average gradation would be classified as Lean Clay following the Unified Soil Classification System (USCS) |
| ***Qbs2*** Deposit laboratory gradations average in 53.5 percent files, 48.4 percent sand, and no gravel, with a liquid limit of 37.2 percent, and a plasticity index of 20.3 percent. This average gradation would be classified as Clayey Sand following the Unified Soil Classification System (USCS). | ***Qbc2*** Deposit laboratory gradations average 76.6 percent fines, 21 percent sand, and no gravel with a liquid limit of 39.8 percent, and a plasticity index of 18.9 percent. This average gradation would be classified as Lean Clay with Sand following the Unified Soil Classification System. |
| | ***Qbcu*** Deposit laboratory gradations average 84.4 percent fines, 14.5 percent sand, and 1.1 percent gravel with a liquid limit of 36.4 percent, and a placticity index of 18.4 percent. This average gradation would be classified as Lean Clay following the Unified Soil Classification System (USCS). |

Figure 79. General geologic descriptions of sediments of both lines provided by the U. S. Bureau of Reclamation.

### 5.1 Line 1 Interpretation

Line 1 is located on a SW-NE trending section of the dam (Figure 78). The geologic section for Line 1 to depths of 200 ft shows layered sediments with the deepest layer consisting of a Lean Clay as classified by the Unified Soil Classification System. This layer is overlain by a sequence of a Clayey Sand, followed by a Lean Clay, and at the surface a Clayey Sand layer. All of these layers are overlain by the earthen dam embankment (Figure 79).

At depths greater than 200 ft, only more general information exists for areas nearby the Willard Bay Reservoir in the Weber Delta district about 6 miles from the reservoir, as seen in Feth et al., (1966) (Figure 80). The Lake Bonneville Group extends to about 4,000 ft above sea level (Feth et al., 1966), which is about where the detailed geologic information ends in Figure 79. Results from previous geophysical studies in the area indicate that the unconsolidated fill could be upwards of 6,000 ft thick in the deepest part of the trough underlying the Weber Delta district (Feth et al., 1966). Though the Bonneville deposits do not represent a large part of the overall depositional history in the basin, geophysical data suggest that underlying sediments consist of the same types of materials as the lacustrine Bonneville Group deposits (Feth et al., 1966). Below the Weber Delta, at depths of at least 800 ft, deposits consist primarily of sand and gravel in fan-like patterns extending from the mouth of the Weber canyon (Feth et al., 1966). It is likely that deposits beneath the Willard Bay Reservoir site consist of the same types of sediments based on the proximity to the Weber Delta district.

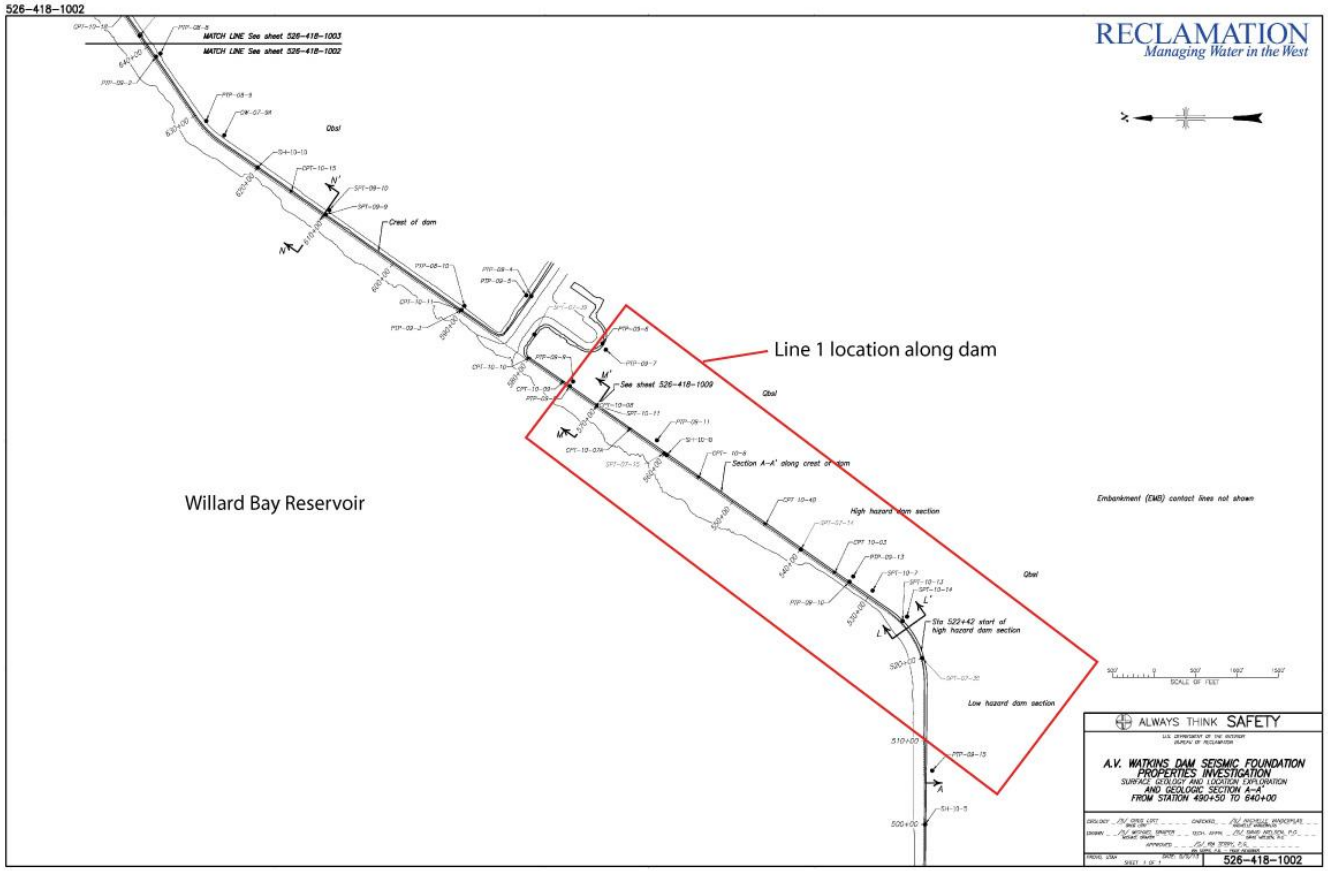


Figure 80. Approximate location of Line 1 along the A. V. Watkins dam surrounding the Willard Bay Reservoir. The cross section is the approximate length of the SW=NE trending line shown in the red box. Provided by the U.S. Bureau of Reclamation.

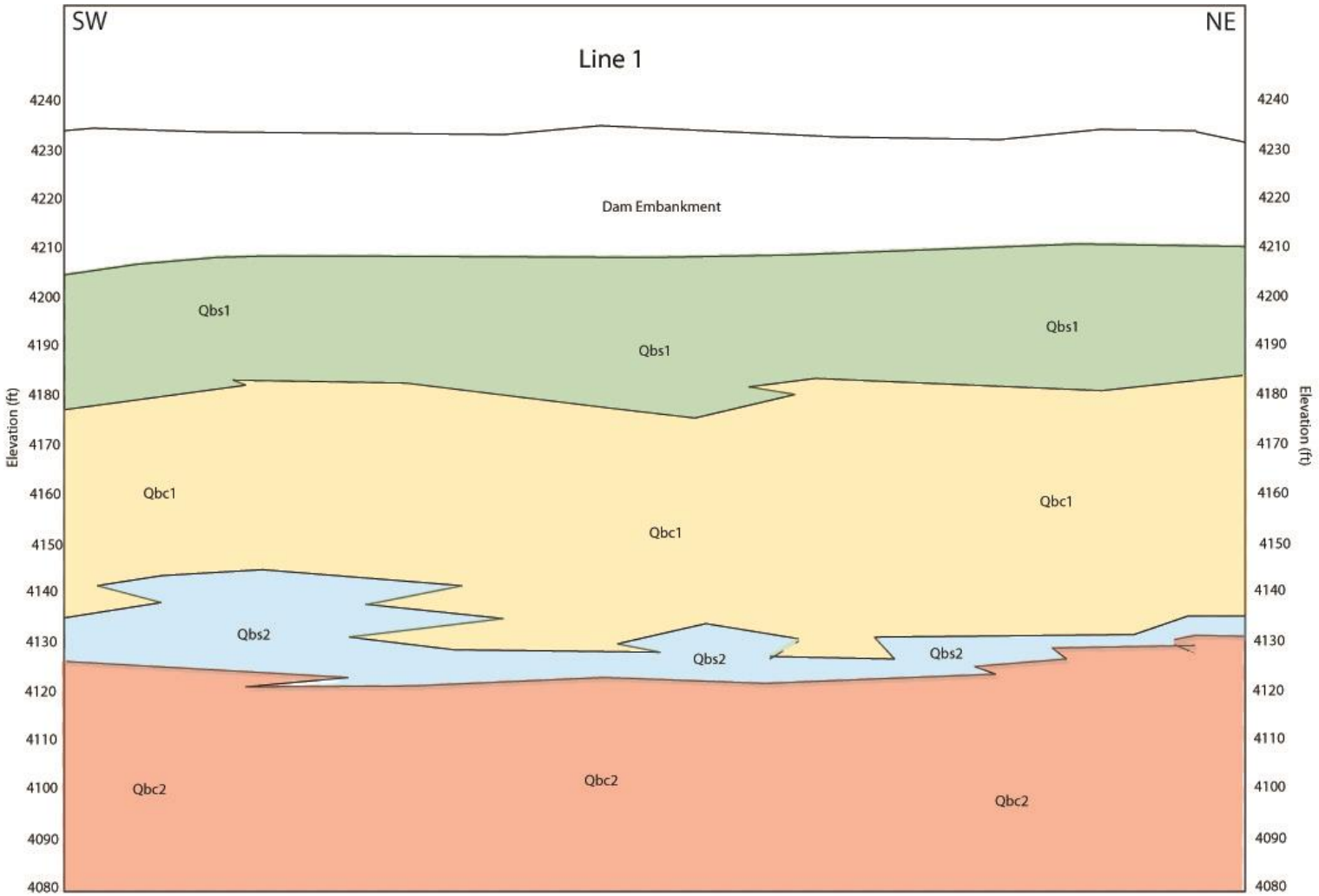


Figure 81. Geologic interpretation of Line 1 based on wells drilled by the U.S. Bureau of Reclamation. Data is available to depths of about 200 ft.

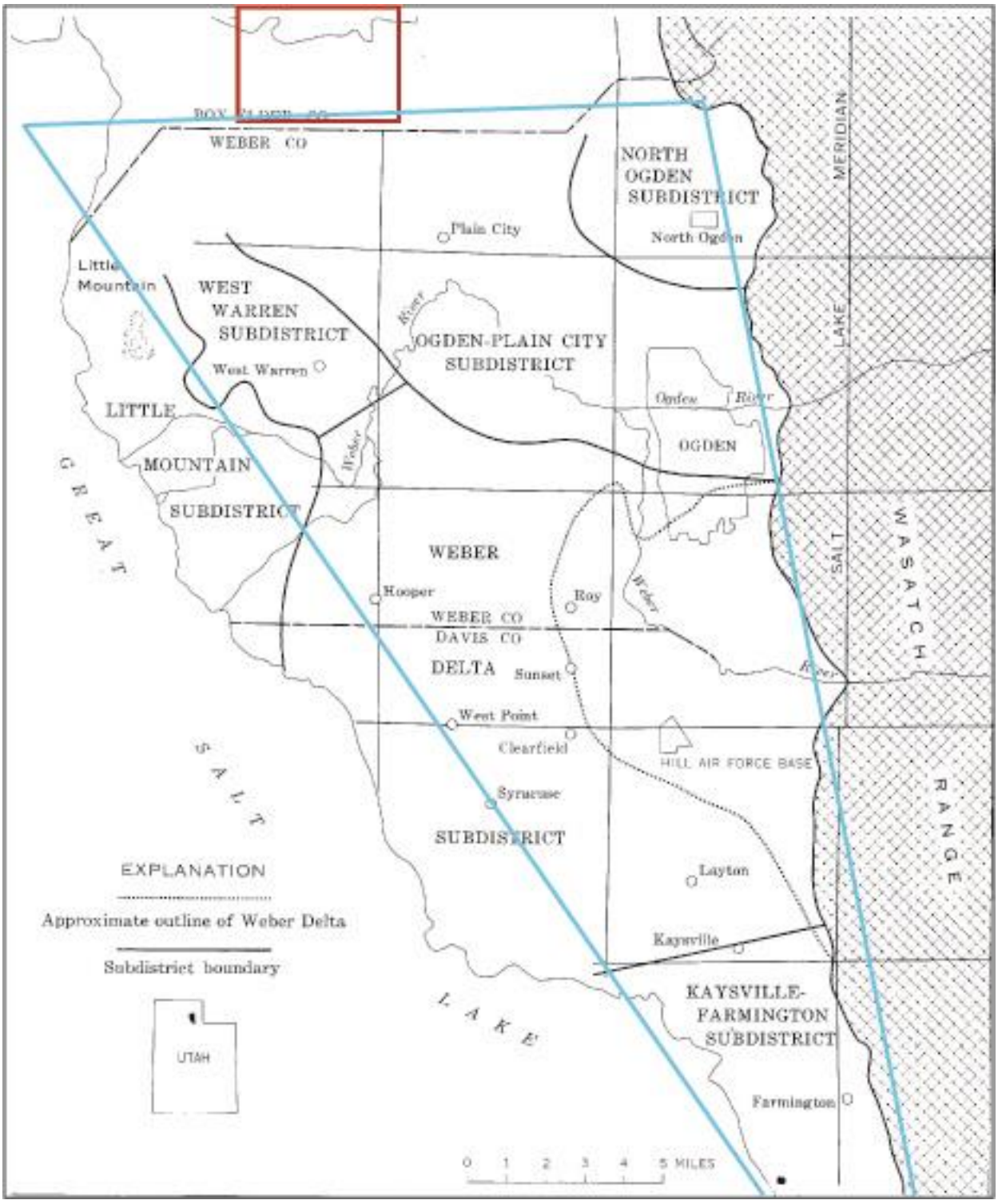


Figure 82. Map of the Weber Delta district (outlined in blue) in relation to the approximate location of the southern portion of the Willard Bay Reservoir (inside red box) to show proximity (Modified from Feth et al., 1966).

One possible geologic interpretation of the seismic data is given based on the geologic information for the upper ~200 ft on-site and information from wells in the adjacent Weber Delta district (Figure 81, 82). Below ~200 ft, interpretations are very general with greater uncertainty but it is clear that the materials here consist entirely of unconsolidated sediments based on geologic cross sections for the area. Below 200 ft packages of reflections are divided according to how their appearances compare to the known reflection packages in the upper 200 ft. There are fewer continuous reflections relative to other portions of the section from 200-275 ft much like the classified layer of Lean Clay above it, suggesting this layer largely consists of clayey material (blue). Reflections from 275-425 ft are similar to the known layers consisting of clayey sand and therefore could also consist of clayey sand (red). The next section from 425 ft – 575 ft shown in green is interpreted to consist clay layers based on the geologic information from the upper 200 ft. Reflection characteristics are similar between this layer (green) and the known lean clay layers. Reflections from 575 ft to 750 ft (yellow) are interpreted to consist of clayey sand. Reflection characteristics are similar to the clayey sand layers in the upper 200 ft. Reflections from 750 ft – 950 ft (purple) are interpreted to have similar characteristics to the known clayey sand layers. Data from the Weber River delta suggest that at these depths gravel is present. The deepest set of reflections (grey) are interpreted to have a Lean Clay make up.

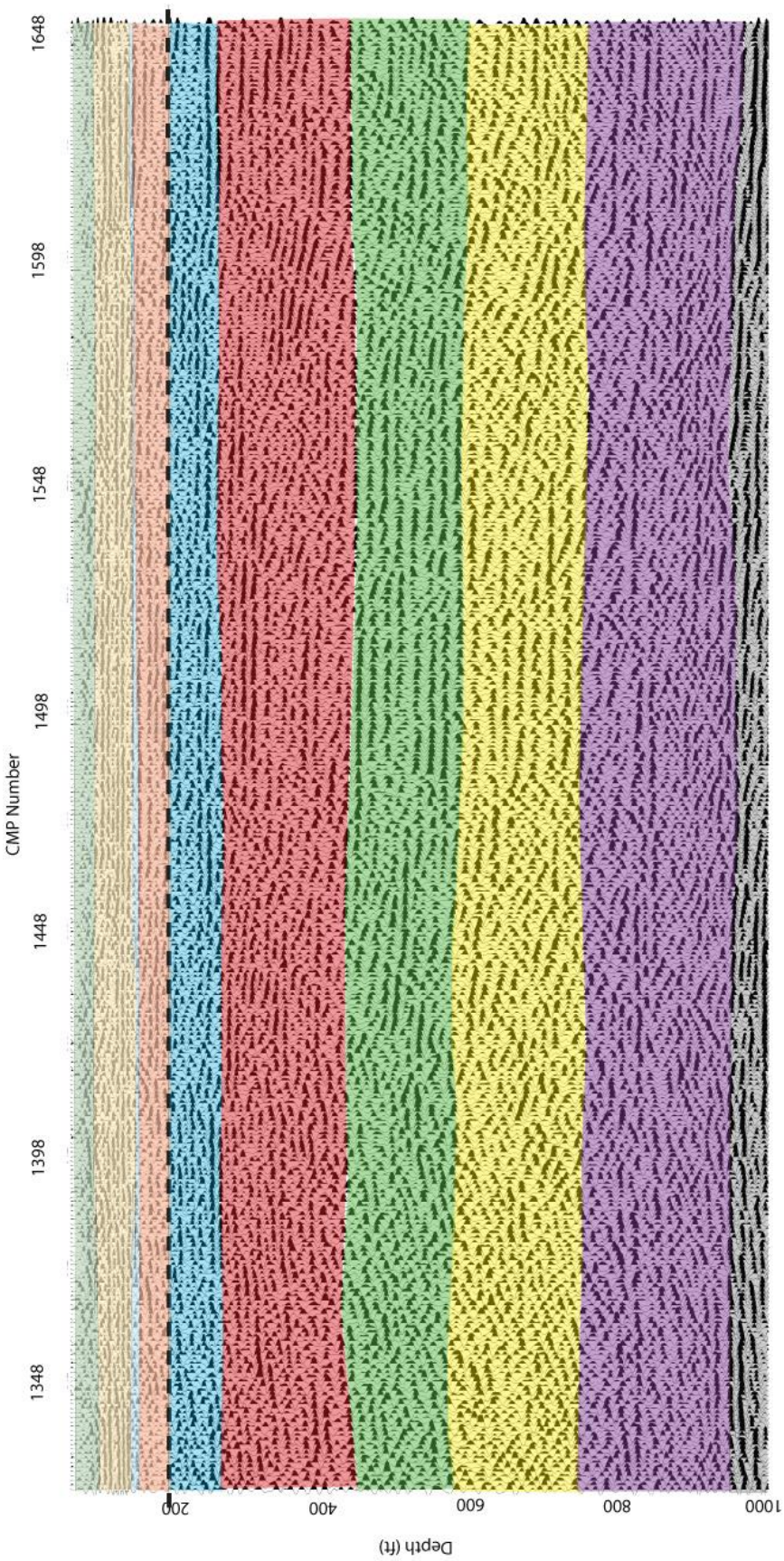


Figure 83. NE portion of Line 1 with one possible interpretation shown. The black dotted line indicates where the detailed geologic information ends and the more general interpretation begins.

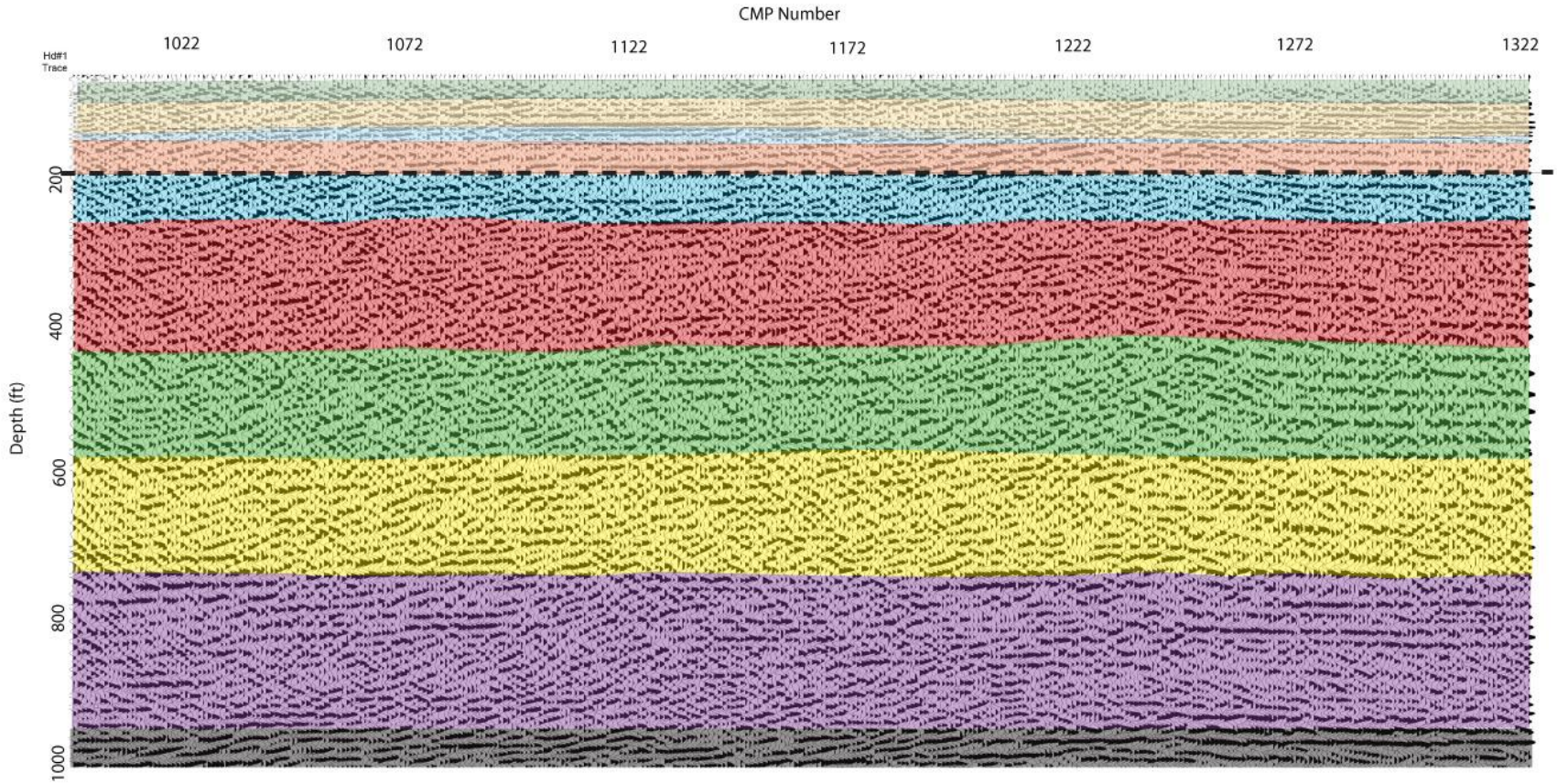


Figure 84. SW portion of Line 1 with one possible interpretation shown. The black dotted line indicates where the detailed

## 5.2 Line 2 Interpretation

Line 2 is located on a SW-NE trending section of the dam (Figure 83). The geologic section for Line 2 to depths of around 200 ft shows sediments with uncertain boundaries that could not be well defined from borehole information (Figure 84). The deepest layer on this section consists of a Lean Clay as classified by the Unified Soil Classification System. Within this layer there are deposits of Clayey Sand and a Lean Clay with a different make up. This layer is overlain by both Quaternary Bonneville clay deposits and specifically a Bonneville Lean Clay. The uppermost layer is classified as a Clayey Sand deposited in a beach environment.

The upper ~200 ft is again where the most detailed geologic information exists. At depths below 200 ft general interpretations are made based on the information from the upper 200 ft and from limited geologic information from nearby boreholes in the Weber River delta area (Feth et al., 1966).

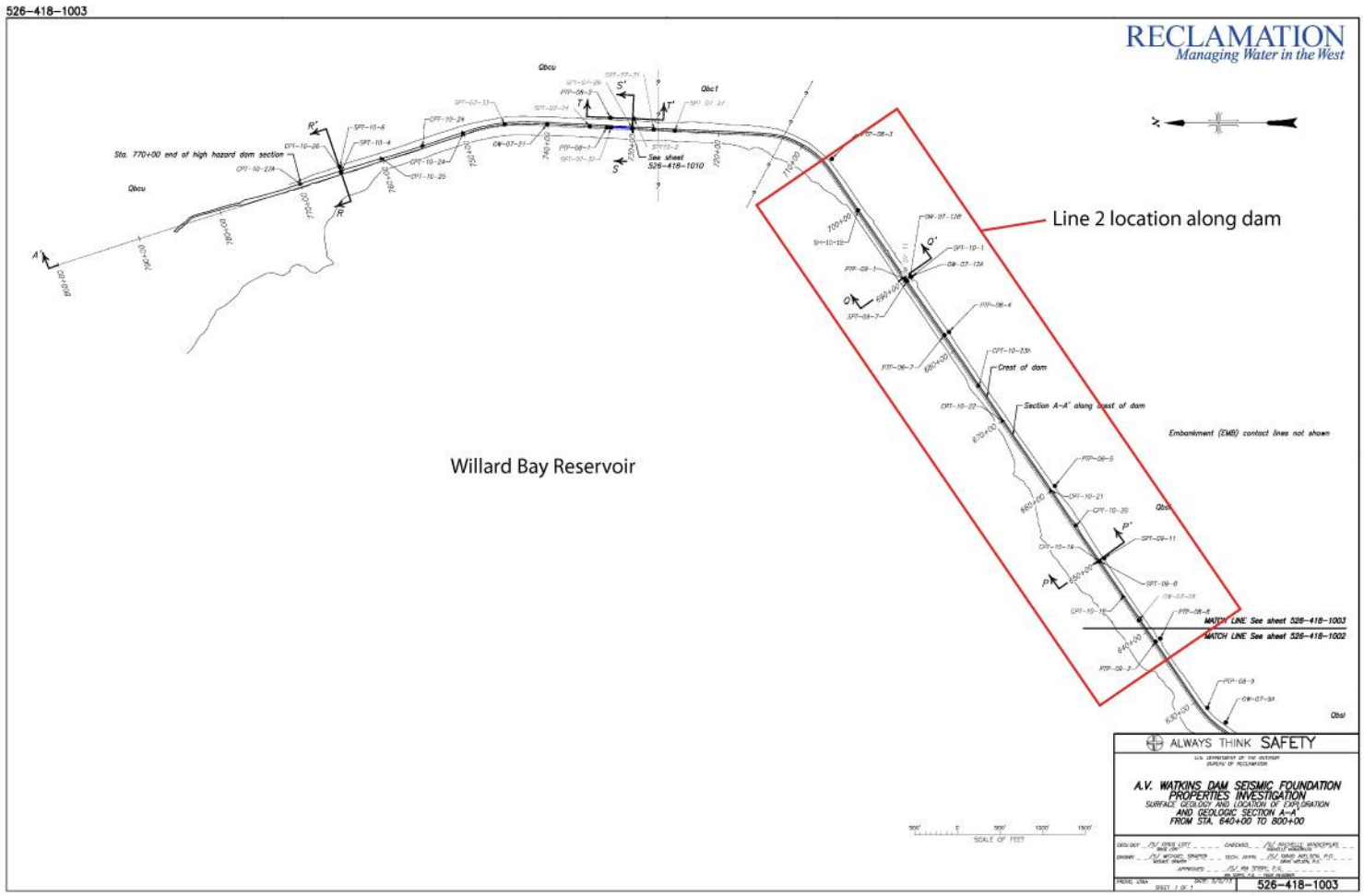


Figure 85. Location of Line 2 along the A.V. Watkins dam where geologic information is available

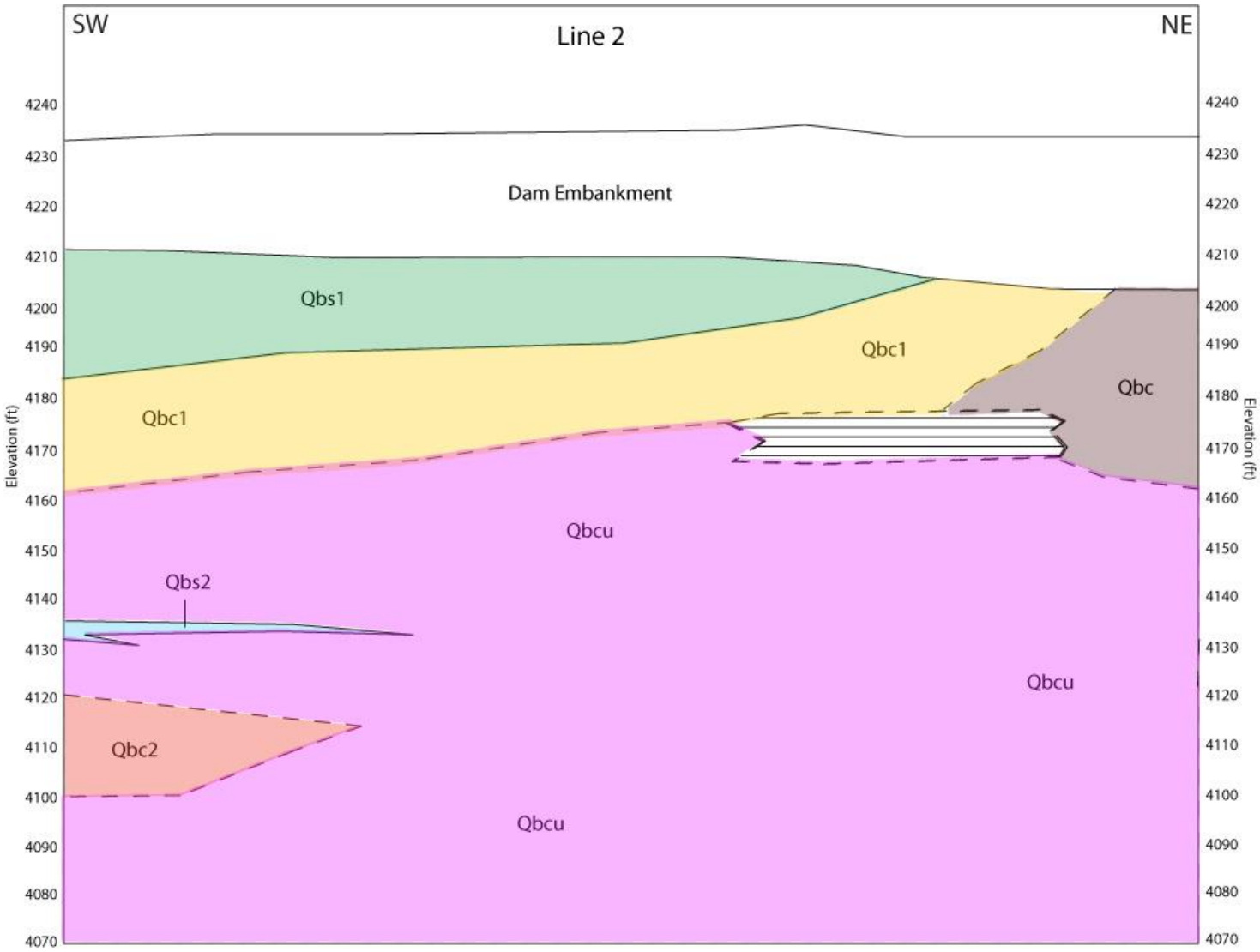


Figure 86. Geologic interpretation of Line 2 based on wells drilled by the U.S. Bureau of Reclamation. Data is available to depths of about 200 ft.

One possible geologic interpretation of the seismic data is given based on the geologic information for the upper ~200 ft and information from wells in the adjacent Weber Delta district (Figure 85, 86). Below ~200 ft interpretations are very general, but certainly consist entirely of unconsolidated sediments based on borehole information. The section of reflections directly below the last geologic information at 200-350 ft (on the unfaulted section) (blue) is identified as consisting of clayey material that is very likely similar to the identified clayey layer overlying it. Reflection characteristics are similar between the two sections. Reflections from 350–425 ft (red) are interpreted to have similar characteristics to a Lean Clay layer in the upper 200 ft. This section is interpreted to consist of a Lean Clay. Reflections from 425–800 ft (green) have similar characteristics to an identified Lean Clay layer. This section is interpreted as consisting of Lean Clay. Reflections from 625–800 ft is interpreted to be a clayey sand layer with fairly coherent reflections. Reflections from 800–1050 ft (purple) are interpreted to consist of clayey sand and gravel based on geologic observations from the Weber Delta boreholes. Reflections in the deepest section from 1050-1100 ft (grey) have similar characteristics to known Lean Clay layers and is interpreted to be Lean Clay.

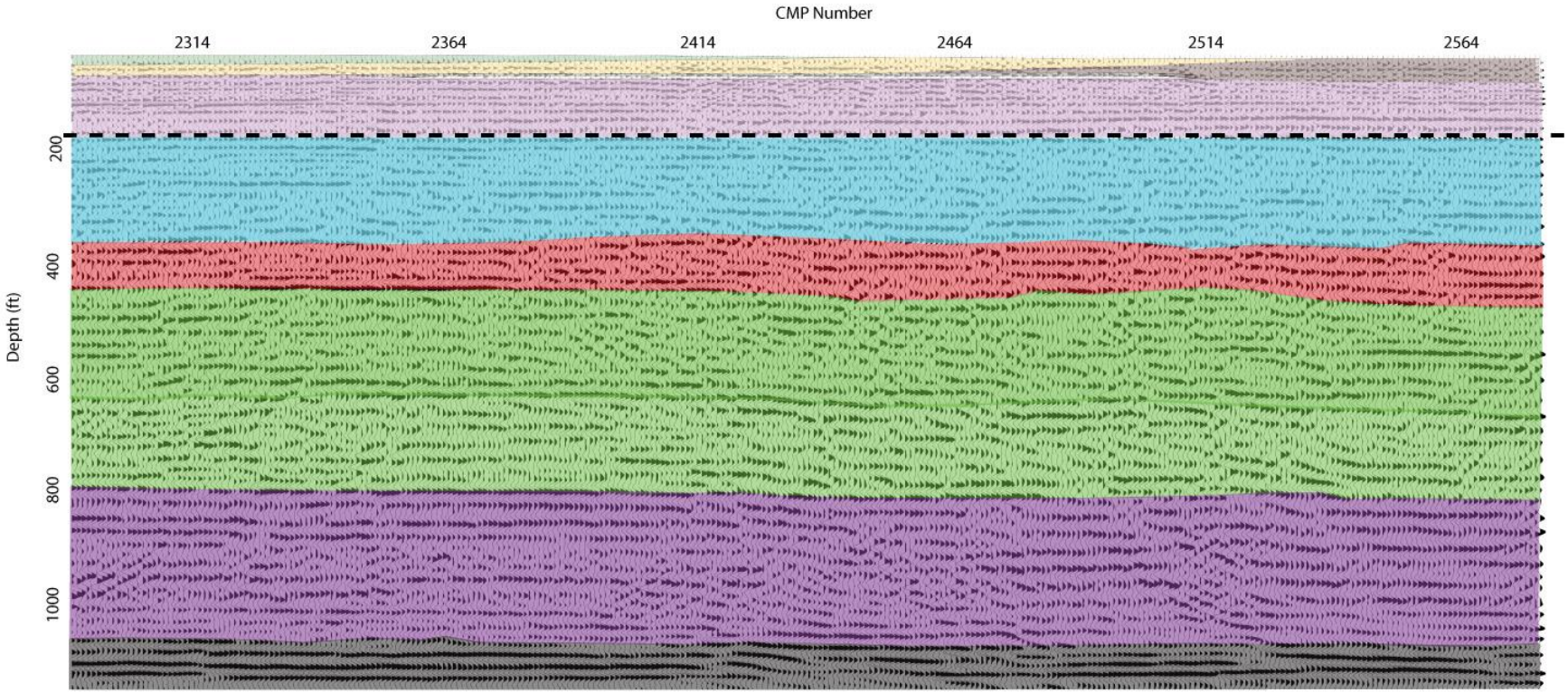


Figure 87. NE portion of Line 2 with one possible interpretation shown. The black dotted line indicates where the detailed geologic information ends and the more general interpretation begins.

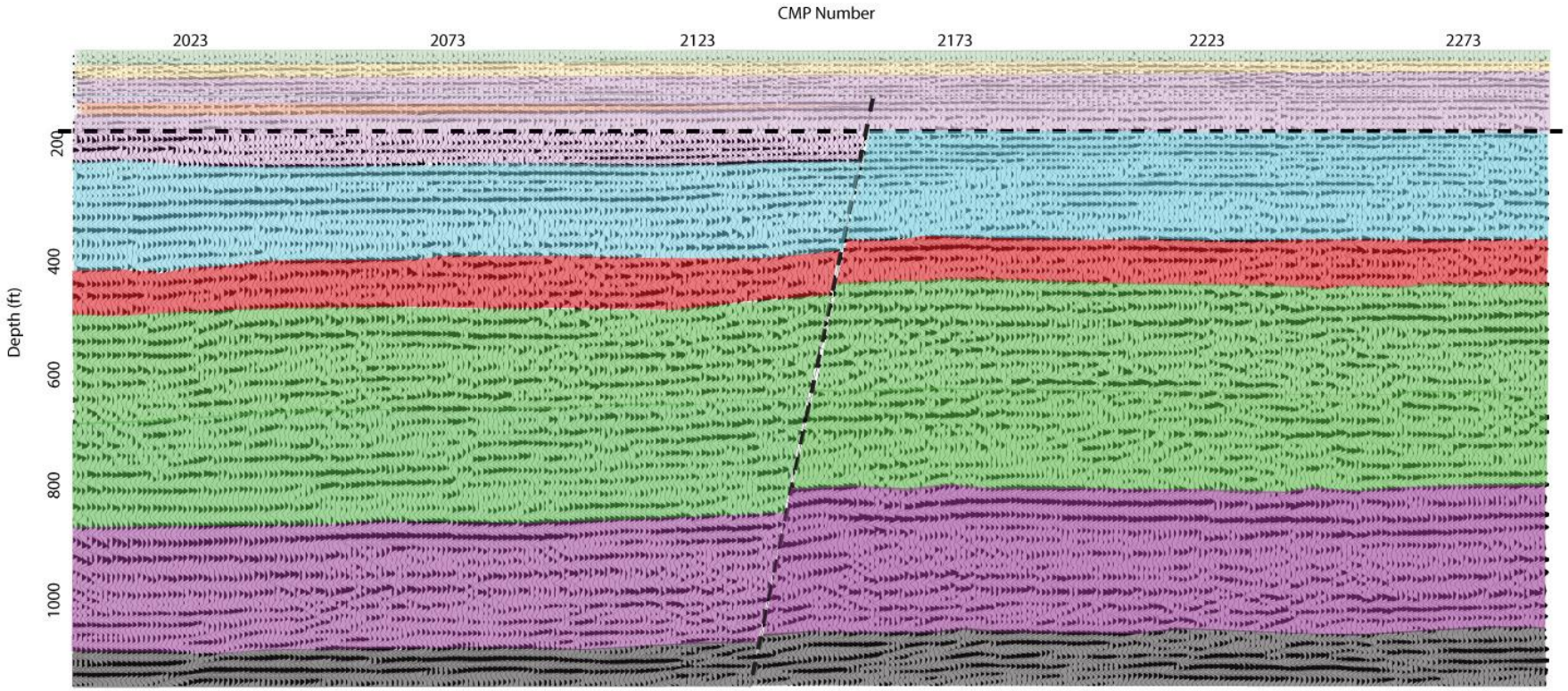


Figure 88. SW portion of Line 2 with one possible interpretation shown. The black dotted line indicates where the

# Chapter 6: Discussion

Though S-wave studies have many benefits in theory, they are not used as often as high-resolution P-wave reflection studies in near-surface settings according to the available literature. This is in part due to the difficulty of collecting and processing broad bandwidth S-wave data with a shear source. The S-wave reflection data presented here provides examples of mapping and Love wave inversion of S-wave data, as well as highlights the pitfalls associated with S-wave acquisition and processing as a broader scale study of S-wave data. This study ultimately provides important information about the characteristics of the subsurface at a site where geohazards such as earthquakes are a threat to surface structures.

## 6.1 Standard Correlation

In theory, in unconsolidated saturated sediments, S-wave reflection surveying is generally capable of achieving higher resolution than their P-wave counterparts if the same dominant frequencies can be produced and recorded due to the slower S-wave velocities. While this study does not compare P-wave data to S-wave data, these S-wave data provide high resolution. Though these data have a low dominant frequency of ~35 Hz, the velocities are slow enough to provide a vertical resolution of as small as 5 ft. Given the equation for wavelength: $\lambda = \frac{V}{F}$, and an average velocity of $V = 700\ ft/s$, and a dominant frequency of $F = 35\ Hz$, wavelength is equal to 20 ft. Dividing 20 ft by four according to the resolution criterion, the vertical resolution is around 5 ft (Dobecki, 1993). The unconsolidated saturated sediments at the site had unusually slow S-wave velocities, creating an environment well suited for achieving high-resolution with S-wave reflection (Castagna et al., 1985).

The conventionally correlated stacked sections from this site, though reaching depths of only a little over 1,100 ft, provide important information about the structure of the sediments beneath the A. V. Watkins dam. A fault on Line 2 shows disturbed layers at depths of less than 200 ft. The detection of faults in Quaternary sediments is an important indicator of how active faulting is at distances from the main fault in a seismically active region. The fault in this particular location is especially important because of its proximity to a dam and the implications its carries when considering the historic seismic activity along the main Wasatch fault. S-wave reflection successfully detected this fault in a setting when there was no other easy way of detecting the existence of this fault. The location of this site prohibits trenching, there is no surface expression and the offset is too small to produce a gravity anomaly.

### 6.2 S-wave processing pitfalls

While S-wave surveying can have many advantages, S-wave data can be plagued by processing pitfalls and difficulties. The main difficulty associated with SH polarized data with the velocity structure observed at the site is the interference of Love waves with the reflection data. Love waves can appear hyperbolic on shot gathers due to their velocities being similar to body S-waves near the source point apex, masking reflections and thus increasing ambiguity when trying to separate true reflections from Love waves. If Love waves cannot be separated from reflectors, they can stack coherently on a CMP stacked section and be mistaken for reflections in the near-surface. By leaving Love waves unmuted in the data, this study demonstrated how coherent noise can appear to be high-amplitude, low-frequency reflections at the top of a stacked section. The unexperienced processor or interpreter could easily mistake these for real data leading to misinterpretations of the subsurface. Love waves by their very

nature are dispersive, which can make removing them completely from data a difficult to impossible task.

Low signal-to-noise ratio in this dataset was a primary difficulty encountered during processing. Removing noise from Line 1 was very difficult. Line 2 contained higher signal-to-noise ratio than Line 1, even though power lines were present along the second half of the line. Harmonic distortion from the vibratory source was present in both lines, but Line 1 was more contaminated with acquisition notes describing "rattling" as the machine swept on a variable surface (Figure 87).

Due to various noise problems, much of the frequency spectrum had to be cut to eliminate as much noise as possible. This led to a narrow bandwidth characterizing the final stacked sections preventing additional noise from being removed due to the signal and noise having the same frequencies.

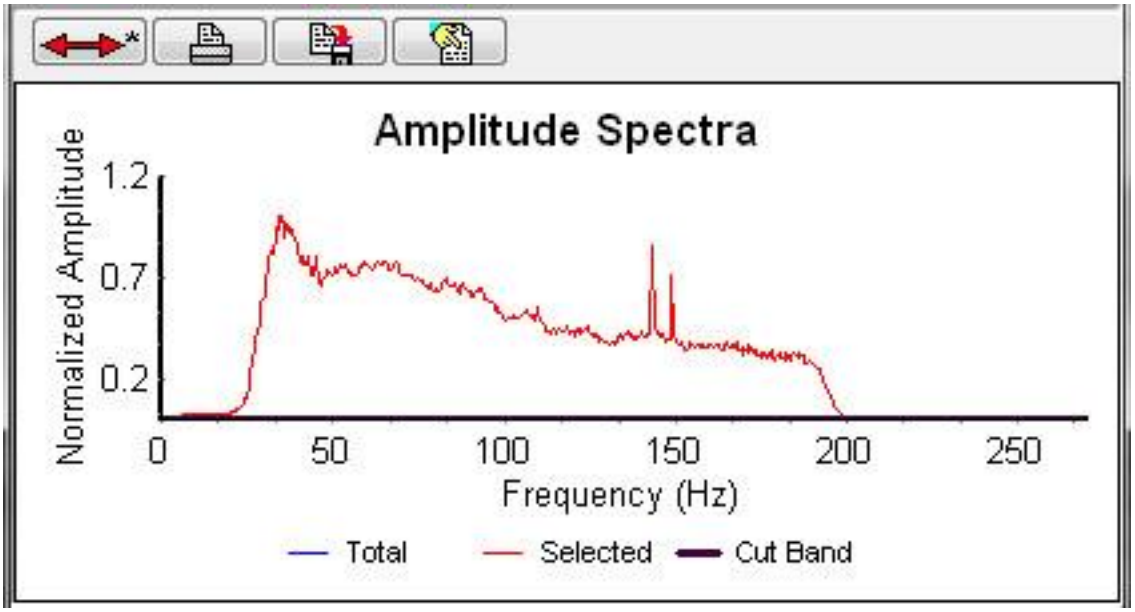


A.

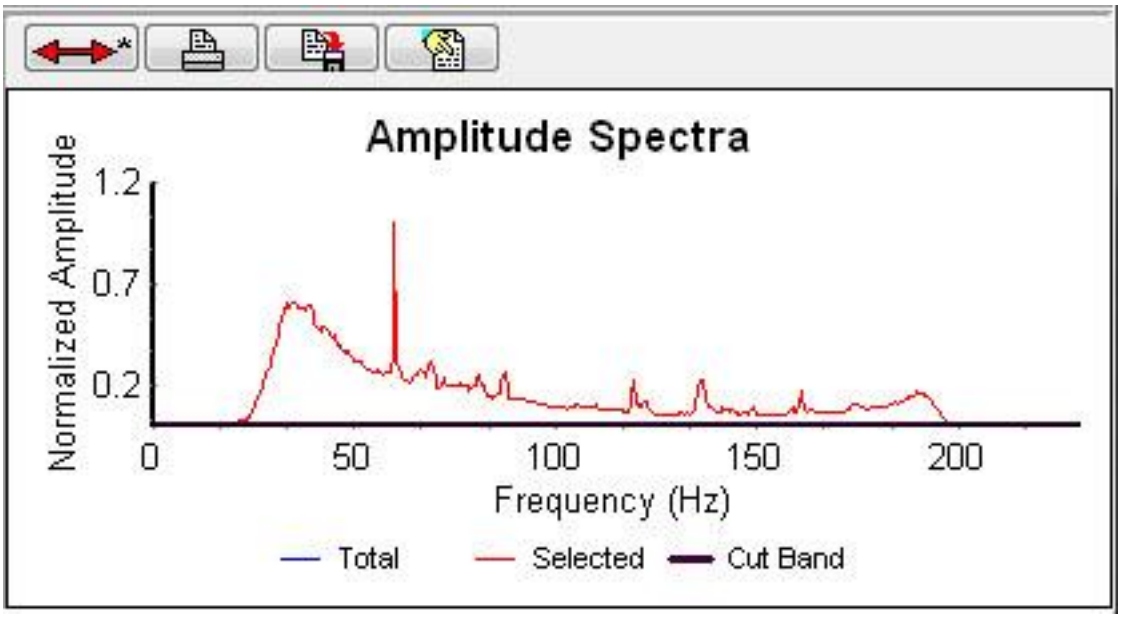


B.

Figure 89. (A) Amplitude spectra from Line 1 showing higher amplitude noise throughout. (B) Amplitude spectra for Line 2 showing more single frequency noise that is easier to remove than the noise on Line 1.

### 6.3 Extended Correlation

Extended Vibroseis correlation is sometimes employed in industry when exploration scale data is available but crustal scale information is desired, but the referenced literature has no examples of extended correlation being used in a near-surface study. The self-truncating extended correlation method was successfully implemented on S-wave data in this study. Data was lengthened by 1 s, to give a record of 2.8 s. Time-depths reached through conventional Vibroseis correlation were almost doubled through the use of extended correlation. With extra time, extra reflections were brought out in the data giving more key information about the deeper, less understood part of the subsurface.

### 6.4 Love wave inversion and surface elevation corrections

In general when S-wave data are acquired for most applications Love waves that are present are considered noise and are attenuated during processing. This study demonstrated that Love waves can be successfully inverted to create a $V_S$ profile to give more detailed information about the very near-surface material for static or engineering application. Raw, uncorrelated data was used to create Love wave dispersion curves. Dispersion curves from Line 1 were keasily discernable and the fundamental modes were easily separable from higher modes. Line 2 dispersion curves were often ambiguous and many records could not be used due to higher mode contamination of the fundamental mode. Fundamental modes were picked in the records where they were easily identifiable and uncontaminated by higher modes. The dispersion curves were then inverted and a $V_S$ profile was created. The profile from Line 1 reached a depth of 25 ft, while the profile from Line 2 reached a depth of only 13 ft. This was due to the better dispersion curves from Line 1 data which allowed for the picking of more low frequency data.

The $V_S$ profiles were then used to correct for minimal surface elevation statics and assess lateral velocity variations. Based on the velocities measured in the profiles, average velocities were calculated for the layers specified in a model. A datum was chosen above these layers and below the surface elevations collected at the site. Data was then corrected to the datum. Data corrected for surface elevation static show important information that was not shown in the regular data. Line 1 shows structure that was not visible in the data before it was corrected for surface elevation. There is a dipping layer that could indicate the presence of a fault. Line 2 shows a layer at a depth of less than 200 ft that was previously continuous, but shows offset possible from faulting when elevation statics are applied. This is a significant finding because it has implications for the activity of the fault. Had that layer remained continuous it would be possible to conclude that the fault was no longer active. However, if near-surface layers are showing offset as well, it is possible that the fault is still active and could pose a potential threat to any structures on the surface.

### 6.5 Geologic interpretation

Based on the limited available geologic information for the area interpretations were made for both lines. More detailed geologic information for depths greater than 200 ft are needed to confidently interpret lithology and identify lithologic boundaries.

Offset in unconsolidated saturated sediments is clearly imaged and identified. Many different reflections are clearly shown on the S-wave seismic sections for both lines. It is possible that not as much offset would have been imaged with potentially lower resolution P-wave data. In addition, fewer reflections might have been imaged due to acoustic impedance changes not being sufficient to produce reflections from within saturated sediments. If sediments in the deeper

subsurface (greater than 200 ft) could be confidently identified it would be possible to obtain the relative age of the offset of the fault offsetting sediments on Line 2.

### 6.6 Other applications

The applications for which the methods outlined in this study are used for are by no means exclusive uses for the methods. The near-surface branch of geophysical studies is broad in scope, needs and situations. The methods used here might be applied successfully to other areas of investigation such as hydrogeological, engineering, geotechnical, mining, and many other shallow near-surface applications.

The inversion of Love waves is a method that could benefit greatly from development of the algorithms and be put to use in practical applications. One example of the detailed information that can be provided by inversion of Love waves includes a measure of anisotropy when compared to inverted Rayleigh wave data. Theoretically, Love and Rayleigh waves are associated with different shear-wave velocities, so inverting them independently can show differences in vertical and lateral velocity variations.

Advantages to researchers developing Love wave inversion as a tool include the fact that Love wave dispersion curves are generally cleaner and sharper than those of Rayleigh waves rendering phase velocities easier to pick (Xia et al., 2012). Love wave inversion is also more stable than Rayleigh wave inversion and "mode kissing", a phenomenon whereby misidentification of modes causes velocities to appear to be much higher than they actually are is not a problem as with Rayleigh waves (Xia et al., 2012).

### 6.7 Future research

Many aspects of this research could benefit from further study and utilization in the near-surface community. Development of a standard processing flow for S-wave reflection data containing Love waves and low signal-to-noise ratio would be a useful guide for future researchers. More extensive information and examples of S-wave processing pitfalls and difficulties and suggestions to overcome them would be useful information to have in the literature base for the near-surface community. In addition, the literature base would benefit from more examples of the use of extended correlation in near-surface surveys.

Inversion of Love wave data for supplemental shear velocity profiles is a technique that would be of great use to the near-surface community if developed further. Love wave data are often present in SH reflection data and could be of great use to researchers rather than being discarded. Xia, (2009), Xia et al., (2010), Mari, (1984), and Safani et al., (2005) provide good starting points for this research.

## Conclusion

S-wave reflection data is a very useful tool for near-surface studies if processing pitfalls can be overcome and true reflections can be separated from Love waves. S-wave reflection sections from this study contained high percentages of noise, but were still processed to give important information about the subsurface. The use of extended correlation is also a useful tool for near-surface studies where it can be necessary due to acquisition limitations. Inverting Love waves for $V_S$ profiles provides information about shallow $V_S$ structure. The $V_S$ profiles can also be used to perform static corrections. Applying static corrections to the data in this study helped determine previously thought continuous layers were actually faulted on Line 2 and that there may be a fault on Line 1 as well.

**References**

Allmendinger, R. W., and, Zapata, T. R., 2000, The footwall ramp of the Subandean decollement northernmost Argentina, from extended correlation of seismic reflection data. Tectonophysics, **321**,37-55.

Banner, R. E., 2006, Physiographic Provinces and Surface Geology of Utah. Rangelands Archives, **14**, no. 2,106-108.

Bansal, R., and, Gaiser, J. E., 2013, An introduction to this special section: Applications and challenges in shear-wave exploration. The Leading Edge, **32**, no. 1,12.

Benjumea, B., Hunter, J. A., Pullan, S. E., Burns, R. A., and, Good, R. L., 2001, Near-surface seismic studies to estimate potential earthquake ground motion amplification at a thick soil site in teh Ottawa river valley, Canada. Proc. SAGEEP,4-7.

Benson, A. K., and, Mustoe, N. B., 1991, Delineating concealed faults and shallow subsurface geology along the Wasatch Front, Utah, USA, by integrating geophysical and trench data. Quarterly Journal of Engineering Geology and Hydrogeology, **24**, no. 4,375-387. doi: 10.1144/gsl.qjeg.1991.024.04.05.

Best, J. A., 1991, Mantle reflections beneath the Montana Great Plains on Consortium for Continental Reflection Profiling Seismic Reflection Data. Journal of Geophysical Research, **96**, no. B3,4279-4288.

Bexfield, C. E., McBride, J. H., Pugin, A. J. M., Ravat, D., Biswas, S., Nelson, W. J., Larson, T. H., Sargent, S. L., Fillerup, M. A., Tingey, B. E., Wald, L., Northcott, M. L., South, J. V., Okure, M. S., and, Chandler, M. R., 2006, Integration of P- and SH-wave high-resolution seismic reflection and micro-gravity techniques to improve interpretation of shallow

subsurface structure: New Madrid seismic zone. Tectonophysics, **420**, no. 1-2,5-21. doi: 10.1016/j.tecto.2006.01.024.

Black, R. A., Steeples, D., and, Miller, R. D., 1994, Migration of shallow reflection data. Geophysics, **59**, no. 3,402-410.

Brittle, K. F., Lines, L. R., and, Dey, A. K., 2000, Vibroseis deconvolution: a comparison of cross-correlation and frequency domain sweep deconvolution Geophysical Prospecting, **49**, no. 6,675-686.

Burger, R. H., Sheehan, A. F., and, Jones, C. H. 2006, Introduction to Applied Geophysics: W. W. Norton & Company, Inc.

Carr, B. J., Hajnal, Z., and, Prugger, A., 1998, Shear-wave studies in glacial till. Geophysics, **63**, no. 4,1273-1284.

Castagna, J. P., Batzle, M. L., and, Eastwood, R. L., 1985, Relationships between compression-wave and shear-wave velociites in clastic silicate rocks. Geophysics, **50**, no. 4,571-581.

Coruh, C., and, Costain, J. K., 1983, Noise attenuation by Vibroseis whitening (VSW) processing. Geophysics, **48**, no. 5,543-554.

Deidda, G. P., and, Ranieri, G., 2001, Some SH-wave seismic reflections from depths of less than three meters. Geophysical Prospecting, **49**,499-508.

Dobecki, T. L., 1993, High Resolution in Saturated Sediments - a case for shear wave reflection. Symposium of the Application of Geophysics to Engineering and Environmental Problems, 1993.

Eardley, A. J., 1938, Sediments of Great Salt Lake, Utah. Bulletin of the American Association of Petroleum Geologists, **22**, no. 10,1305-1363.

Feth, J. H., Barker, D. A., Moore, L. G., Brown, R. J., and, Veirs, C. E., 1966, Lake Bonneville: Geology and hydrology of the Weber delta district, including Ogden, Utah. Geological Survey professional paper, **518**.

Garotta, R. 1999, Shear waves from acquisition to interpretation. Vol. 3: Society of Exploration Geophysicists.

Ghose, R., 2002, High-frequency shear wave reflections from shallow subsoil layers using a vibrator source: Sweep cross-correlation versus deconvolution and groundforce derivative. SEG, Expanded Abstracts, **21**, no. 1408-1411.

Goforth, T., and, Hayward, C., 1992, Seismic reflection investigations of a bedrock surface buried under alluvium. Geophysics, **57**, no. 9,1217-1227.

Guy, E. D., Nolen-Hoeksema, R. C., Daniels, J. J., and, Lefchik, T., 2003, High-resolution SH-wave seismic reflection investigations near a coal mine-related roadway collapse feature. Journal of Applied Geophysics, **54**, no. 1-2,51-70. doi: 10.1016/s0926-9851(03)00055-7.

Haines, S. S., and, Ellefsen, K. J., 2010, Shear-wave seismic reflection studies of unconsolidated sediments in the near surface. Geophysics, **75**, no. 2,B59-B66.

Harris, J. B., 2010, Application of shallow shear-wave seismic reflection methods in earthquake hazards studies. The Leading Edge,960-963.

Hasbrouck, W. P., 1991, Four shallow-depth, shear-wave feasibility studies. Geophysics, **56**, no. 11,1875-1885.

Helbig, K., and, Mesdag, C. S., 1982, The potential of Shear-wave observations. Geophysical Prospecting, **30**, no. 4,413-431.

Hintze, L. F. 2005, Utah's Spectacular Geology: How it came to be: Department of Geology, Brigham Young University.

Hunter, J. A., Benjumea, B., Harris, J. B., Pullan, S. E., Burns, R. A., and, Good, R. L., 2002, Surface and downhole shear wave seismic methods for thick soil site investigations. Soil Dynamics and Earthquake Engineering, **22**,931-941.

Hunter, J. A., Pullan, S. E., Burns, R. A., Gagne, R. M., and, Good, R. L., 1984, Shallow seismic reflection mapping of the overburden-bedrock interface with the engineering seismograph-Some simple techniques. Geophysics, **49**, no. 8,1381-1385.

Inazaki, T., 2004, High-resolution seismic reflection surveying at paved areas using an S-wave type land streamer. Exploration Geophysics, **35**, no. 1,1-6.

Inazaki, T., 2005, High-resolution seismic reflection survey using land streamer in a large urban area. Symposium of the Application of Geophysics to Engineering and Environmental Problems, 2005,979-988.

Inazaki, T., Kusaka, N., Takigawa, S., and, Yoshimi, S., 2001, High-Resolution S-wave reflection surveying using land streamer for the safe driving of a shield tunnel. Society of Exploration Geophysicists.

Johnson, W. J., and, Clark, J. C., 1992, Improving Subsurface Resolution with the Seismic Reflection Method: Use S-waves. Ground Water Management, **11**,655-663.

Jongerius, P., Brouwer, J., and, Helbig, K., 1985, Shallow high resolution seismics: Geologic applications. 1985 SEG Annual Meeting,152-154.

Joyner, W. B., 2000, Strong motion from surface waves in deep sedimentary basins. Bulletin of the Seismological Society of America, **90**, no. 6B,S95-S112.

Kelly, K. R., 1983, Numerical study of Love wave propagation. Geophysics, **48**, no. 7,833-853.

Kendall, R. R., and, Davis, T. L., 1996, The cost of acquiring shear waves. The Leading Edge, **15**, no. 8,943.

Krawczyk, C. M., Polom, U., and, Beilecke, T., 2013, Shear-wave reflection seismics as a valuable too for near-surface urban applications. The Leading Edge, **32**, no. 3,256-263.

Krawczyk, C. M., Polom, U., Trabs, S., and, Dahm, T., 2012, Sinkholes in the city of Hamburg—New urban shear-wave reflection seismic system enables high-resolution imaging of subrosion structures. Journal of Applied Geophysics, **78**,133-143. doi: 10.1016/j.jappgeo.2011.02.003.

Kurahashi, T., and, Inazaki, T., 2007, Seismic reflection survey using shear-wave vibrator for an active fault. Symposium of the Application of Geophysics to Engineering and Environmental Problems, 2007,566-573.

Lemons, D. R., and, Chan, M. A., 1999, Facies architecture and sequence stratigraphy of fine-grained lacustrine deltas along the eastern margin of late Pleistocene Lake Bonneville, northern Utah and southern Idaho. AAPG Bulletin, **83**, no. 4,635.

Mari, J. L., 1984, Estimation of static corections for shear-wave profiling using the dispersion properties of Love waves. Geophysics, **49**, no. 8,1169-1179.

Miller, R. D., and, Steeples, D., 1990, A shallow seismic reflection survey in basalts of the Snake River Plain, Idaho. Geophysics, **55**, no. 6,761-768.

Miller, R. D., Xia, J., and, Park, C. B., 2001, Love waves: A menace to shallow shear wave reflection surveying. Annual Meeting of Society of Exploration Geophysicists Expanded Abstracts.

Mussett, A. E., and, Khan, M. A. 2000, Looking into the earth: an introduction to geological geophysics: Cambridge Univeristy Press.

Nazarian, S., and, Stokoe, K. H., 1985, In situ determination of elastic moduli of pavement systems by Spectral-analysis-of-surface-waves Method: Practical Aspects. Transportation Res. Record, **Report No. 368-1F**.

Okaya, D. A., and, Jarchow, C. M., 1989, Extraction of deep crustal reflections from shallow Vibroseis data using extended correlation. Geophysics, **54**, no. 5,555-562.

Park, C. B., Miller, R. D., and, Xia, J., 1999, Multichannel analsis of surface waves. Geophysics, **64**, no. 3,800-808.

Pugin, A., Larson, T., and, Phillips, A., 2002, Shallow high-resolution shear-wave seismic reflection acquisition using a land-streamer in the Mississippe River floodplain: potential for engineering and hydrogeologic applications. SAGEEP, CD-ROM.

Pugin, A., Pullan, S. E., and, Hunter, J. A., 2013, Shear-wave high-resolution seismic reflection in Ottawa and Quebec City, Canada. The Leading Edge, **32**, no. 3,250-255.

Pugin, A. J., Larson, T., Sargent, S., McBride, J., and, Bexfield, C., 2004, Near-surface mapping using SH-wave and P-wave seismic land-streamer data acquisition in Illinois, USA. The Leading Edge, **23**, no. 7,677-682.

Pugin, A. J., Pullan, S. E., and, Hunter, J. A., 2007, Imaging of ultra-shallow subsurface using SH-wave seismic reflection. SEG Annual Meeting.

Pullan, S. E., Hunter, J. A., and, Neave, K. G., 1990, Shallow shear-wave reflection tests. SEG Annual Meeting.

Reust, D. K., 1995, Vibrator force control: How simple can it get. The Leading Edge, **1**, no. 11,1129-1133.

Ristow, D., and, Jurczyk, D., 1975, Vibroseis Deconvolution. Geophysical Prospecting, **23**, no. 2,363-379.

Safani, J., O'Neil, A., and, Matsuoka, T., 2006, Full SH-wavefield modelling and multiple-mode Love wave inversion. Exploration Geophysics, **37**,307-321.

Safani, J., O'Neil, A., Matsuoka, T., and, Sanada, Y., 2005, Applications of Love wave dispersion for improved shear-wave velocity imaging. . Journal of Environmental and Engineering Geophysics, **10**, no. 2,135-150.

Schrodt, J. K., 1987, Techniques for improving Vibroseis data. Geophysics, **52**, no. 4,469-482.

Seriff, A. J., and, Kim, W. H., 1970, The effect of harmonic distortion in the use of vibratory surface sources. Geophysics, **35**, no. 2,234-246.

Sheriff, R. E. 2006, Encyclopedic Dictionary of Applied Geophysics. Edited by Eugene F. Scherrer. Vol. 4: Society of Exploration Geophysicists.

Sheriff, R. E., and, Geldart, L. P. 1995, Exploration Seismology: Cambridge University Press.

Shtivelman, V., Frieslander, U., Zilberman, E., and, Amit, R., 1998, Mapping shallow faults at the Evrona playa stie using high-resolution reflection method. Geophysics, **63**, no. 4,1257-1264.

Stewart, R. R., Gaiser, J. E., Brown, R. J., and, Lawton, D. C., 2003, Converted-wave seismic exploration: Applications. Geophysics, **68**, no. 1,40.

Stumpel, H., 1984, The use of seismic shear waes and compressional waves for lithologic problems of shallow sediments. Geophysical Prospecting, **32**, no. 4,662-675.

Tatham, R. H., and, Stewart, R. R., 1993, Present status and future directions of shear-wave seismology in exploration. CREWES Research Report, **5**.

Telford, W. M., Geldart, L. P., Sheriff, R. E., and, Keys, D. A. 1976, Applied Geophysics: Cambridge University Press.

von Steht, M., Jaskolla, B., and, Ritter, J. R., 2008, Near surface shear wave velocity in Bucharest, Romania. Natural Hazards and Earth System Science, **8**, no. 6,1299-1307.

Wang, Z., Madin, I. P., and, Woolery, E. W., 2003, Shallow SH-wave seismic investigation of the Mt. Angel Fault, Northwest Oregon, USA. Tectonophysics, **368**, no. 1-4,105-117. doi: 10.1016/s0040-1951(03)00153-7.

Waters, K. H. 1987, Reflection Seismology. Edited by Inc. John Wiley & Sons. Vol. 3: Wiley-Intersciene.

Wei, Z., Phillips, T. F., and, Hall, M. A., 2010, Fundamental discussion on seismic vibrators. Geophysics, **75**, no. 6,W13-W25.

Woolery, E. W., and, Street, R. L., 2002, Quaternary faullt reactivation in the Fluorpar Area fault complex of western Kentucky: Evidence from shallow SH-wave reflection profiles. Seismological Research Letters, **73**, no. 5,628-639.

Woolery, E. W., Street, R. L., and, Wang, Z., 1993, Near-surface deformation in the New Madrid seismic zone as imaged by high resolution SH-wave seismic methods. Geophysica Research Letters, **20**, no. 15,1615-1618.

Xia, J., 2009, Estimation of near-surface shear-wave velocity by inversion of Love waves. SEG Technical Program Expanded Abstracts, **2009**,1390-1395.

Xia, J., Miller, R. D., Cakir, R., Luo, Y., Xu, Y., and, Zeng, C., 2010, Revisiting SH-wave data using Love-wave analysis. Symposium of the Application of Geophysics to Engineering and Environmental Problems, 2010,569-580.

Xia, J., Miller, R. D., and, Park, C. B., 1999, Estimation of near-surface shear-wave velocity by inversion of Rayleigh waves. Geophysics, **64**, no. 3,691-700.

Xia, J., Xu, Y., Luo, Y., Miller, R. D., Cakir, R., and, Zeng, C., 2012, Advantages of using multichannel analysis of Love waves (MALW) to estimate near-surface shear-wave velocity. Surv Geophysics, **33**,841-860.

Yilmaz, O. 1987, Seismic Data Processing. Vol. 2: Society of Exploration Geophysicists.

Young, R. A., and, Hoyos, J., 2001, Near-surface, SH-wave surveys in unconsolidated, alluvial sediments. The Leading Edge, **20**, no. 9,936-948.

Zimmer, M. A., Prasad, M., Mavko, G., and, Nur, A., 2007, Seismic velocities of unconsolidated sands: Part 2-Influence of sorting-and compactions-induced porosity variation. Geophysics, **72**, no. 1,E15-E25.